Investigations of the Loadbearing Behaviour of Timber Bending Beams Reinforced Using Prestressed CFRP-Lamellas

Dissertation

zur Erlangung des akademischen Grades

Doktor-Ingenieur (Dr.-Ing.)

an der Fakultät Bauingenieurwesen

der

Bauhaus-Universität Weimar

vorgelegt von

MSc. Dipl. Ing. FH Martin Lehmann

aus Bern

Weimar

Gutachter: 1. Prof. Dr. Ing. Karl Rautenstrauch

2. Prof. Dr. Ing. Parviz Navi

3. Prof. Dr. Ing. Jan-Willem van de Kuilen

Tag der Disputation: 29. April 2015

Abstract

The refurbishment of old buildings often goes hand in hand with an increase in both the dead and live loads. The latter, combined with the higher safety factors, often make the reinforcement of the old structures necessary. Most reinforcement methods involve transforming a structural timber member into a composite beam. Composite sections have a long tradition in timber construction. In the early days, multiple timber beams were connected with interlocking tooth and wooden shear connecters, which resulted in an elastic connection. Although historical timber structures are frequently upgraded, no method has yet been established and fully accepted by all stakeholders such as owners, builders, architects, engineers and cultural heritage organisations. Carbon fibre-reinforced polymers (CFRP) have already shown their efficiency in structural reinforcement especially in concrete structures. Moreover, previous studies have shown that CFRP has the potential to meet the expectations of all parties involved. In order to reach the service-limit state, a high amount of carbon fibres has to be used, or considering the cost of reinforcement, prestress has to be applied. However, prestressing often goes hand-in-hand with delaminating issues. The camber method presented here offers an efficient solution for prestressing timber bending members and overcoming the known obstacles.

In the method proposed, the timber beam is cambered using an adjustable prop at midspan during the bonding of the CRFP-lamella to the lower side of the bending member. After curing the adhesive, the prop is removed and the prestressed composite beam is ready to be used. The prestress introduced in the system is not constant, but has a triangular shape and peaks at midspan, where it is used the most. The prestress force, which declines towards the end of the beam, leads to a constant shear stress over the whole length of the reinforcement, avoiding a concentrated anchorage zone.

An analytical calculation model has been developed to calculate and design prestressed timber-bending members using the camber method. Numerical modelling, using a multi-surface plasticity model for timber, confirmed the results from the analytical model, and clearly reduced delaminating issues, comparing very favourably to traditional prestressing methods. The experimental parametric study, including the determination of the short-term load-bearing capacity of structural-sized beams, showed agreement with the analytical and numerical calculation. The prestressed reinforcement showed a benefit of nearly 50% towards the ultimate-limit state and up to 70% towards the service-limit state. Calculations revealed that the use of high modulus CFRP allows even higher benefits, depending on the configurations and requirements. The long-term design of the prestressed composite beam was investigated by extending the analytical model. The creep of the timber leads to a load transfer from the timber towards the CFRP, and therefore increases the benefit towards the ultimate-limit design. Applying high modulus CFRP-lamellas allows for a complete utilisation of the design capacity of timber and carbon fibre-reinforced polymer.

The thorough investigation conducted demonstrated that the camber method is an efficient technique for prestressing and reinforcing timber-bending members. Furthermore, the calculation model presented allows for a safe design and estimation of long-term behaviour.

Zusammenfassung

Die Sanierung von bestehenden Gebäuden bringt häufig eine Erhöhung der Nutz- und Auflasten mit sich. Dies und die von den neuen Normen geforderten höheren Sicherheitsfaktoren erfordern oft eine Verstärkung der bestehenden Tragstruktur. Die meisten Massnahmen verwandeln den Holzbalken in einen Verbundquerschnitt. Zusammengesetzte Querschnitte haben in der Holzkonstruktion eine lange Tradition. Zu Beginn wurden die Konstruktionen durch Verzahnen und / oder durch Hartholzdübel respektive Keile miteinander verbunden. Kohlefaser verstärke Kunststoffe (CFK) haben bereits den Nachweis der Effizienz zur Verstärkung bestehender Strukturen erbracht, dies insbesondere im Betonbau. Verstärkungen im Holzbau werden bereits durchgeführt, jedoch hat sich bis heute noch keine Methode etabliert welche für alle involvierten Parteien wie Bauherr, Bauunternehmung, Architekt Ingenieur und Denkmalpflege zufriedenstellend ist. Verschiedene Untersuchungen zeigten, dass CFK das Potenzial hat diese Ansprüche zu erfüllen. Um mit dem Hochleistungsmaterial CFK auch die Durchbiegung reduzieren zu können ist entweder eine Vorspannung notwendig oder es muss andererseits sehr viel CFK eingesetzt werden, was die Methode unnötig verteuert. Leider kommt eine Vorspannung meist Hand in Hand mit Delaminierungsproblemen. Die Ursache dafür sind konzentrierte Schubspannungen an den Lamellenenden. Hier setzt die in der Dissertation präsentierte Methode zur Vorspannung von Biegebalken an und löst die bekannten Probleme.

Die Vorspannung wird durch Überhöhung des zu sanierenden Balkens während der Verklebung mit der Kohlefaserlamelle erzeugt. Dies erfolgt mit Hilfe einer Schalungsstütze in der Mitte des Balkens. Durch das Entfernen der Schalungsstütze wird der verstärkte Balken vorgespannt und kann belastet werden. Das durch die Überhöhung induzierte Biegemoment ist dreieckförmig. Daher ist die Schubspannung in der Klebefuge gleichmässig über die Länge verteilt und auf eine konzentrierte Verankerung der Vorspannkraft wird verzichtet. Die Vorspannkraft ist in der Mitte, wo sie am meisten benötigt wird, am grössten und gegen aussen abnehmend.

Ein analytisches Berechnungsmodel zur Berechnung und Dimensionierung von Balken, welche mit der präsentierten Methode vorgespannt sind, wurde entwickelt. Nummerische Modellierungen mit einem nichtlinearen Materialmodell für Holz bestätigten die Resultate der analytischen Berechnungen und das klar reduzierte Risiko gegenüber Delaminierung. Die Laborversuche beinhalteten eine Parameterstudie sowie die Ermittlung der Bruchlast von vorgespannten Holzbalken mit baupraktischen Abmessungen. Die Tragfähigkeit konnte um ca. 50 % gesteigert werden. Der Beitrag zur Gebrauchstauglichkeit war, abhängig vom Gefährdungsbild, bis zu 70 %. Berechnungen zeigten, dass bei der Verwendung von hochmoduligen CFK-Lamellen diese Werte je nach Anforderung und Gefährdungsbild noch höher ausfallen. Das Langzeitverhalten des Verbundquerschnittes wurde analytisch untersucht. Durch das Kriechen des Holzes wird es über die Zeit leicht entlastet und der CFK übernimmt mehr Last. Bei hochmoduligen CFK-Lamellen kann die Kapazität von Holz und CFK vollständig ausgenutzt werden.

Die ausführlichen Untersuchungen bewiesen die Effizienz der präsentierten Verstärkungsmethode. Mit dem analytischen Berechnungsmodell können verstärkte Balken sicher dimensioniert und das Langzeitverhalten abgeschätzt werden.

Acknowledgments

Over the last few years I have received support and encouragement from many people, and I wish to express my thanks to all of them. Further, I would like to especially acknowledge those who made a specific contribution.

The doctoral thesis was done beside my work as assistantand scientific collaborator at the Bern University of Applied Sciences. I like to thank the University for giving me permission to publish the experimental results I obtained from my research work there. I also wish to express my thanks to Dr. Frédéric Pichelin and to René Graf for their flexibility concerning my employment and working hours as well as for the motivating support they have always given to me, especially towards the end of the thesis.

I would like to thank Professor Dr. Ing. Karl Rautenstrauch for giving me this opportunity and for supervising my doctoral thesis. Furthermore, I wish to thank him for the guidance and support he has given me during this time. I would also like to thank Professor Dr. Ing. Navi and Professor Dr. Ing. Van de Kuilen for finding the time to act as an examiner of my thesis.

My acknowledgments and thanks go to the members of the examining committee for the time and effort they put into examining the thesis.

I wish to thank Dr. Maurice Brunner for his remarks, discussions and interesting suggestion regarding the analytical calculation model.

Last but not least, I thank my partner, Hilde, and our little daughter, Tilia Estelle, for the understanding and support they have given me during the time I spent on the preparation of this thesis.

Bern, December 2012 Martin Lehmann

Contents

1 Introduction

The refurbishment of old buildings often goes hand-in-hand with an increase of the dead and live load. This, together with the higher safety factors, often make the reinforcement of an old structure necessary. At the same time, the use of steel is often regarded as an inadequate solution in a timber construction due to the increased self-weight of the structure, the appearance and the corrosion in marine environments that result. The use of Carbon Fibre-Reinforced Polymers (CFRP), however, allows methods that avoid these effects, and are nearly invisible.

Most reinforcing methods transform a structural-timber member into a composite. Composite sections have a long tradition in timber constructions. In the early stages, the multiple timber beams were connected with interlocking tooth and wood shear connecters, which resulted in an elastic connection. The first known construction using adhesive to overcome the limited size and straight shape of timber beams was built in 1860 in Southampton, England [89]. Otto Hetzer is usually regarded as the pioneer, using adhesives to laminate timber and contributing to the invention of glue-laminated timber (glulam). Glulam can be regarded as a composite section made of several timber boards. Glulam technology allowed the production of large beams, and with the development of finger joints, the size of timber beams was only limited by production facilities. Furthermore, the lamination and grading of different boards resulted in a certain degree of homogenisation of the timber.

Timber-concrete composite slabs, which are quite frequently used in the Swiss timber building industry, are the first composite constructions involving two different materials. In order to use both materials most advantageously, the timber is placed on the tension side, and the concrete on the compression side. The efficiency of this composite depends mainly on the shear connector. Timber-concrete composites are also used to strengthen timber floors. This technique also increases the stiffness, helps to avoid vibrations and contributes to sound isolation. The disadvantages of such interventions are the added weight, the humidity brought into the building, and the necessary construction height.

CFRP is a relatively new class of composite materials manufactured from artificial fibres and a polymer matrix, and which has demonstrated efficiency in the field of reinforcement and in the rehabilitation of structures. However, while timber has been successfully reinforced over the past few decades using various materials and reinforcing techniques, only a few of those methods have reached the commercial market. In order to gain the necessary contribution of the CFRP reinforcement to the service-limit state, a solution involving prestressing is required; otherwise the amount of carbon fibre would be very high and therefore the method would not be cost efficient. Prestressed carbon fibres are commercially used to strengthen concrete and steel structures, and especially old cast-iron structures. Until now, the methods had not been applied to timber successfully, mainly because of the delaminating of the carbon fibre strip due to concentrated shear stress at the beam end. The idea to overcome this obstacle by using adhesives with a higher bonding strength resulted mostly in timber failure due to tension perpendicular to the grain. This failure was usually 2 to 3 cm above the carbon strip.

In cultural heritage buildings, the reversibility of the reinforcement as well as the preservation of the old structure as load-bearing elements are both important. The reversibility of a reinforcement is often in conflict with the impact on the appearance, this especially for bonded CFRP lamellas: For externally bonded lamellas the reversibility is given but they are clearly visible. The opposite is true for adhesively bonded lamellas slotted into the timber.

In the proposed method, the timber beam is cambered with an adjustable prop at midspan during the bonding of the CRFP-lamella on the bottom side of the bending member (Figure 1). Measures have to be taken to avoid the force of the prop being transmitted through the CFRP-lamella. Otherwise, the adhesive thickness would locally be reduced to nearly zero. Because of its simplicity, this method can be readily used in-situ. In cases where the weight of the structure on top of the beam is insufficient, measures need to be taken to hold down the beam ends. The moment introduced in the beam has a triangular shape. Therefore, the shear stress in the glue line is constant and quite low, and the stress introduced in the FRP lamella varies over its length. The prestress level is related to the force present in the prop during the bonding process. It is crucial for the bending capacity of the composite section that the force applied during the cambering of the beam is within the elastic limit of the timber beam; otherwise the crushing that occurs during cambering would be on the tension side during service life.

Figure 1: *The black line shows the system prior to intervention. In red is the cambered system after installation of the prop. The red arrow indicates the adjustable prop.*

1.1 Objective

The purpose of this study was to investigate the load-bearing behaviour of CFRP reinforced timber bending members when prestressed using the camber method. In order to conduct the study, the following objectives were defined:

- Experimental investigation of the governing parameters, such as adhesive type, prestress level and load-bearing behaviour
- Development of an analytical calculation method to allow a safe design for engineers
- Numerical investigation of the stresses present in the anchorage zone of the CFRP-lamella
- Experimental verification of the calculation model and the numerical investigations.

1.2 Outline

The research presented in this thesis consists of three main subjects: the first is the development of the analytical calculation model, the second concerns the experimental work, and the third deals with numerical simulation using the finite element method.

The outline of the chapters is as follows:

Chapter 2 presents the state of research. A brief overview of the materials involved in the research is included. Finally, conclusions are drawn from the state of the research.

Chapter 3 deals with the development of the analytical calculations model. The presented model allows for the design of a structure that is prestressed using the camber method. Furthermore, different verification methods are considered and the compliance of these methods with the Swiss building codes is discussed.

Chapter 4 explains and discusses the experimental work. The chapter is divided into two parts: first the investigation done using small clear timber is presented; the second section deals with the experiments done using structural-sized glulam beams.

Chapter 5 describes the numerical investigations. First the used material properties and models are presented. The modelling of the experiments is followed by verification. The optimisation using finite-element modelling (FEM) leads into the discussion and conclusions drawn from the numerical investigations.

Chapter 6 presents the overall discussions and conclusions. Finally, topics for future research are suggested.

1.3 Scope

The scope of the presented research is limited to the tasks presented above. As externally-bonded CFRP-lamellas are more prone to delaminating than slotted-in lamellas, also called near-surface mounted lamellas, the investigations were limited to externally-bonded CFRP-lamellas.

The method presented in this doctoral thesis for prestressing bending beams is mainly thought for the reinforcement of historical constructions. The method can only be applied if the bending member, which needs to be reinforced, has a sound timber quality. The assessment of the timber prior to reinforcement is out of the scope of the presented research.

Experiments considering climatic variations as well as the long-term behaviour of prestressed timber beams are also out of the scope of the presented dissertation. However, some primary investigations were carried out at the Swiss Federal Laboratories for Materials Science (EMPA) in collaboration with the author (Richter, Lehmann and Properzi [93]).

2 State of the Research

Timber is one of the oldest building materials used by human beings, and is currently gaining popularity due the fact that it is a CO_2-neutral. Timber and other building materials have been researched since ages. Therefore only a brief overview of the related work is presented below. For further reading it is recommended to consider the cited literature.

2.1 The structure of timber

Because timber is a naturally-grown material, there is wide variability in is structure and properties, both between and within species. Wood is an inhomogeneous and anisotropic material.

The cross-section of a tree consists of different zones (Figure 2, left). Bark, the outermost layer, protects the tree to a certain degree from damage (mechanical, UV, and fire). The secondary *phloem*, often called inner bark, is where the sap is transported downwards. The *cambium* is the part where new cells grow. The cambium builds cells for the timber and also for the bark. As the bark does not grow over the years, it is replaced continuously, leading to the often characteristic flakes and cracks in the outer bark. The wood under the bark is usually divided into two zones: the *sapwood* and the *heartwood*. In the sapwood, the sap is transported upwards. When the tree reaches a certain age, the sap-flow is concentrated in the outer growth rings. These rings in the centre are then transformed into heartwood. Not all species form heartwood, however; and the width of the sapwood varies from species to species. At the centre of the stem, the pith is found.

Timber is a naturally-grown polymer. According to Fengel and Wegener [31] the three major substances constituting timber are *cellulose*, *polyoses* (hemicelluloses) and *lignin* with the cell walls containing between 97 and 99% of those three macromolecular substances. Cellulose, the major component of wood, can be described as a linear polymer chain with a high degree of polymerisation. This polymer chain contains only β-D-glucose. Cellulose is the main structural component of wood. The molecular chains of the polyoses are much shorter than the one of celluloses and they contain different natural sugars. The polymers of hemicelluloses have side-groups and may be branched. Lignin is structured quite differently from the two polysaccharides mentioned above. Lignin is an irregular branched-polyphenolic polymer. Its complex structure varies according to the species.

Compared to hardwood, the cell structure of softwoods is quite simple. As the research presented in this thesis was done using softwood, the structure of hardwood is not explained further. The softwood structure contains mainly *tracheids*, which are responsible for the mechanical support of the tree and the transport of liquids within the tree. The majority of the tracheids are orientated longitudinally (parallel to the growth direction) with only the tracheids of the medulla rays orientated radially (perpendicular to the growth direction). In regions with a vegetation period of less than 12 months, the trees have the characteristic growth rings (Figure 2, left). The early wood contains tracheids with thin walls and large lumens. The late wood, which grows towards the end of the vegetation period, has thick-walled tracheids with a smaller diameter (Figure 2, right). The properties of these two types of wood differ in that

the late wood is denser, stiffer and darker, and has a higher resistance than the early wood. This is valid for softwood only.

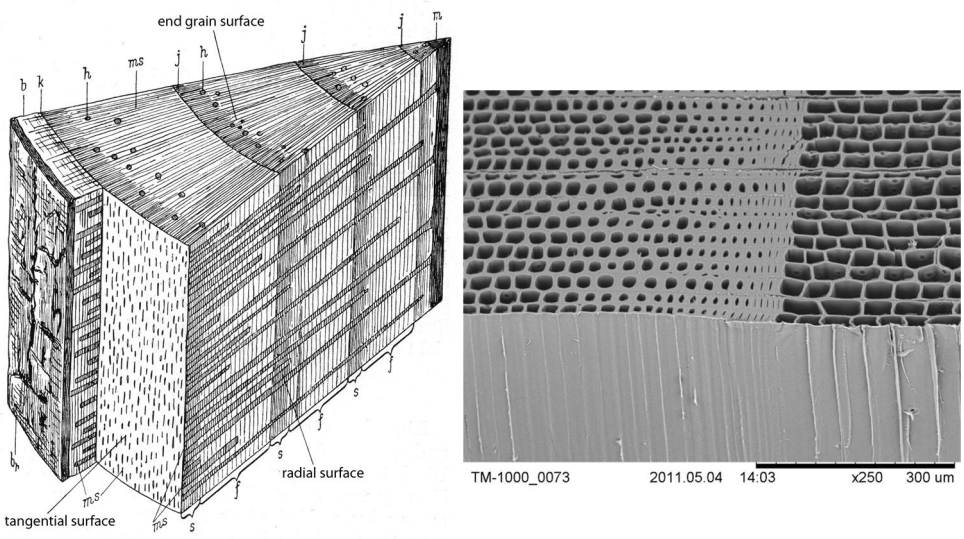

Figure 2: ***Left****: section of a four-year-old fir tree (br, bark; b, inner bark; k, cambium; h, resin streak; ms, medulla ray; j, growth ring border; m, pith; s, late wood; f, early wood) [48];* ***Right:*** *Picea Abies: the border between late and early wood is clearly visible (© wood anatomy laboratory Biel)*

The cell wall is composed mainly of cellulose, and is divided into the primary, secondary and tertiary walls. The secondary wall itself is composed of three layers (S1 to S3) with different microfiber angles (Figure 3). The S3 layer can only be found in parenchyma tracheids. The S2 layer by far the thickest is responsible for the mechanical resistance of the timber. The different cells are connected by the middle lamella which is mainly composed of hemicelluloses and lignin.

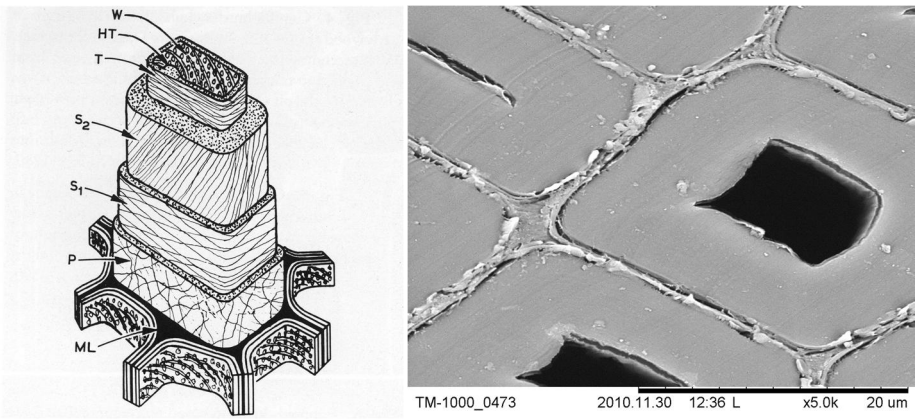

Figure 3: ***Left:*** *Structure of a tracheid (ML, middle lamella; P, primary wall; S1, first layer of the secondary wall; S2, second layer of the secondary wall; T, tertiary wall; HT, helical thickening; W, warty layer) [25]* ***Right:*** *Picea Abies: the primary, secondary and tertiary walls with the middle lamella are clearly visible (© wood anatomy laboratory Biel)*

2.2 Rheological behaviour of timber

In timber, strain under a constant load increases over time. This behaviour is generally called creep. Creep is generally divided into three different phases: 1) primary creep, which is the creep strain that occurs shortly after loading, and is characterised by a decreasing strain rate that becomes constant over time; 2) secondary creep is characterised by a constant strain rate, and the creep strain during this phase is usually less important than the primary creep; 3) tertiary creep is characterised by an exponential increasing strain rate, leading to failure of the specimen (Figure 4). For timber, the tertiary creep stage only occurs above a certain load level, otherwise the strain rate decreases towards zero during stage two. According to Navi and Heger [81], creep can be regarded as linear for loads up to 40% of the short-term load-bearing capacity.

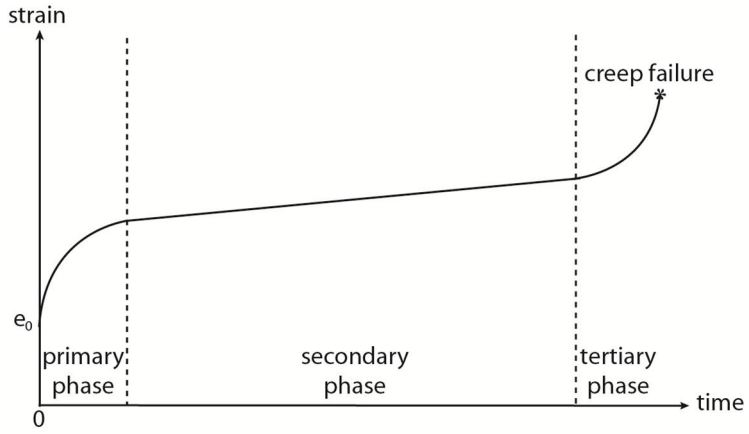

Figure 4: *Definition of the three creep phases*

One has to remember that several different mechanisms are responsible for the strain occurring in a timber specimen under constant load:

- elastic strain
- viscoelastic strain
- viscoplastic strain (non-linear creep)
- mechano-sorptive strain
- moisture-induced strain (swelling / shrinking)
- thermal strain

Usually the different strains are regarded independently, and the total strain is determined by adding all the strains (1). The total strain under constant load is therefore a function of time, humidity and temperature.

$$\varepsilon(t,u,T) = \varepsilon_0(u,T) + \varepsilon_{ve}(t,T) + \varepsilon_{vp}(t,T) + \varepsilon_{ms}(u,T) + \varepsilon_u(u) + \varepsilon_T(T) \qquad (1)$$

Where:

$\varepsilon(t,u,T)$ = total strain under constant load as a function of time humidity and temperature

$\varepsilon_0(u,T)$ = elastic strain as a function of humidity and temperature

$\varepsilon_{ve}(t,T)$ = viscoelastic strain as a function of time and temperature

$\varepsilon_{vp}(t,T)$ = viscoplastic strain as a function of time and temperature

$\varepsilon_{ms}(u,T)$ = mechano-sorptive strain as a function of humidity and temperature

$\varepsilon_u(u)$ = moisture-induced strain as a function of humidity

$\varepsilon_T(T)$ = thermal strain as a function temperature

As the influence of the temperature on the strain is quite low for timber, it can be neglected for engineering proposes. Generally the non-linear part of the creep is neglected for permanent loads up to 40% of the maximal load-bearing capacity [40, 81, 91]. Therefore, simplified creep strain can be defined as the sum of viscoelastic strain and mechano-sorptive strain (2).

$$\varepsilon_c(t,u) = \varepsilon_{ve}(t) + \varepsilon_{ms}(u) \tag{2}$$

Where:

$\varepsilon_c(t,u)$ = creep strain as a function of time and humidity

$\varepsilon_{ve}(t)$ = viscoelastic strain as a function of time

$\varepsilon_{ms}(u)$ = mechano-sorptive strain as a function of humidity

Equation (3) describes viscoelastic behaviour under uniaxial stress while equation (4) describes it under uniaxial strain.

$$\varepsilon(t) = \int_{-\infty}^{t} J(t-\tau)\frac{d\sigma}{d\tau}d\tau \tag{3}$$

$$\sigma(t) = \int_{-\infty}^{t} E(t-\tau)\frac{d\varepsilon}{d\tau}d\tau \tag{4}$$

$$J(t) = \frac{\varepsilon(t)}{\sigma_0} \tag{5}$$

$$E(t) = \frac{\sigma(t)}{\varepsilon_0} \tag{6}$$

Where:

$\varepsilon(t)$ = strain as a function of time

$\sigma(t)$ = stress as a function of time

J(t) = retardation function (5)

E(t) = relaxation function (6)

t = time

σ = stress

σ_0 = constant stress

ε = strain

ε_0 = constant strain

In literature, several ways of numerical modelling for creep in timber are presented. A mathematically quite simple approach is to use a power function for the creep strain in function of time, as only a few parameters are needed (7). According to Rautenstrauch [91], even for constant loads, the precision of equation (7) is limited.

$$\varepsilon_c(t) = a \cdot t^m \quad (7)$$

Where:

$\varepsilon_c(t)$ = creep strain as a function of time
a = parameter to derivate from experimental data
t = time
m = parameter to derivate from experimental data

Rheological models are used most often, usually as a combination of dashpots and springs. The dashpot represents the viscous part and follows the viscosity law of Newton (8). The spring represents the elastic part and follows Hook's law (9). Therefore, a single dashpot leads under constant load to infinite strain and under constant strain to complete relaxation, whereas a spring shows no time dependency (Figure 5).

$$\sigma = \eta \cdot \dot{\varepsilon} \quad (8)$$

$$\sigma = E \cdot \varepsilon \quad (9)$$

Where:

σ = stress
η = dashpot constant
$\dot{\varepsilon}$ = strain rate
E = spring rate
ε = strain

Figure 5: *Schematic drawing of a dashpot (left) and spring (right).*

In order to model viscoelastic behaviour, a combination of the basic elements is needed. If the two elements are combined parallel, it is called Kelvin element (Figure 6 left). Under constant load, this combination creeps to a limit that is defined by the spring rate. Relaxation under constant strain cannot be modelled using a Kelvin element. The combination of a dashpot and a spring in a series is a Maxwell element (Figure 6, right). The behaviour of this element leads, under constant load, to infinite creep; and under constant strain, to complete relaxation. Equation (10) describes the behaviour of a Kelvin element under constant stress. Equation (11) describes the behaviour of a Maxwell element under constant strain.

$$\varepsilon(t) = \frac{\sigma_0}{E} \cdot \left(1 - e^{\frac{-t}{\Theta}}\right) \quad (10)$$

$$\sigma(t) = \varepsilon_0 \cdot e^{\frac{-t}{\tau}} \quad (11)$$

Where:

$\sigma(t)$ = stress as a function of time
t = time

σ_0 = constant stress

Θ = retardation time

ε_0 = constant strain

τ = relaxation time

E = spring rate

$\varepsilon(t)$ = strain as a function of time

Figure 6: ***left:*** *Schematic drawing of a Kelvin element* ***right:*** *Maxwell element*

Due to the fact that material is never true viscoelastic one single element is not suitable to model retardation (creep) or relaxation of materials therefore the so called standard solid model combines the Maxwell or Kelvin element with a Hook spring (Figure 7).

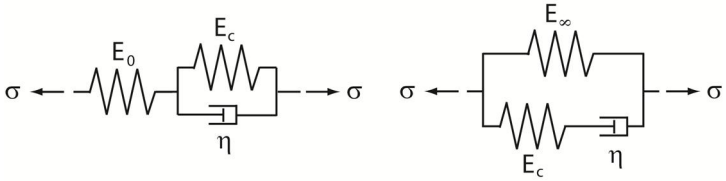

Figure 7: ***left:*** *Schematic drawing of the standard solid models based on a Kelvin element* ***right:*** *based on a Maxwell element*

For timber usually generalised standard solid models are used. This means that one spring is used in combination with several Maxwell (parallel) respectively Kelvin (series) elements. According to Hartnack [40], a spring followed by five Kelvin elements is suitable for modelling the creep behaviour of a timber specimen under compression.

The numerical modelling of long-term behaviour is out of the scope of the presented work. Therefore, the long-term behaviour was estimated using a simplified analytical approach based on the reduction of the MOE of the timber for calculations taking the creep into account.

2.3 Adhesives

Humans have used adhesives since the early Stone Age. Birch-tar was used in producing tools and spears. Traces of birch-tar on flint stones have been found in Italy that are approximately 200'000 years old [74].

Adhesives are used in many industries. Due to the large marked for industrial bonding, the main research in adhesions technology does not focus on the building or timber industries. Structural on-site bonding involving timber is not commonly done, and therefore the adhesive industry does not develop special adhesives for this application. Nevertheless, the huge product ranges of the adhesive producers mean that more or less suitable adhesives can be found on the market.

According to Habenicht [38], the adhesives can be divided into groups according to the setting mechanism. Chemical-setting adhesives contain monomers or prepolymers, and the

final polymerisation occurs during the curing of the adhesive. The chemical-setting adhesives usually contain two components that are either mixed prior to application or sometimes one component is provided by the adherent (e.g. water for the one component polyurethane adhesive as often used in the timber industry). Physical-setting adhesives, which consist of one main component, are already polymerised during production. The wettability is reached by means of solvents or temperature and/or pressure. No chemical reaction occurs during the curing of the adhesive. The reactive hot-melt adhesives are a combination of those two setting mechanisms and are based mainly on polyurethane or epoxy formulations.

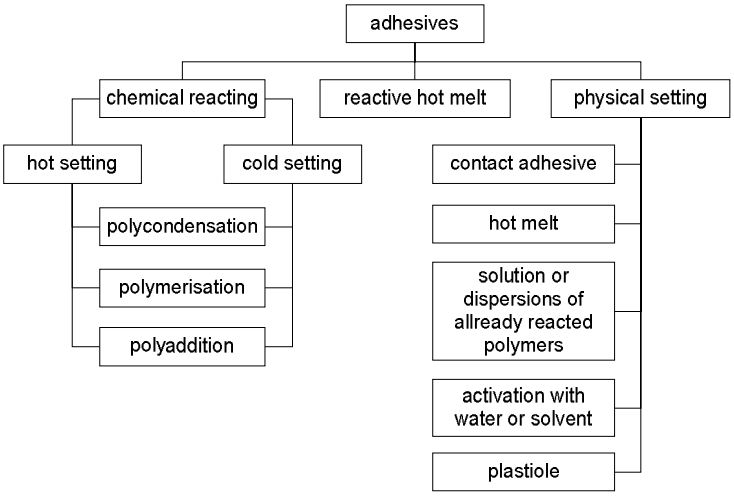

Figure 8: *Adhesives grouped by the setting mechanism according to Habenicht [38]*

In the aircraft and space industry, adhesives have been widely used for over 60 years. According to Habenicht [38], the main reasons for the success of adhesives are:

- no or only low head-introduction (important for non-heat resistant high-strength metal alloys)
- higher dynamic resistance due to avoiding of stress concentrations (e.g. rivet connections show high-peak stresses around the holes)
- higher buckling strength (Figure 9)
- long durability

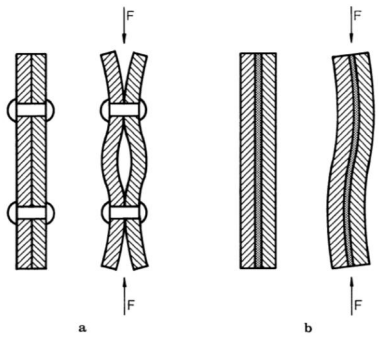

Figure 9: *Buckling behaviour of a rivet and adhesive connection [38]*

The above points also explain why adhesives are crucial for modern vehicle engineering. Additionally the ductile behaviour of adhesive connections is crucial in the crash behaviour of

vehicles. These industries use mainly chemical-setting adhesives and reactive hot melts. For further information see Habenicht [38].

2.3.1 Adhesives used in combination with timber

In the wood-panel industry, hot-setting adhesives such as melamine (MF), urea- (UF), melamine-urea- (MUF) and phenol-formaldehyde (PF) are mainly used. UF is a low-cost adhesive with poor water resistance, and in order to enhance the water resistance it can be copolymerised with melamine (MUF). PF has a high-water resistance but is more costly. Due to the formaldehyde emission that occurs with these adhesives, other types based on isocyanate gain popularity in the panel industry. Tannin-based adhesives with hexamine as a hardener allow the production of wood-based panels without formaldehyde emissions due to the adhesive [63, 87, 95]. Furthermore, tannin is a natural polyphenol extracted from bark and/or timber and is therefore environmentally friendly. This short overview is not compete but considers the large quantities of adhesives used the panel industry.

Timber is a good thermal isolator so there are certain obstacles in using hot-setting adhesives for large sections such as glulam and cross laminated timber. The glulam industry therefore uses mainly cold-setting adhesives such as melamine-urea formaldehyde (MUF), polyurethane (PUR) or phenol-resorcinol formaldehyde (PRF). Some producers use high-frequency presses, however, for hot-setting adhesives with short pressing times. PRF resins are not often used anymore because of the long curing time necessary with the cold-setting system. Glulam produced using PRF has an excellent performance in humid conditions, however. The successful use of PUR and PRF adhesives in bonding CFRP with timber has also been documented by various authors, for example, [15, 33, 72].

Epoxy-based adhesives (EP) are chemical setting and can be cured at ambient or elevated temperatures. In the timber industry, mainly cold-setting epoxy adhesives are used for load-bearing connections involving steel or FRP. According to Habenicht [38], cold-setting epoxy adhesives have a lower ultimate strength and a shorter pot life than hot-setting epoxies. The lower strength is due to the fact that the OH group of the epoxy component (Figure 10) fails to cross-link below 65°C. Thermal treatment of an already reacted cold-setting EP generally leads to a higher glass-transmission temperature and ultimate strength. Epoxy resins are often used for the external reinforcement of structures. Several authors have also confirmed the suitability of these adhesives for timber structures e.g.[15, 23, 61, 65-67, 69, 70, 72, 98].

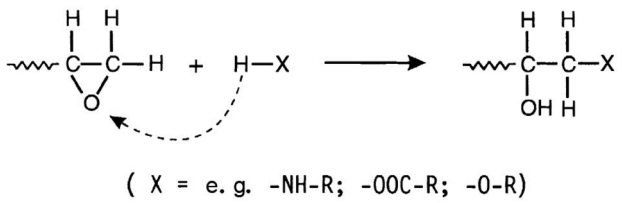

Figure 10: *Typical addition reaction of an epoxy according to Habenicht [38]*

Although physical-setting adhesives are also used in the timber industry, these are not usually utilised for load-bearing structures. Although the furniture industry uses mostly dispersion or hot-melt adhesives.

Due to the porous structure of timber, the mechanical adhesion is vital for the resistance of adhesively-bonded joints. Some adhesives do also form chemical adhesion, for example, isocyanate-based adhesives react with the OH groups of the celluloses and lignin. Obstacles to good adhesion to timber can be:

- extractives
- dust
- swelling/shrinking due to variation in humidity
- low-surface quality
- high density
- elevated moisture content (depending on the adhesive type)

Lehmann, Vallée, Tannert et al. [71] have shown that epoxy and polyurethane-based adhesives are an efficient alternative to the pinned connections generally used in timber structures. The load-bearing behaviour is quite different: no slip occurs which results in lower deformation. However, adhesively-bonded joints usually fail quite brittle and the timber structure loses its ductile elements. Vallée, Tannert, Lehmann, et al. [118] present a probabilistic strength model for adhesively-bonded lap joints composed of wood adherents. The calculations show a good correlation with the experiments conducted using adhesive thickness and bond length.

2.3.2 Bonding on-site

As most structural adhesives are chemically setting, the quality control and maintenance during the manufacturing of adhesively-bonded joints is very important. In industrial facilities such as glulam factories, the necessary measures are applied. However, reinforcements or the assembly of large structures need to be done on the construction-site where no controlled environment is normally available. The adhesives used for structural bonding on-site are usually polyurethane or epoxy based. Richter, Cruz and Negrão [92] outline the following obstacles for bonding on-site:

- A lack of well-structured and concise knowledge on bonded reinforcement or repair techniques for timber
- Bonding on-site process and conditions are difficult to control (e.g. bond-line thickness, surface properties, bond-line stresses and environmental conditions)
- Adhesives for bonding on-site are not specifically developed for timber
- Appropriate test methods and standards for bonding adhesives on-site are lacking
- Sufficiently rapid on-site assessment methods (control of mixture and penetration, viscosity) are missing.

Due to these obstacles and to the special circumstances of bonding on-site, the adhesive used in factories to produce engineered timber products are not suitable for on-site usage. In case of retrofitting or reparation, no adhesive suitable for all tasks exists. The viscosity, for example, needs to be chosen depending on the job: for crack filling, a low viscosity is preferable; however, for overhead installation a higher viscosity and thixotropy are needed.

According to Cruz and Custódio [28], the correct surface preparation of adherents is imperative. The main reasons for preparing the wood surface before bonding are:

- To produce a close fit between the adherents
- To produce a freshly-cut or planed surface, free from machine marks or other surface irregularities, extractives or other contaminants
- To produce a mechanically-sound surface without crushing or burnishing it, which would inhibit adhesive wetting and penetration.

One of the most crucial tasks is to ensure sufficient quality control of a bonding on-site job involving timber. Smedley, Cruz and Paula [103] present a systematic overview of the measures needed to ensure adequate quality control.

2.4 Fibre-reinforced polymers (FRP)

Fibre-reinforced polymers (FRP) are composites composed of fibres that are enclosed in a polymer matrix. For structural purposes mainly thermosetting matrixes are used.

2.4.1 Production

FRP is widely used in the industry, and its production is well-developed and documented (e.g. Michaeli and Wegener [79] and Bourban, Carlsson and Mercier [21]); therefore only the production methods and a brief description of the methods relevant for retrofitting are listed below:

- Lay-up (wet or dry)
- Spray-up
- Autoclave
- Compression moulding
- SMC (sheet-moulding compound)
- DMC (dough-moulding compound)
- GMT (glass-mat thermoplastics)
- Injection-compression moulding (ICM)
- Pultrusion
- Filament winding
- Centrifugal casting
- Bladder-inflation moulding
- Resin-transfer moulding (with or without vacuum assistance)
- Vacuum bag moulding

However, at present, only two methods are mainly used in the construction industry: the hand lay-up and the use of prefabricated pultruded rods or lamellas. Systems using sprayed-up FRP are currently being developed in Japan [34, 35]. Other systems that could be interesting for the construction industry are vacuum-bag moulding and filament winding. The winding process could be used for the post-strengthening of columns against seismic loading. The vacuum-bag method could be used in combination with the systems mentioned above in order to avoid air enclosures within the FRP or at the interface between FRP and substrate [90].

Before applying the FRP post-strengthening the structure needs to be prepared (grinded) and cleaned. It is important that the surface is free of loose components and dust (vacuum

cleaned). The surface needs to be reasonable even otherwise it is necessary to level it with special mortars. In case the FRP needs to be wrapped around an edge, the minimum diameter (~20mm) needs to be respected. The substrate needs to meet the minimum requirements in strength in order to prevent failure of the substrate above the glue line, due to shear stress.

2.4.1.1 Hand lay-up

The hand lay-up systems involve production of the FRP on-site. There are two different methods of hand lay-up, the wet and the dry process. In the case of a wet lay-up, the fabrics are impregnated on-site with resin prior to the application. For the dry process, the fabric is imbedded and impregnated with resin during the application (Figure 11). The first step is the preparing of the substrate along the specifications of the FRP-system producer. After the vacuum cleaning of the surface, a primer is applied. Within a certain time frame, the first layer of resin is applied on top of the primer (Figure 11, left). It is important to avoid any folds or air enclosures when the fabric is laminated to the substrate using a roller (Figure 11, right).

Figure 11: *Hand lay-up dry system applied on a concrete girder [3]*

The hand lay-up method is used for shear post-strengthening in concrete constructions. This method is also used for retrofitting concrete columns for seismic loads. It is important that there are no air enclosures present in the FRP or on the interface between the FRP and the substrate. Otherwise, the ultimate strength of the post-strengthened member will be significantly reduced. This method is also used in timber constructions in order to post-strengthen timber columns [104].

2.4.1.2 Pultrusion

The pultrusion production is not done on-site the rods or lamellas are prefabricated in a factory. The FRP for post-strengthening has an epoxy-based matrix. The matrix itself usually has a low MOE compared to the fibres, which increases the strain of the product at ultimate load. The production process is similar to the extrusion except that the fibres are pulled through the die and not pushed. (Figure 12) The resin is cured in the die, either by means of dielectric heating of the resin or by heating the die itself.

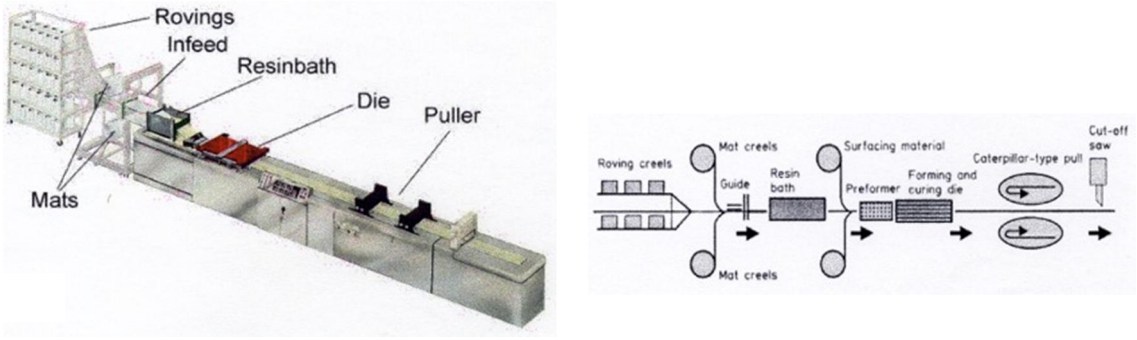

Figure 12: *Pultrusion production process [73]*

The pultruded rods or lamellas are mainly used for post-strengthening beams in bending. The lamellas are glued onto the structure with epoxy resin. It is possible to pre-tension the lamellas before they are glued to the structure. FRP rods are also used for the external post-tensioning of structures.

2.4.1.3 Spray-up FRP

The spray-up technique is used in industry to produce large and/or complex shapes. Automation of this production process is possible, depending on the shape of the product. The resin and fibres are mixed during the spraying process (Figure 13, left). The fibres are supplied as a string to the spray gun and then automatically chopped before being sprayed (Figure 13, right). After the spray process, the fibres need to be pressed to the substrate using a roller or another suitable device. It is important to avoid any air enclosures in the FRP or at the interface between the substrate and FRP.

Figure 13: *Spray-up FRP [73]*

2.4.1.4 Vacuum-bag moulding

Vacuum-bag moulding can be used in combination with other production methods such as spray-up or hand lay-up. The vacuum-bag moulding is used in the industry to apply pressure to the FRP and also to ensure that there are no air enclosures in the FRP. The system can be adopted for on-site production. The vacuum bag needs to be placed around the member, the ends sealed and a vacuum pulled in the bag. The sealing of the vacuum bag needs to be reasonably tight in order to pull the necessary vacuum (Figure 14).

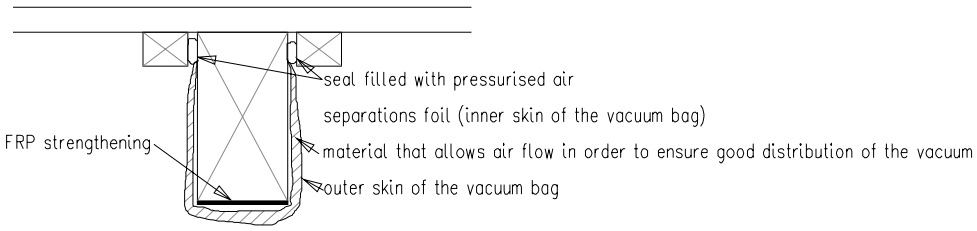

Figure 14: *Proposed method of a vacuum-bag moulding for on-site application [90]*

2.4.1.5 Filament winding

This technique is used in industry to produce large items such as silos, pipes or tanks. The fibres are impregnated with a pre-catalysed resin and wrapped around a mould. In industrial production, the mould is turned (Figure 15). In an on-site production, the applicator needs to rotate around the column. Instead of single fibres, a pre-woven fabric can also be used.

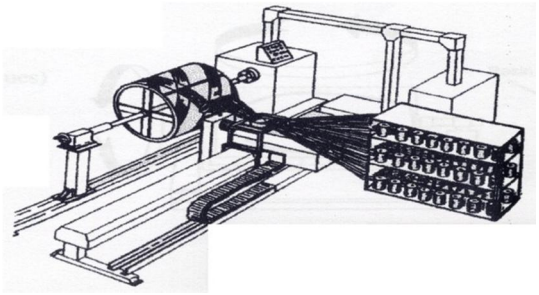

Figure 15: *Filament winding [73]*

2.4.2 Matrix

Generally, two different types of matrixes are distinguished: thermoplastic and thermosetting. Thermoplastic matrixes are prone to creep, especially at elevated temperatures. For structural purposes, mainly thermosetting matrixes based on epoxies or unsaturated polyester resins are used (Table 1). In the aircraft industry phenol-formaldehyde is preferred because of its head resistance.

Table 1: *Properties of thermosetting matrixes for FRP according to [122]*

	Epoxy	**Phenol**	**Polyester**
tension strength [MPa]	40-140	42-63	35-92
MOE [MPa]	3000-4500	2800-3500	1500-2000
ultimate strain [%]	2-10	1.5-2	2-4
density g/cm^3	1.15-1.35	1.3-1.32	1.1-1.5

Ulga and Meier [117] investigated the production of CRFP-lamellas for structural purposes using thermoplastic matrixes. The results show that the strength and stiffness of the developed lamella is lower than a standard lamella produced using the same fibres. They also report some obstacles overcoming the creep tendency and the low-heat resistance.

2.4.3 Fibres

In the building industry, three types of fibres are used: carbon, glass and aramid; furthermore polyethylene, polyamide and boron are also mentioned in the literature [76, 79] as possible fibres for FRP. The first three fibres and therefore also the composites have different properties and advantages: glass fibres are the least expensive ones; aramid has a high toughness and is therefore excellent for impact loading; whereas carbon has high modulus of elasticity (MOE) and strength. Table 2 shows the strength of the fibres shortly after production. Any damage caused during further processing can reduce the strength to 2/3 or even 1/3 of its original value.

Table 2: *Mechanical properties of different fibres according to [79]*

	Glass		**Carbon**				**Aramid**	
	E	S	HT	HST	IM	HM	Standard	HM
strength [GPa]	3.4–3.5	4.4–4.6	2.7–3.0	3.9–7.0	3.4–5.9	2.0–3.2	2.8–3.0	2.8–3.4
MOE [GPa]	72–73	86–87	228–238	230–270	280–400	350–490	58–80	120–186
ultimate strain [%]	3.3–4.8	4.2–5.4	1.2–1.4	1.7–2.4	1.1–1.9	0.4–0.8	3.3–4.4	1.9–2.4
density [g/cm^3]	2.6	2.45	1.75–1.8	1.78–1.83	1.72–1.8	1.79–1.91	1.39–1.44	1.25–1.47

Glass fibres show an isotropic behaviour, whereas carbon and aramid fibres show a highly orthotropic behaviour. According to Meier [76], the ratio between the modulus of elasticity parallel to perpendicular is for carbon fibres between 1000 and 3000, and for aramid fibres between 500 and 600.

Figure 16 clearly shows that only carbon fibres have a higher MOE than steel [79].

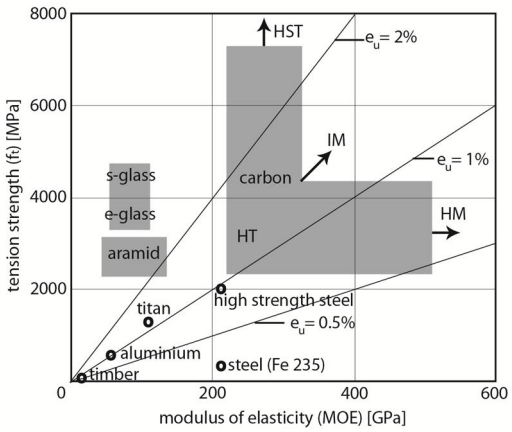

Figure 16: *Strength of fibres as function of the modulus of elasticity according to [79]*

Depending on the desired properties, carbon fibres can contain from 92 to 100% carbon. Pure carbon can have two different states: graphite and diamond. According to Michaeli and Wegener [79], theoretically, graphite possesses the highest strength and stiffness of all known materials. Graphite has a layered structure and between the layers only low-bonding forces exist which leads to a quite low-shear strength of carbon fibres.

2.4.4 Composite

The mechanical properties of FRP strongly depend on the fibre content in each direction and on the fibre itself (Figure 17). Unidirectional fibre-reinforced polymers (FRP) are highly orthotropic.

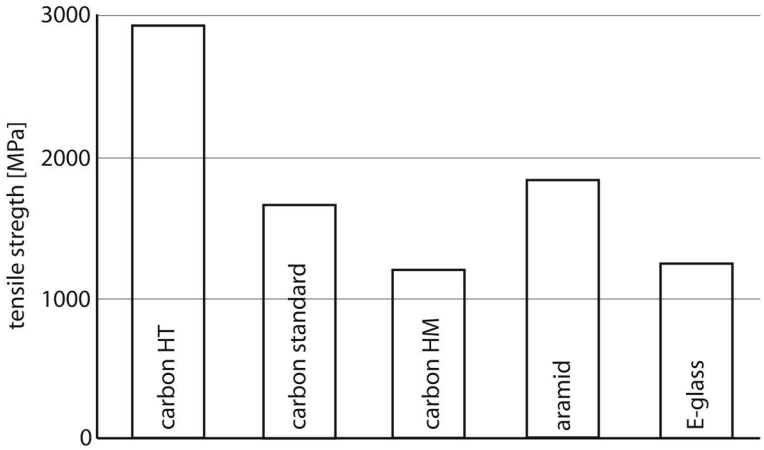

Figure 17: *Tension strength of different unidirectional reinforced FRP, according to [79]*

The ultimate strength of unidirectional reinforced CFRP is much higher than the strength of prestressing steel. However, the design stresses is not higher than for prestressing steel (Table 3). Nevertheless the advantages of CFRP are its low density, its resistance to corrosion and to most chemicals, as well as the fact that fatigue does not occur.

Table 3: *Selected mechanical properties in tension of different construction materials according to [5, 49-51]*

Material	$f_{d,t}$* [MPa]	$f_{u,t}$** [MPa]	**MOE** [GPa]	**Density** [g/cm^3]
CFRP	714–1600	1500–3200	150–300	1.6
reinforcing steel	450–1600	650–1860	210	7.85
steel (FE 235)	235	360	210	7.85
timber (GL24h)	12	18	11	0.38
timber (GL36h)	18	27	14	0.45

*Yield stress for steel.

**5% percentile for CFRP and timber.

2.5 Reinforced structures

Tension reinforcing of structures is nothing new to the construction industry. As concrete has very low-tension strength, nearly all concrete structures are reinforced on the tension side.

Externally-bonded reinforcement is often used for retrofitting concrete constructions. An early and well-documented example for extensive retrofitting using glue on steel plates is the telecommunications building in Zürich at the Füsslistrasse [1, 2, 47, 54, 58, 60]. The retrofitting was done in stages between the years 1971 and 1975. New telecommunication installations made it necessary to reinforce the concrete slabs in bending and the concrete girders in bending and shear. Steel plates and lamellas were bonded to the concrete using epoxy res-

in. In order to ensure the feasibility of the reinforcement, the EMPA carried out bending tests in the laboratory using reconstructed, preloaded and reinforced slab and girder [58]. The installation of the retrofitting was complex and labour-intense; mainly due to the weight of the steel plates and lamellas used in this case.

Different materials have been used and/or researched to reinforce timber, and various authors have reported the use of steel or aluminium as reinforcement [18, 30, 55, 56, 59, 102, 105, 106, 108]. Krueger and Eddy, and Krueger and Sandberg replaced the lower lamella of glulam beams with steel wires embedded in an epoxy matrix [55, 56].

According to Steurer [106], the reinforcing material for timber should still be in its elastic state at the load where the timber fails. Therefore, standard steel (FE 235) is unsuitable for the externally-bonded reinforcement of timber-bending beams. As the ratio of the MOE of timber to the MOE of steel is large, the yield stress of the steel is already reached at 11.7 MPa tension stress in timber. Steurer [106] reports that the yield stress of the used steel should be between 525 and 840 MPa. Therefore, he concludes that for externally-bonded reinforcement in fibre direction, high-strength steel or other materials with high strength and stiffness should be used.

2.5.1 Use of CFRP in concrete constructions

Retrofitting of reinforced concrete with carbon fibre-reinforced polymer (CFRP) lamellas or sheets can be regarded as the state-of-the-art. The advantages of this method when compared with steel are the lower weight and higher strength that make the installation much easier and compensate for the higher material costs. The Westgate Bridge in Melbourne is an excellent example of retrofitting with CFRP using different techniques [86]. Lamellas were used either singly or multilayered, and in combination with sheets. The sheets, which were impregnated on-site, were used to avoid debonding problems at the end of the lamellas. The lamellas were glued into slots or just glued onto the concrete.

Debonding is quite a large obstacle with glued-on CFRP-lamellas. Therefore, glued-on lamellas without any additional anchorage at the ends can only be capitalised between 8 and 25% [96, 119]. The main parameter for the maximum anchorage force for glued-on lamellas without additional anchorage is the surface tensile strength of the concrete [11]. Debonding of the CFRP-lamellas does not always originate in the anchorage zone that Ulaga presents in the [116] experiments in which he located the start of the debonding. Depending on the geometry and the loading situation, debonding starts in the anchorage zone or in the zone with the highest bond stress. In order to avoid debonding in the Swiss standard SIA 166:2004 externally-bonded reinforcement [11], the strain of the CFRP-lamella is limited to 0.8%, and the bond stress is limited to 2.5 times the concrete shear-design stress.

Furthermore, a calculation model for the design anchorage force is given. In cases of additional anchorage, it is requested, that the model used should be based on theoretical or experimental research. For near-surface mounted (slot-in) lamellas, the debonding is not such an obstacle [119]. Due to the slot, no movement perpendicular to the adhesive layer is possible, and a three-dimensional state of stress takes place (similar to that of the standard reinforcing bars in concrete). This factor allows capitalising the whole tensile force of a near-

surface mounted CFRP-lamella [86]. The cross section of slot-in lamellas is usually quite small it is limited mainly by the concrete cover of the reinforcing bars.

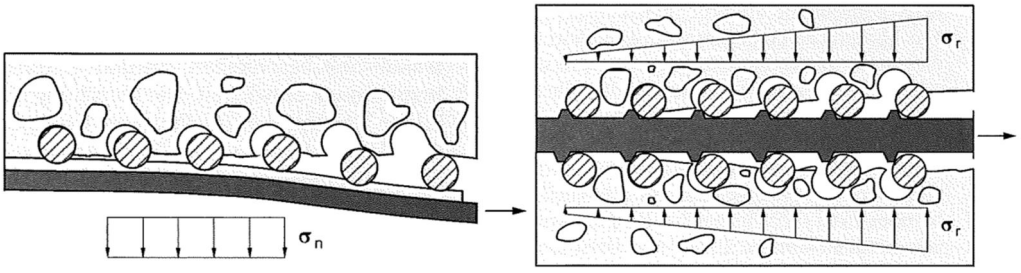

Figure 18: *Comparison of an externally-bonded reinforcement and an ordinary reinforcing bar in concrete [83]*

The application of prestressed externally-bonded CFRP-lamellas as retrofitting of concrete structures is a relatively new technique that is not yet widely used. To avoid delaminating prestress systems, additional end-anchorage systems are used, which in most cases involves mechanical fasteners and steel components that are prone to corrosion. However, researchers at EMPA have developed a device that allows anchorage of prestressed CFRP-lamellas without any means other than epoxy resin [78]. The anchorage of the prestressed lamella is done in gradients over a distance of about 80 cm. For the mounting of the lamella, the device is bolted to the concrete slab, and the process works as follows: by turning the wheels (no. 2 in Figure 19) the prepared CFRP-lamella is prestressed to the level required. Then, the lamella is pressed to the concrete, and the first section of the adhesive (no 7 in Figure 19) is cured by heat. Afterwards, the wheels are turned backwards and the next section of the adhesive (no. 8 in Figure 19) is cured by heat. This process is repeated until the whole prestress force is anchored. The curing of the adhesive between the anchorage zones (no. 6 in Figure 19) can be done as for CFRP-lamellas that are not prestressed.

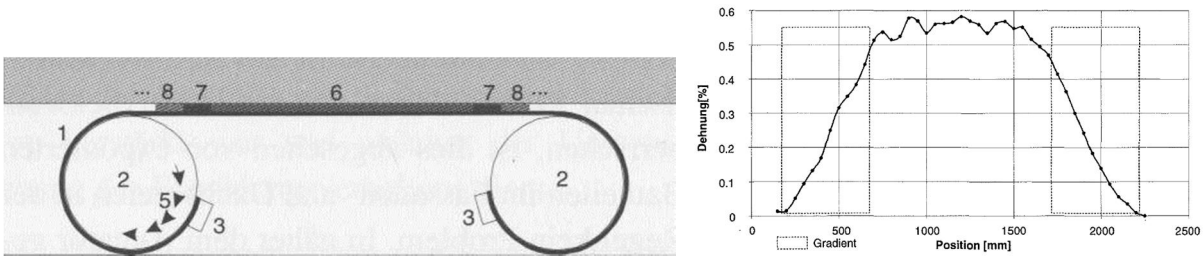

Figure 19: ***Right:*** *Sketch of the device used to attach prestressed CFRP-lamellas in gradients [78]* ***Left:*** *Stain distribution in the CFRP-lamella over the length of the beam [107]*

This method was used to reinforce a concrete slab with tree prestressed CFRP-lamellas after removing a supporting wall [107]. Visually, the prestressed lamellas using the described anchorage method cannot be distinguished from the lamellas that are not prestressed. Unfortunately, the company owning the equipment is more interested in developing CFRP for use on race-sailboats and other lucrative markets rather than promoting the gradient anchorage technology. An example where prestressed carbon lamellas (with additionally steel end anchorage) were used to retrofit a prestressed concrete bridge is presented by Hammer, Müller and Bücheler [39]. The costs for the additional anchorage for prestressed systems are often

higher than the benefit. Therefore, prestressed lamellas are mainly used to help reach the service-limit state and/or if crack-width reduction is needed.

2.5.2 Use of CFRP in timber construction

The use of CFRP-lamellas to reinforce timber structures is not as common as in concrete structures. Several research projects and applications have shown that externally-bonded or slot-in CFRP-lamellas are suitable for reinforcing timber structures. The first documented application of CFRP-lamellas to reinforce large timber structures was the retrofitting of a timber bridge near Sins in Switzerland. The externally-bonded reinforcement was installed in the year 1992 by the EMPA [101]. Two beams were reinforced with one lamella bonded to the top and the other, to the lower side. In order to observe the influence of the MOE of the CFRP-lamella, one beam was reinforced using high modulus CFRP with an MOE of 305 GPa, and the other one using standard CFRP with an MOE of 152 GPa. The long-term behaviour was controlled over several years and no significant obstacles could be detected.

Buell and Saadatmanesh [24] investigated timber beams reinforced by wrapping using carbon fabrics. The solid sawn-timber beams were removed from a rural farm road bridge and had a cross section of 203mm x 483mm. Six beams were tested in bending, one was unreinforced as control, and the others were reinforced using different wrap layups. One beam was reinforced using two CRP-lamellas. This beam failed due to horizontal shear at a lower load than the control specimen. The strength increase of the wrapped beams, based on one single control, was between 40 and 53%. The stiffness increased from 17 to 27% compared to the stiffness determined before reinforcing. Furthermore, four beams were tested in 4-point bending using a short span to determine the shear strength. Two were reinforced using different wrap layups. One of the control specimens failed at a load significantly higher than one of the reinforced beams. Buell and Saadatmanesh [24] reported that this result was due to fewer defects in the critical zones. They still conclude that the wrapping leads to a significant increase in shear strength. Moreover, they conclude that beams wrapped with one-piece full longitudinal wrap perform better than beams wrapped with multiple sheets with an overlap. This conclusion is valid for the bending and shear capacity.

Blass et al. investigated the influence of FRP-reinforcement on the bending stiffness and load-bearing capability of glulam, testing different reinforcement layouts, qualities of timber and adhesives. [14, 16, 17] The CFRP-lamellas were at the bottom in some specimens, in others, the CFRP was covered with one timber lamella, and in another set, three small CFRP-lamellas were vertically slotted into the bottom part of the timber beam (Figure 20). Blass et al. concluded that a facing timber lamella has a negative influence on the load-bearing behaviour compared to the other layout, and that CFRP is suitable for reinforcing timber bending beams. The beams with slotted in CRFP-lamellas showed linear elastic behaviour nearly up to the loadbearing capacity. No delaminating occurred with near-surface mounted lamellas. According to Blass, Krams and Romani [14], one specimen had a shear failure above the CRFP-lamellas, combined with a bending failure in midspan. Due to the abrupt failure, it was not possible to detect if shear or bending was the governing failure mode.

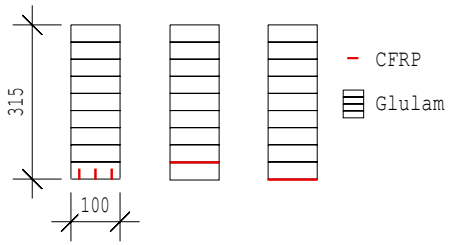

Figure 20: *Cross sections of reinforced beams as tested by Blass et al. [14] (in the left beam the lamellas are slotted in; the beam in the centre has a facing lamella)*

Schober and Rautenstrauch investigated the reinforcement of historic timber beams with CFRP-lamellas [100], using three different layouts for the reinforcement. The total amount of CFRP was equal in all sections (Figure 21) but the historic timber cross section was not constant.

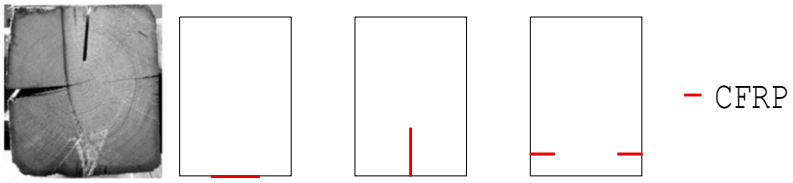

Figure 21: ***Left:*** *cross section of historic beam as used in the research by Schober and Rautenstrauch [100];* ***Right:*** *sketches of the three layouts used to reinforce the historic timber*

Schober and Rautenstrauch [100] compared the bending stiffness prior to and after the reinforcement, and determined the ultimate bending-capacity of the reinforced beams. The investigation proved that the use of epoxy adhesive to bond CFRP-lamellas to timber is a suitable method for reinforcing historic timber beams. They concluded that the CFRP reinforcement bridges local defects and arrests cracks in the timber, especially if the lamella is slotted into the timber. However, some specimens failed due to old cracks in the historic timber; therefore the use of an appropriate method for shear-reinforcing areas with large horizontal cracks is recommended.

Schober [99] presents a new method of reinforcing timber-bending beams. This method involves epoxy-based polymer concrete to reinforce the compression side, and CFRP-lamellas to strengthen the tension side of a timber-bending beam (Figure 22). The polymer concrete used has a compression strength that can be compared with high performance concrete C100/115, and a bending-tension strength about three times higher than C100/115.

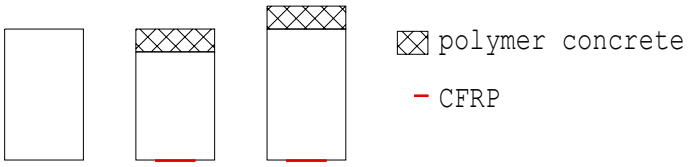

Figure 22: *Sketch of the cross sections tested by Schober [99].* ***Left****: unreinforced timber section;* ***centre:*** *reinforced cross section using the substitutive method;* ***right****: reinforced cross section using the additive method.*

Schober achieved an improvement in the bending bearing-capacity of 56% using the substitutive method, and up to 186% using the additive method. The short-term bending stiffness

was significantly increased, especially with the additive method. Unfortunately, the polymer concrete used is prone to creep, and the gain in stiffness is almost lost over time. In the case of the substitutive method, the reinforced section has an even lower long-term bending stiffness than the original cross section. The relative creep deformation is about 1.8 to 2.5 times greater for the reinforced beams than for the original timber beams.

Triantafillou [112] investigated shear reinforcement of timber beam using FRP on rather small and clear timber specimens. Triantafillou used 0.167mm thick CFRP fabrics in different layups (one- or two-ply parallel, one perpendicular or one parallel combined with one perpendicular to the wood fibres). In order to ensure shear failure of the specimen, the shear span of the bending specimens was reduced (Figure 23).

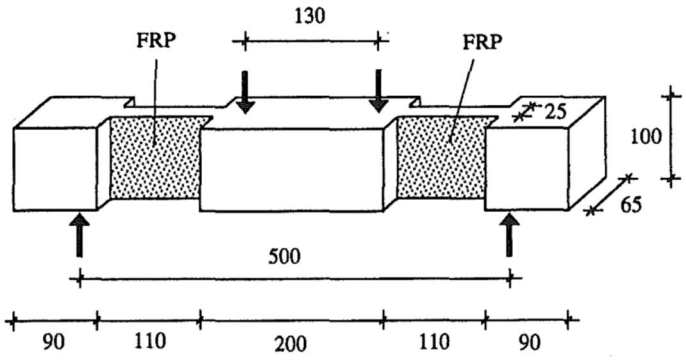

Figure 23: *Specimen geometry as used by Triantafillou [112]*

He used the standard equation (12) for composite beams to determine the shear stress in the timber.

$$\tau = \frac{Q \cdot S}{b \cdot I_y} \qquad (12)$$

Where:

τ = shear stress
Q = shear force
S = first moment of area of the composite section
I_y = moment of inertia of the composite section

The reinforced beams had an up to 30% higher shear capacity than the control specimens. This shows that CFRP fabrics can be quite efficient for shear reinforcement; however the long-term behaviour needs to be investigated, especially for large glulam beams in uncontrolled environments.

Borri, Corradi and Grazini investigated timber beams that were reinforced using CFRP-fabrics or bars [19, 20]. The different layups tested are shown below (Figure 24).

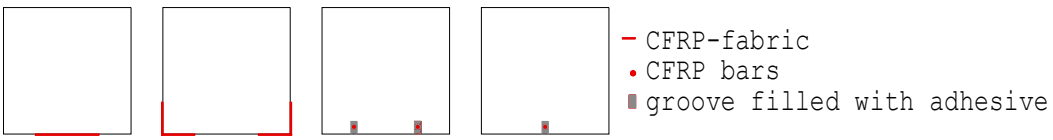

Figure 24: *Reinforcement layouts as used by Borri, Corradi and Grazini*

Compared with the control beams, these reinforced beams showed an increase of about 30% in stiffness and up to 60% for the beams reinforced with three CFRP fabric layers on the lower face of the beam. The beam reinforced with one fabric on each edge of the lower side performed better than the one with two fabrics at the bottom face. The beams with slotted-in CFRP bars all had a lower stiffness and capacity than the ones reinforced using fabrics. However, they still performed better than the control beams. Borri, Corradi and Grazini report that cambering a beam during the bonding process does not increase the stiffness or the load-bearing capacity. The authors did not consider or evaluate the camber or the stress distribution in a prestressed beam.

2.5.3 Prestressed timber

The methods, involving the externally-bonded CFRP reinforcements, presented above lead to a significant improvement of the load-bearing capacity. Unfortunately, the contribution of these methods to the bending stiffness is small, and in some cases, even detrimental. Furthermore, because the CFRP-lamella is not used to its full capacity at ultimate load, the expensive material is not used cost efficiently. In order to overcome these two obstacles the CFRP reinforcement has to be prestressed.

Currently, prestressed concrete constructions are widely used, especially for large spans. Prestressing allows the engineers to overcome the weak tension strength of concrete and to avoid fissures on the tension side during service. Reports of prestressed concrete go back to the 19th century. As timber-bending beams also fail on the tension side, prestressing may also be applied in this case. Several authors have presented studies of prestressed timber beams (see below) with the research having started in the second half of the 20th century.

Bohannan studied prestressed timber beams loaded in bending [18], testing six reinforced glulam beams with closely matched controls in four-point bending. To ensure that the controls and the prestressed beams were as alike as possible, he graded and split the timber lamellas prior producing the beams, placing one half of the matched lamellas in the control and the other half in the prestressed specimen at the same position. The Douglas-fir beams had a cross section of 127 x 271mm and were prestressed with 124.5 kN, which is equal to 3.6 MPa compression stress in the timber. The steel wires were placed eccentrically on the tension side of the beam (Figure 25).

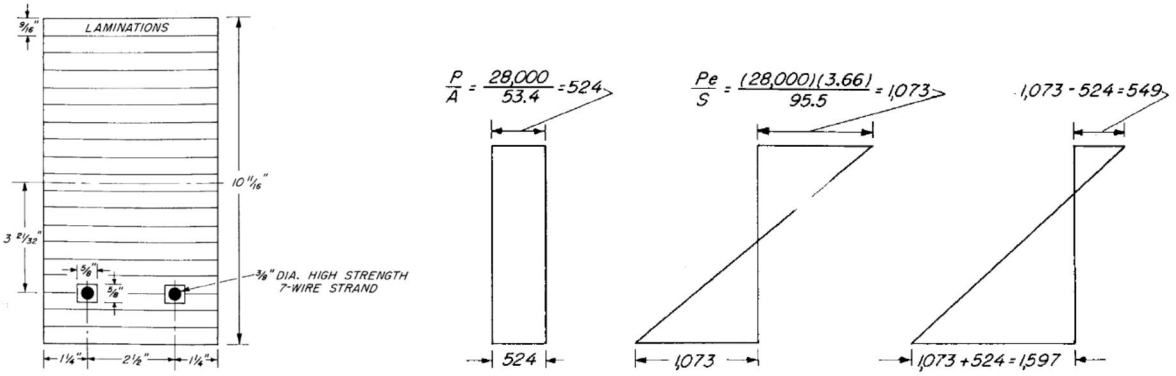

Figure 25: *Cross section of the prestressed beam and the resulting stress distribution in the timber; the measurements are in inches, pound force and pound force per square inch [18]*

Bohannan concludes that for beams consisting of high-grade lamellas, the gain in load capacity is not as predominant as for beams with lower-grade laminations. Therefore the prestressing leads to a reduction of the scatter in failure loads. He recommends the application of higher prestress in order to ensure significant crushing on the compression side of the timber, which would lead to an even higher capacity and lower variability. He also states that the prestressing has almost no influence on the bending stiffness but leads to a camber of about 1.3mm.

Luggin [72] studied in his dissertation the behaviour of prestressed timber. He used a pretensioning frame, which involves introducing the prestress force in the timber after curing the adhesive (see also Figure 36). Luggin used two meter-long glulam specimens of 100 x 192mm to analyse the prestress distribution in the CRFP-lamella of different layouts and reinforcing ratios (Figure 26). He used strain gauges on the CFRP to measure the strain distribution over the length of the beam.

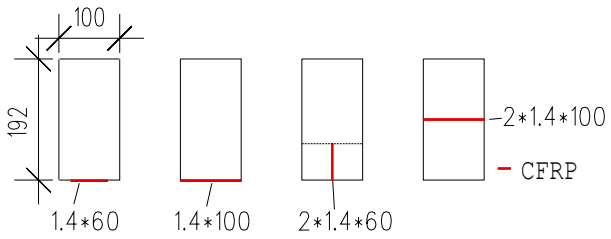

Figure 26: *Reinforcing layouts to determine the prestress distribution over the length of the CRFP-lamella as used by Luggin*

Luggin observed delaminating issues for the specimen with an externally-bonded CRFP-lamella. All specimens with a prestress higher than 550 MPa (calculated from the force in the jack) in the CFRP-lamella failed, due to delaminating while releasing the jack or shortly afterwards. The specimens with a vertically-orientated CRFP-lamella did not have any delaminating issues even with forces twice as high than the externally-bonded lamellas of the same width. Luggin observed the same result for the specimen with the CFRP-lamella in the centre.

Figure 27 [72] shows the prestress distribution over the length of the beam on different load-releasing levels (LST). The specimens had an anchoring length of about half a meter.

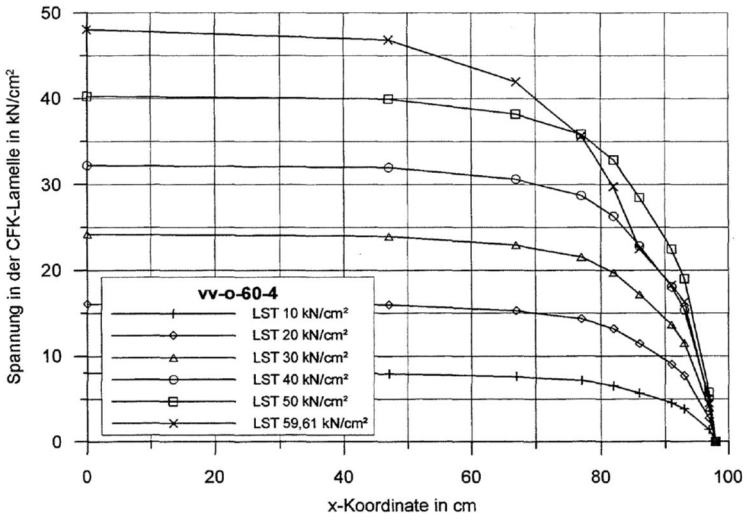

Figure 27: *Measured prestress as a function of the lamella length (0 is in the centre of the beam) on different load-releasing levels (LST) [72]*

Luggin [72] tested reinforced and control beams in four-point bending using different reinforcing ratios (0%, 0.35% and 0.7%) and also different prestress force levels (0kN and ~60kN). The CFRP-reinforcement was vertically slotted into the 200 x 100mm glulam beam. A reinforcing ratio of 0.7% led to an increase in the bending stiffness of about 14%. The load-bearing capacity at the first failure of the prestressed specimen with the highest reinforcing was 65% higher than the one of the control. After the first failure, the load could be increased on most of the reinforced specimens up to 70% higher for some than for the control. The load-bearing capacity of the prestressed specimens was about 10% higher than the unstressed ones with the same reinforcing ratio. The reinforced specimens showed severe crushing on the compression side after testing. In some specimens, the CFRP ruptured during total failure of the beam, and this always occurred after the first tension failure of the timber.

Schnüriger, Brunner and Lehmann [98] tackled the delaminating by using a special device that allows the attaching of prestressed CFRP-lamellas in gradients. The device was developed for reinforcing concrete by the EMPA [107] (see also Figure 19). Schnüriger, Brunner and Lehmann tested two series of prestressed timber beams. Two glulam beams (320 x 80mm) were reinforced using three CFRP-lamellas on top of each other. Only the first lamella had the same length as the beam; the second started after the anchorage zone of the first one; and the third was again shorter to avoid interaction with the anchorage zone of the previous one (Figure 28).

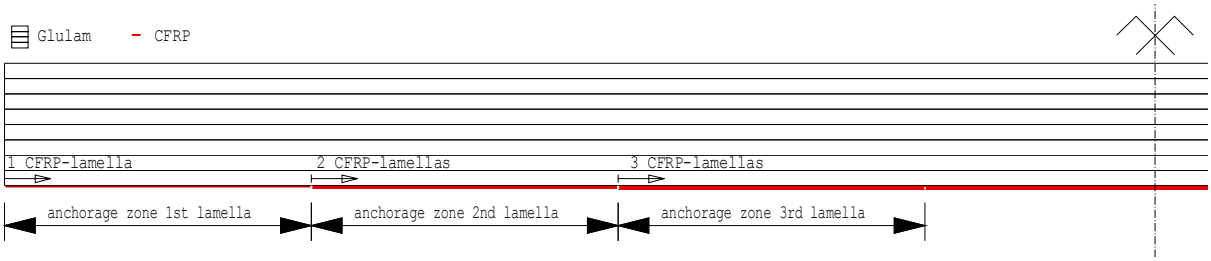

Figure 28: *Glulam beam prestressed with three CFRP-lamellas as tested by Schnüriger, Brunner and Lehmann*

The jacking force (P) of each CFRP-lamella was 60 kN. Due to elastic losses, the calculated prestress force (P_0) was 126.6 kN in the middle of the beam. The camber, due to prestressing, was around 30mm (span divided by 200). After prestressing, the reinforced glulam beams were tested in four-point bending. Unfortunately, the outer CRFP-lamella delaminated before the maximal load was reached. The first lamella was running over the support, and therefore compression perpendicular to the bond may have helped to prevent the total delamination of the CFRP. Lehmann, Brunner, Schober et al. [65] presented numerical simulation of these bending tests. The FEM calculation showed that if a more elastic adhesive were used, the stresses in the anchorage zone could be greatly reduced, and debonding probably avoided without any significant loss in prestress force (P_0). Schnüriger, Brunner and Lehmann [98] also tested two glulam beams (240 x 60mm), prestressed with one lamella. The jacking force (P) was 60 kN and again anchored in gradients. The lamella was anchored before the support as it would be in the case of retrofitting (Figure 29). The four-point bending of those beams showed that no delaminating occurred if only one lamella is applied.

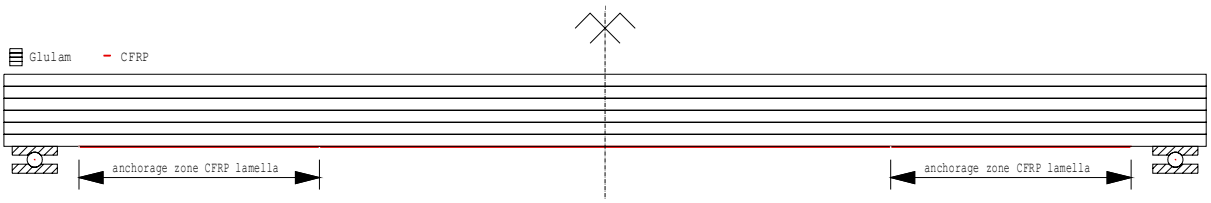

Figure 29: *Glulam beam prestressed with one CFRP-lamella as tested by Schnüriger, Brunner and Lehmann*

Strahm [108] presents a 40m span truss with a prestressed tension member (Figure 30). The trusses are the roof structure of a new production facility of the *neue Holzbau AG Lungern*, which is the first large industrially-built prestressed-timber structure in Switzerland. The tension member was prestressed using two steel rods. The prestress level was chosen so that the tension member is almost stress-free under permanent loads. Strahm reports how, in order to make the prestressing economically viable, the distance between the trusses had to be at least 7.5m. Due to the prestressing, the cross section of the tension member could be reduced by 50%. He concludes that the system is prone for even larger structures.

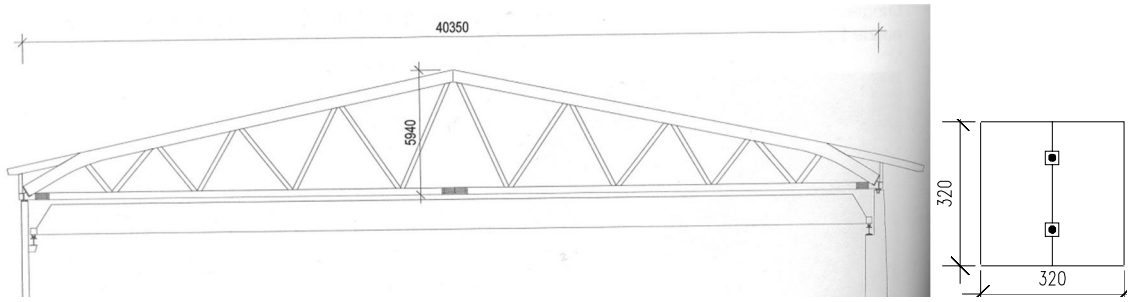

Figure 30: ***Left****: post-tensioned truss [108];* ***Right****: cross section of the prestressed tension member*

The report by Widmann, Meier, Brönnimann et al. [121] of a pedestrian bowstring arch bridge at the EMPA site with a 12m span shows that the bridge has an experimental character and is constructed entirely from CFRP and GFRP timber. The bridge is laterally and longitudinally prestressed, and the CFRP is joined to the timber without adhesives. The six bowstrings are

non-laminated pin-loaded thermoplastic CFRP strips. The installation of the prestressed bowstrings increased the bending stiffness of the bridge deck by about 3 to 4 times (Figure 31).

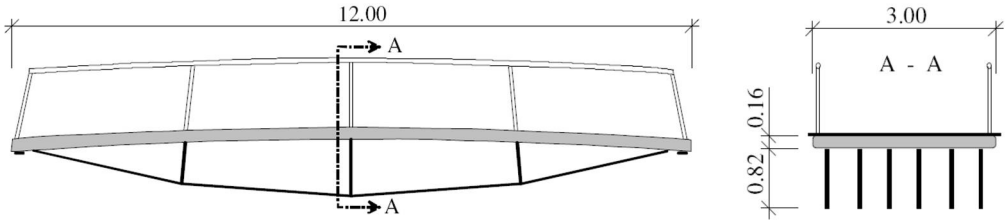

Figure 31: *Prestressed pedestrian bowstring bridge at the EMPA site [121]*

2.5.4 Calculation models for reinforced beams

The Swiss construction standard SIA 166 for 'externally-bonded reinforcement' [11] is valid for various construction materials such as concrete, masonry, steel and timber. However, the calculation models presented are based mainly on experiments using concrete as substrate and on the experience gained from reinforcing concrete structures. Therefore, the calculation models presented are based on the behaviour of concrete and are of limited use in designing a timber structure. The SIA 166 [11] distinguishes two different zones over the length of the reinforcement: the active and anchorage zones. The ultimate-limit state of the active zone is given by the tension capacity of the lamella. The ultimate-limit state of the anchorage zone strongly depends on the means used for the anchorage; and in the case of adhesively-bonded anchorage, depends on its length and the pull-off strength of the substrate. In concrete structures, the anchorage zone has to be located in the theoretically non-fissured part (at ultimate load) of the structure. The region containing cracks is regarded as the active zone. For timber structures, no explanations on how to distinguish between the anchorage and the active zones are given. However, the tension behaviour of timber is more or less linear elastic up till failure, and therefore one can assume that the standard theories for composite beams are applicable. This means that for adhesively-bonded lamellas, the stress in the anchorage zone is equal to the shear stress present in the adhesive, which is determined using standard equations for linear elastic composite sections. For concrete structures SIA 166 [11] recommends using equations (13) - (15) to determine the anchoring resistance. A similar approach may be used for prestressed-timber beams to determine the maximal-prestress force that can be anchored using an adhesive bond and a standard prestressing system as used for concrete structures; the validity of this approach has yet to be confirmed by further research, however.

$$l_{b,0d} = \frac{\pi}{2}\sqrt{2 \cdot \frac{G_{Fbd} \cdot E_l \cdot t_l}{{\tau_{l0d}}^2}} \qquad (13)$$

$$F_{b,Rd} = b_l \cdot \sqrt{2 \cdot G_{Fbd} \cdot E_l \cdot t_l} \cdot sin\sqrt{\frac{{\tau_{l0d}}^2 \cdot {l_{bd}}^2}{2 \cdot G_{Fbd} \cdot E_l \cdot t_l}} \qquad if\ l_{bd} \leq l_{b0d} \qquad (14)$$

$$F_{b0,Rd} = b_l \cdot \sqrt{2 \cdot G_{Fbd} \cdot E_l \cdot t_l} \qquad if\ l_{bd} \geq l_{b0d} \tag{15}$$

Where:

$l_{b,d}$ = design value of the anchorage length
$l_{b,0d}$ = design value of the maximal-effective anchorage length
G_{Fbd} = design value of the fracture energy of the substrate
E_l = MOE of the lamella
t_l = thickness of the lamella
τ_{l0d} = design value of the maximal-shear strength of the substrate
$F_{b,Rd}$ = design value of the anchorage resistance
$F_{b0,Rd}$ = design value of the maximal-anchorage resistance
b_l = width of the lamella

Holzenkämpfer presents in his dissertation engineering models for the bond behaviour of adhesively-bonded reinforcement for concrete structures [44]. He presents the solution of the differential equation for various kinds of bond behaviour (linear, bilinear and non-linear). Holzenkämpfer conducted experiments on concrete specimens with externally-bonded steel lamellas to verify his models. Furthermore, he developed design models for reinforced-concrete structures. The models for bending consider debonding in the anchorage and/or in the zone with high-bending moments (active zone). The models for debonding in the active zone are based on the bending or shear crack size present in the concrete. The model for the anchorage zone is based on the concrete-tension strength and the fracture energy of the concrete. The model allows the determination of the maximal force that can be anchored using adhesive bond. The equations presented by Holzenkämpfer [44] for the anchorage strength are quite similar to the equation presented in the Swiss standard [11]. Holzenkämpfer uses a hyperbolic-tangent function instead of sinus and therefore the equation is valid for every anchoring length. The equations used to estimate the shear strength and the fracture energy of the concrete are different in the two models. However, both models base the estimations on the tension strength of the concrete. Holzenkämpfer uses a modifications factor for different widths of the lamella and the substrate. Holzenkämpfer [44] recommends using 80% of the result of equation (16) as the characteristic value. This difference leads to a significant variation in the characteristic resistance calculated using the two models (Figure 32). Holzenkämpfer estimates higher values for short anchoring length. The maximal resistance is equal for 104mm wide lamellas. For smaller lamellas, Holzenkämpfer estimates higher, and for wider lamellas, lower values than the SIA model. He also presents the lower limit of equation (16) valid for short-anchoring length (equation (17)). Furthermore. the upper limit of equation (16) he deems valid for long-anchoring length (equation (18)), which is identical to the one presented in SIA 166 [11]. There is no description about the range of the anchoring length where equation (17) can be applied.

$$F_{anch} = b_l \cdot \sqrt{2 \cdot G_F \cdot E_l \cdot t_l} \cdot tanh \sqrt{\frac{{\tau_{l1}}^2 \cdot l^2}{2 \cdot G_F \cdot E_l \cdot t_l}} \tag{16}$$

$$F_{anch} = b_l \cdot \tau_{l1} \cdot l \tag{17}$$

$$F_{anch} = b_l \cdot \sqrt{2 \cdot G_F \cdot E_l \cdot t_l} \qquad (18)$$

Where:

G_F = fracture energy of the substrate
E_l = MOE of the lamella
l = anchorage length
τ_{l1} = maximal-shear strength of the substrate
F_{anch} = anchorage resistance
b_l = width of the lamella

Equation (17) represents the maximal anchoring resistance concerning the strength of the substrate, whereas equation (16) considers the fracture mechanics, and equation (18) presents the limit given by fracture mechanics.

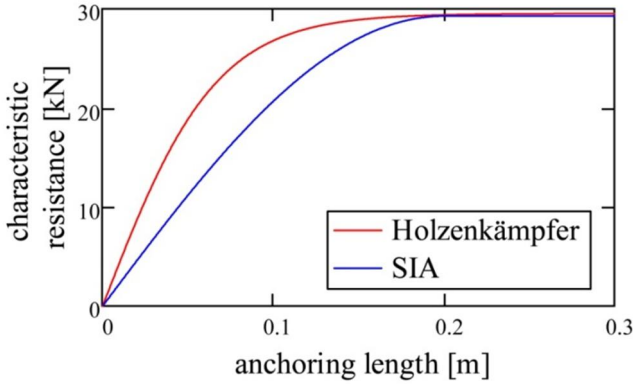

Figure 32: *Comparison of the characteristic anchoring resistance calculated using the equations provided in SIA 166 (**blue**) and Holzenkämpfer (**red**). The calculation is based on a C25/30 concrete and a CFRP-lamella with an MOE of 165 GPa, a thickness of 1.2mm and a width of 100mm.*

Plevris and Triantafillou developed a calculation model for FRP-reinforced timber in bending and bending combined with compression for different failure modes [88]. The model was calibrated with experiments carried out on small clear specimens with various volume fractions of FRP-reinforcement. The results demonstrated that even small area fractions of FRP leads to a significant improvement in the load-bearing capability. The calculation model developed by Plevris and Triantafillou [88] considers four different failure modes of small clear timber specimens reinforced with FRP. The timber is regarded as linear elastic until failure on the tension side, and also linear elastic up to yield strain on the compression side. For strain higher than yield strain, the stress strain curve is described by a falling branch (Figure 33).

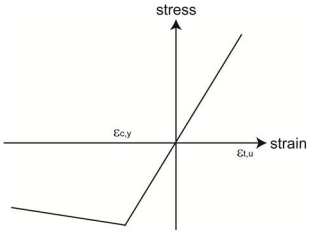

Figure 33: *Sketch of the stress-strain relationship as used by Plevris and Triantafillou [88]*

Tension strain in timber is taken as the failure criteria of the composite section. The modes considered are:

1. Timber and FRP remains in its linear-elastic state
2. Timber remains in its linear-elastic state and FRP has ruptured
3. Timber yields on the compression side and FRP remains in its linear-elastic state
4. Timber yields on the compression side and FRP has ruptured

Rupture can occur in all four modes described above. However, no report of tension failure in the CFRP before failure in timber has been found in any of the literature that considers structural-sized specimens.

Dziuba tested timber beams reinforced with glued-in steel wires in bending [30]. The area fraction of the reinforcement was varied between 0 and 4 %; the used wires had an average yield stress of 535 MPa. The cross section of the beams was around 50 x 160mm, and the distance between the centre of gravity of the reinforcement and outermost tension fibre of the timber was 30mm. For the beams with a higher percentage of reinforcement, Dziuba reports failure of the beam due to compression failure of the timber without failure of the tension side. This leads to his failure model that includes a bilinear stress-strain relationship for timber under axial load. The tension side is linear-elastic up until failure; the compression side has a linear-elastic branch followed by an ideal plastic branch, which is limited by an ultimate strain ($\varepsilon_{c,u}$) where failure occurs (Figure 34).

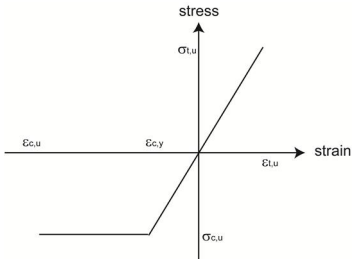

Figure 34: *Sketch of the stress-strain relationship as used by Dziuba [30], Blass and Romani [15, 94]*

Romani and Blass [94] developed a design model for FRP-reinforced beams with a facing timber lamella on top of the FRP-lamella. The model allows for plasticity in timber under compression. The published equations allow the calculation of the ultimate load-bearing capacity based on the ultimate tension and compression strength of the timber. Different failure modes, depending on the ratio between the ultimate stress in compression in timber and tension in timber as well as in the FRP are considered. Blass and Romani [15] extended the design model for FRP-reinforced beams without a facing timber lamella. The design model allows the calculation of the ultimate loadbearing capacity without iteration. However, in the case of active plasticity, the calculation of the stress distribution based on a loading situation is only possible with multiple iterations.

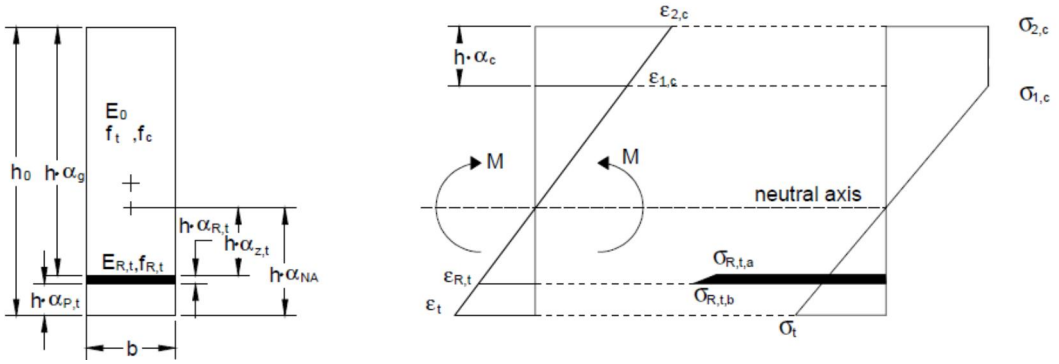

Figure 35: *Stress and strain distribution as used for the calculation model of Romani and Blass [94]*

Herzog presents mathematical investigations on the influence of CFRP reinforcement on the bending capacity of timber beams in his degree thesis [41]. In his calculations, Herzog varies the beams and the size of the CFRP-lamellas as well as the MOE of the CFRP. He considers the compression stress on the top of the timber beam as the failure criterion, which leads to quite a low-reinforcing factor. He also reports that the deflection is more or less independent of the CFRP-lamella properties, and that the increase of bending stiffness due to the CFRP is negligible. Unfortunately, the calculations model used is not described sufficiently as he mentions only using Mathcad for the calculations. Herzog studied the influence of unloading the beam during reinforcing. Cambering of the beam was also considered as unloading. The load applied for unloading was a distributed load. The method of how such load should be applied is not described sufficiently. Likewise, the model used is not described and it is not clear how the prestressing is considered. Herzog also studied the long-term behaviour of a CFRP-reinforced timber beam. For the timber, a model with one spring and nine parallel Maxwell elements was used, but the parameters used for the spring and the Maxwell elements are not presented. For the CFRP, a single Maxwell element was used to model the long-term behaviour. The dynamic viscosity of the damper element presented by Herzog was in accordance with Schnell [97], who did his work on nearly isotropic CRFP-layups. Herzog's long-term calculations do not lead to understandable results. For example, for beams that were cambered during reinforcing, he states that the long-term effects led to a compression stress in the CRFP-lamella, which was bonded to the tension side of the timber beam. Unfortunately, this surprising result is not sufficiently explained or justified. Herzog's results are more or less contrary to the investigations done by others. The fact that the models are not described sufficiently and that Herzog did no experiments to verify his surprising results mean that his work will not be referenced further here. Moreover, the experimental work of Terrasi [110] and considerations of Meier [77] show that unidirectional CFRP-lamellas are not prone to creep, and have completely different long-term behaviour as layups with various fibre directions.

2.5.5 Calculation models for prestressed members

Depending on the prestressing system, the applied prestress force (P) is reduced due to elastic deformation of the structure. This elastic loss (ΔP_{el}) occurs if a system where the jack is mounted on a pre-tensioning frame is used (Figure 36). The prestress force (P_0) present in the member is given by equation (19) below. Most post-strengthening methods for concrete

do not have elastic losses because the prestressing jack is attached to the concrete and the elastic deformation occurs whilst building up the prestress force P (Figure 37).

$$P_0 = P - \Delta P_{el} \tag{19}$$

Where:

P_0 = prestress force present in the member

P = prestress force applied to the system (jacking force)

ΔP_{el} = elastic prestress force loss

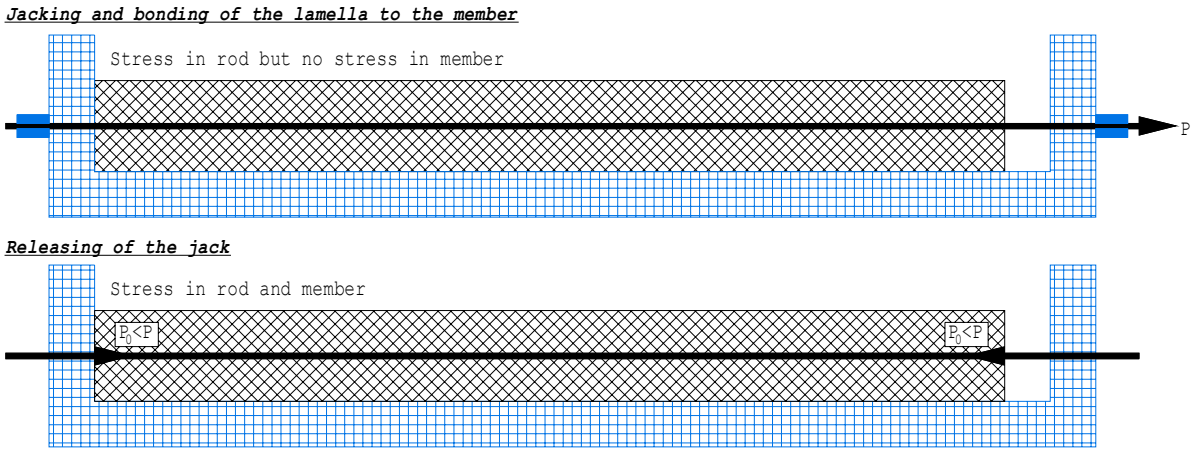

Figure 36: *Sketch of prestressing a member using a pre-tensioning frame or similar device where the jack is mounted on a frame, and therefore elastic loss occurs*

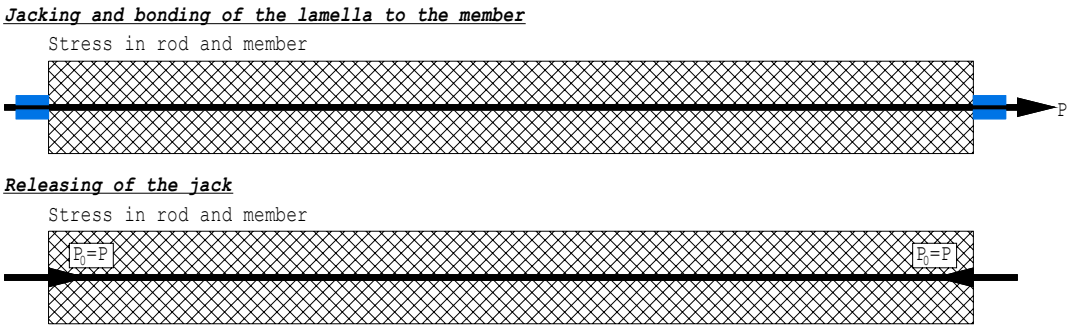

Figure 37: *Sketch of prestressing where the jack is mounted on the member and therefore no elastic loss occurs*

According to Thomsing [111], the prestress force and the moment due to eccentricity act on the conceptual cross section. The moment, due to eccentric prestressing, is determined by the multiplication of the prestress force with the eccentricity.

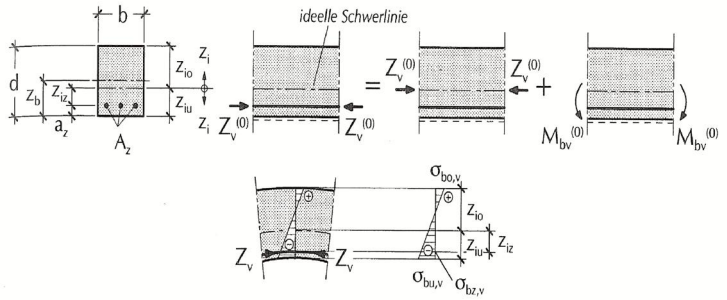

Figure 38: *Determination of the prestress in the case of eccentric prestressing [111]*

Triantafillou and Deskovic [113] investigated the maximal-anchoring force for adhesively-bonded prestressed CFRP-lamellas, assuming concrete or adhesive failure. The analyses they present assume linear-elastic materials, and the governing deformation mode in the adhesive layer as shear. The stress-strain relationship is assumed as a bilinear model where the first part is linear-elastic, followed by a perfect plastic plateau until failure (Figure 39).

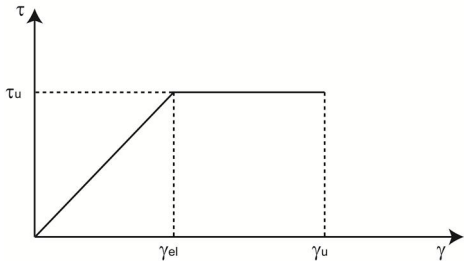

Figure 39: *Shear stress-strain relationship for epoxy adhesive as used by Triantafillou and Deskovic*

The shear stress in the elastic domain of the adhesive can by determined using equation (21) [113].

$$\tau(x) = \frac{\gamma_{el,a} \cdot G_a}{sinh \cdot \left(\frac{\omega \cdot l_{el}}{2}\right)} \cdot \sinh(\omega \cdot x) \qquad (20)$$

$$\omega = \sqrt{\frac{G_a}{h_a \cdot h_{cf}} \left(\frac{1}{E_{cf}} + \frac{4 \cdot h_{cf}}{h_s \cdot E_s}\right)} \qquad (21)$$

Where:

$\tau(x)$ = shear stress due to prestressing in the adhesive as a function of x
$\gamma_{el,a}$ = maximal-elastic shear strain (Figure 39)
G_a = shear modulus of the adhesive
l_{el} = length of the elastic domain
h_a = thickness of the adhesive layer
h_{cf} = thickness of the CFRP-lamella
E_{cf} = modulus of elasticity of the CFRP-lamella
h_s = height of the substrate
x = position over the length of the beam
E_s = modulus of elasticity of the substrate

The shear stress in the area where the adhesive has passed its elastic limits is equal to the ultimate shear stress of the adhesive ($\tau_{u,a}$) (Figure 39).

Triantafillou and Deskovic assume that equation (22) below for the shear deformation is valid for the whole length of the reinforced beam. This assumption is consistent with the commonly-held hypothesis that the strains in the inelastic regime are approximately described by the same relationship characterising elastic response (e.g. bending beam).

$$\gamma(x) = \frac{\gamma_{el,a}}{sinh \cdot \left(\frac{\omega \cdot l_{el}}{2}\right)} \cdot \sinh(\omega \cdot x) \qquad (22)$$

Where:

$\gamma(x)$ = shear strain due to prestressing in the adhesive as a function of x

$\gamma_{el,a}$ = maximal-elastic shear strain (Figure 39)

l_{el} = length of the elastic domain

ω = is given by equation (21)

The equations presented by Triantafillou and Deskovic [113] lead to the following shear stress and strain distribution:

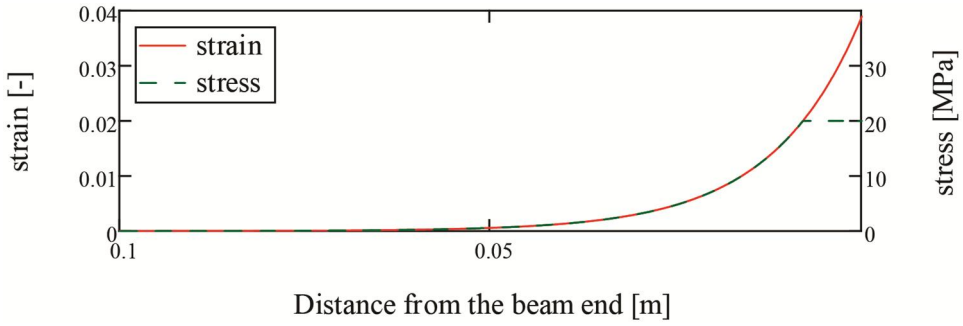

Figure 40: *Shear stress and strain distribution (immediately before delaminating due to prestress force) in the adhesive layer towards the end of the beam, calculated using the equations presented by Triantafillou and Deskovic [113]*

For the ultimate anchorage load, the shear strain at the end of the beam is equal to the ultimate shear strain ($\gamma_{u,a}$). This condition allows the calculation of the length of the elastic domain (l_{el}) (equation (23)).

$$l_{el} = \frac{2 \cdot ln\left(\frac{\beta + \sqrt{\beta^2 + 4}}{2}\right)}{\omega} \qquad (23)$$

$$\beta = \frac{2 \cdot \gamma_{el,a}}{\gamma_{u,a}} \cdot sinh\left(\frac{\omega \cdot l}{2}\right) \qquad (24)$$

Where:

$\gamma_{u,a}$ = ultimate shear strain of the adhesive (Figure 39)

$\gamma_{el,a}$ = maximal-elastic shear strain of the adhesive (Figure 39)

l_{el} = length of the elastic domain

ω = is given by equation (21)

Based on the shear stress distribution in the elastic domain, the normal stress in the CFRP can be determined. Triantafillou and Deskovic assume the normal stress distribution in the inelastic zone as linear. Knowing the normal stress distribution in the CFRP allows the calculation of the ultimate pre-tension force ($P_{0,u}$) (equation (25)).

$$P_{0,u} = EA_{cf} \cdot h_a \cdot \gamma_{el,a} \cdot \omega \cdot \left(coth\left(\frac{\omega \cdot l_{el}}{2}\right) + \frac{\omega \cdot (l - l_{el})}{2} \right) \quad (25)$$

Where:

$P_{0,u}$ = ultimate pre-tension force
EA_{cf} = tension stiffness of the CFRP
h_a = thickness of the adhesive layer
$\gamma_{el,a}$ = maximal-elastic shear strain of the adhesive (Figure 39)
l_{el} = length of the elastic domain
ω = is given by equation (21)

Furthermore, Triantafillou and Deskovic [113] present an equation to calculate the ultimate pre-tension force ($P_{0,u}$), assuming concrete failure (equation (26)):

$$P_{0,u} = \frac{\tau_{u,c} \cdot (l - l_{el})}{4h_{cf}} \cdot \left(A_{cf} + \alpha \cdot \frac{EA_{cf}}{E_c} \right) + \frac{EA_{cf} \cdot h_a \cdot \tau_{u,c} \cdot \omega}{G_a} \cdot coth\left(\frac{\omega \cdot l_{el}}{2}\right) \quad (26)$$

Where:

$P_{0,u}$ = ultimate pre-tension force
EA_{cf} = tension stiffness of the CFRP
h_a = thickness of the adhesive layer
$\gamma_{el,a}$ = maximal-elastic shear strain of the adhesive (Figure 39)
l_{el} = length of the elastic domain
ω = is given by equation (21)

Triantafillou and Deskovic [114] investigated the maximal-anchor resistance for prestressed CRFP-laminates on European beech (*Fagus Silvatica*), using adhesive bond, and assuming timber shear failure. The shear stress-strain behaviour of wood is assumed as bilinear with an elastic start followed by an ideal plastic branch (Figure 39). The equations for timber failure are the same as presented for adhesive failure [113] (equations (20) to (25)), except the stress-strain relationship of wood has to be used instead of the one of the adhesive. In case the CFRP-lamella is not as wide as the timber beam equation (21), it has to be modified (equation (27)).

$$\omega = \sqrt{\frac{G_a \cdot b_s}{h_a \cdot A_{cf}} \left(\frac{1}{E_{cf}} + \frac{4 \cdot A_{cf}}{AE_s} \right)} \quad (27)$$

Where:

G_a = shear module of the adhesive
h_a = thickness of the adhesive layer
A_{cf} = cross section area of the CFRP-lamella
E_{cf} = modulus of elasticity of the CFRP-lamella

b_s = width of the substrate

AE_s = tension stiffness of the substrate (area multiplied by the module of elasticity)

Triantafillou and Deskovic [113, 114] report that the theoretical investigations were satisfyingly verified with experiments using rather small and clear specimens. Furthermore, they tested three timber beams in bending in order to determine the influence of prestressed CFRP-lamellas on the bending capacity [114]. They conclude that, in order to avoid sudden collapse, the members have to be designed to yield in the compression first before fail by tensile fracture.

2.6 Numerical modelling of timber

Kim and Harries used an orthotropic-linear elastic-solid model to analyse timber beams reinforced with CFRP [46]. Tension strain was introduced as failure criteria for the timber. The model was able to predict the failure load of the beams with an average error of 8.2%. This model is only valid if no crushing occurs on the compression side of the timber, therefore the decrease of the load-deformation curve towards the maximal load cannot be modelled. Kim and Harries validated their model with beams produced from Douglas fir, and investigated other species by changing the mechanical properties. The parametrical study, including a study with larger reinforcing degrees and different timber species, was carried out numerically without experimentally verifying the hypothesis of the linear elastic behaviour of timber up till failure. According to other authors, significant non-linear behaviour can be observed for reinforced-bending members [20, 23, 30, 55, 56, 68, 69, 88, 98, 100, 106, 114]. Therefore, a numerical study discussing failure loads and modes should include the non-linear behaviour in the compression of timber.

2.6.1 Orthotropic elasticity

The complex cell structure of timber is often regarded as orthotropic elastic within its linear limits. This simplification allows the numerical modelling of timber beams in structural sizes with reasonable computing power.

Hook's law of elasticity describes the dependency between stress and strain (28).

$$\varepsilon_{ij} = S_{ijkl} \cdot \sigma_{kl} \qquad i,j,k,l = 1,2,3 \tag{28}$$

Where:

$\varepsilon_{i,j}$ = strain tensor (tensor second order)

$S_{i,j,k,l}$ = compliance tensor (tensor fourth order)

$\sigma_{k,l}$ = stress tensor (tensor second order)

The strain and stress tensor contains 9 elements and can be written as a 3 by 3 matrix or in Voigt notation as a vector containing 6 elements. This reduction is based on the symmetry of the shear stresses. Figure 41 visualises the stress in a solid.

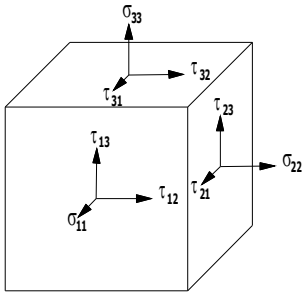

Figure 41: *Definition of the stresses in a solid*

The compliance tensor contains 81 elements. The Voigt notation, due to the symmetry, allows a reduction to 36 elements that can be written as a 6 x 6 matrix. Hook's law (28) may be written in Voigt notation as shown in equation (29).

$$\begin{Bmatrix} \varepsilon_{11} \\ \varepsilon_{22} \\ \varepsilon_{33} \\ 2\cdot\varepsilon_{12} \\ 2\cdot\varepsilon_{13} \\ 2\cdot\varepsilon_{23} \end{Bmatrix} = \begin{bmatrix} S_{11} & S_{12} & S_{13} & S_{14} & S_{15} & S_{16} \\ S_{21} & S_{22} & S_{23} & S_{24} & S_{25} & S_{26} \\ S_{31} & S_{32} & S_{33} & S_{34} & S_{35} & S_{36} \\ S_{41} & S_{42} & S_{43} & S_{44} & S_{45} & S_{46} \\ S_{51} & S_{52} & S_{53} & S_{54} & S_{55} & S_{56} \\ S_{61} & S_{62} & S_{63} & S_{64} & S_{65} & S_{66} \end{bmatrix} \cdot \begin{Bmatrix} \sigma_{11} \\ \sigma_{22} \\ \sigma_{33} \\ \tau_{12} \\ \tau_{13} \\ \tau_{23} \end{Bmatrix} \qquad (29)$$

Where:

$\varepsilon_{i,i}$ = strain in the three principal directions

$\varepsilon_{i,j}$ = shear strain

$S_{i,j}$ = elastic coefficients

$\sigma_{i,i}$ = stresses in the three principal directions

$\tau_{i,j}$ = shear stresses

Due to symmetry (e.g. $s_{i,j} = s_{j,i}$), the compliance tensor has only 21 independent elements. For orthotropic materials only, 12 elastic coefficients are not equal zero. For timber, it is common to assume a symmetric compliance tensor, and therefore only nine constants are independent. However, this is contrary to the results of Neuhaus [84], as he has shown that this assumption is not true for timber. The compliance tensor for timber can by written as shown in equation (30).

$$\begin{Bmatrix} \varepsilon_L \\ \varepsilon_R \\ \varepsilon_T \\ \gamma_{LR} \\ \gamma_{LT} \\ \gamma_{RT} \end{Bmatrix} = \begin{bmatrix} 1/E_L & -\nu_{LR}/E_R & -\nu_{LT}/E_T & 0 & 0 & 0 \\ -\nu_{RL}/E_L & 1/E_R & -\nu_{RT}/E_T & 0 & 0 & 0 \\ -\nu_{TL}/E_L & -\nu_{TR}/E_R & 1/E_T & 0 & 0 & 0 \\ 0 & 0 & 0 & 1/G_{LR} & 0 & 0 \\ 0 & 0 & 0 & 0 & 1/G_{LT} & 0 \\ 0 & 0 & 0 & 0 & 0 & 1/G_{RT} \end{bmatrix} \cdot \begin{Bmatrix} \sigma_L \\ \sigma_R \\ \sigma_T \\ \tau_{LR} \\ \tau_{LT} \\ \tau_{RT} \end{Bmatrix} \qquad (30)$$

Where:

ε = strain in the three principal directions

γ = shear strain

E = modulus of elasticity

G = shear modulus

$_L$ = longitudinal

$_R$ = radial

$_T$ = tangential

σ = stresses in the three principal directions

τ = shear stresses

Neuhaus [84] undertook extensive research concerning the dependency of the 12 elastic constants of *Picea Abies* on the moister content. In this research, he demonstrated that the 12 members of the compliance tensor of timber have a significant dependency on the moister content. Neuhaus used *Picea Abies* from Russia and Scandinavia. He determined the elastic constants in tension and torsion mode. All measurements were done on the same 51 specimens with a nominal cross section of 20 x 20mm and a length of 240mm. The fibre orientation of the timber was chosen so the three principle directions were tested (Figure 42).

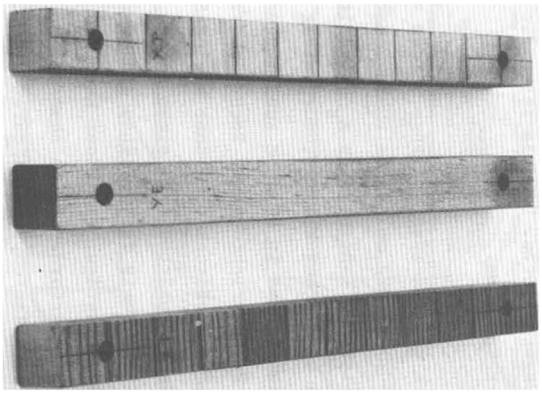

Figure 42: *Specimens after testing as used by Neuhaus [84]*

For the numerical modelling in the presented work, the elastic constants determined by Neuhaus [84] were used except the modulus of elasticity parallel to the grain, which was measured for each specimen in bending mode. As the used specimen had a moister content of around 12%, the moisture dependency of the constants was not considered in the model.

2.6.2 Non-linear methods

The linear orthotropic elasticity does not allow the consideration of plasticity, softening or hardening. Different authors [15, 22, 23, 30, 61, 68, 72, 82, 88, 98] have reported that significant crushing can occur during bending tests done on reinforced timber beams. Therefore, the numerical modelling of the ultimate load should allow for plasticity on the compression side. Grosse [37] presents a good overview of different yield criteria and the suitability for applying it to timber. Therefore, only a brief overview is presented here.

For isotropic and homogeneous materials, von Mises [120] presents a yield criterion which allows the consideration of hardening. Von Mises assumes the incompressibility of the material and that hydrostatic pressure or tension does not lead to failure. The yield criterion of von Mises describes the surface of a pipe rotationally symmetrical to the hydrostatic axis. Isotropic hardening leads to a modification of the yield stress; thus the diameter of the pipe is modified as a function of the plastic strain.

Hill [43] presents a yield criterion for orthotropic materials. This criterion is based on the von Mises criterion but allows different yield stresses for the three main directions. He still assumes incompressibility of the material and that hydrostatic stresses do not lead to failure. The generalised Hill criterion allows different yield stresses for tension and compression in the same direction. The generalised Hill criterion has some restrictions for the yield stresses and they are not completely independent. Grosse [37] shows that under certain conditions the generalised Hill criterion with a hardening function is applicable to timber, especially for plane stress under compression.

Tsai and Wu [115] present a yield criterion that does not assume incompressibility of the material and also allows yielding under hydrostatic stress state. The criteria of von Mises and Hill can be derived from the Tsai-Wu. The yield criterion allows for all failure modes and, where appropriate, parameters are chosen so a realistic yield volume can be generated. In the case of yielding, the primary failure criterion is not clearly determinable. This factor complicates the application of different softening behaviour for each failure criterion. Due to the fact that Tsai-Wu has nearly no restrictions in the material behaviour, not all parameters needed can be directly derived from the engineering constants. Therefore, some of the parameters have to be estimated. Grosse [37] presents methods from various authors and concludes that there are no common methods for derivating the needed parameters for timber.

Multi-surface plasticity allows failure criteria for anisotropic materials to be generated. The allowable stress combinations are not bordered by one single surface but by several surfaces. This allows, for example, the definition of a separate failure stress for each mode and direction, which leads to 12 independent surfaces that have to enclose a volume. Stüssi [109] presented, as early as 1946, a failure criterion for timber under tension or compression as a function of the fibre angle. He used three different equations depending on the failure mode, and verified the model on experiments done by Baumann [12] and Kraemer [53]. He concludes, therefore, that a single surface is not suitable to describe a failure criterion for timber depending on the fibre angle (Figure 43).

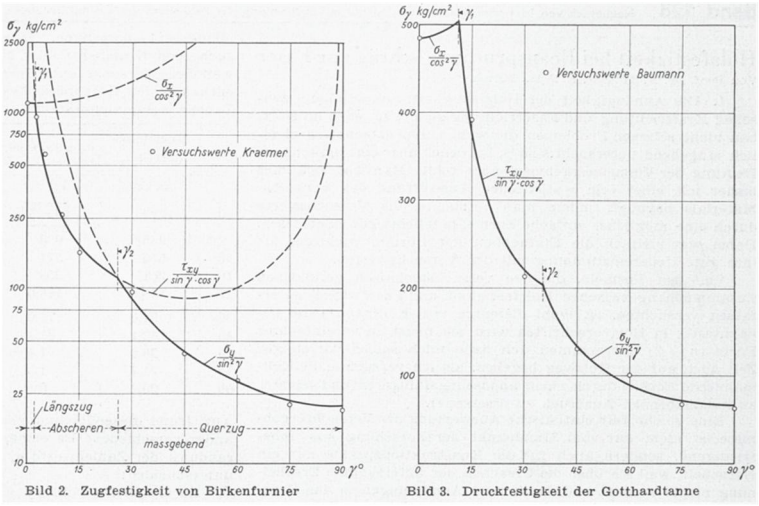

Figure 43: *Failure criteria for timber as presented by Stüssi [109]*

Grosse [37] presents in his dissertation a multi surface plasticity model for timber. He used softening rules to model the post failure behaviour of timber in each failure mode. The model was implemented in Ansys. Grosse specifies seven factors in order to describe a 3D failure criterion for soft wood.

- Rupture of the fibres (surface 1)
- Crushing of the fibres (surface 2)
- Crack development in the LT plane (surfaces 3 and 4)
- Compression radial (surface 5)
- Crack development in the LR plane (surface 6)
- Compression tangential (surface 7)

The surfaces 1, 2, 5 and 7 are maximal-stress criteria, and therefore multi-axial stress states have no influence on those surfaces. On the other hand, tension in the radial direction has a clear influence on the shear capacity LR-plane ($\tau_{RL,u}$). Compression in the radial direction has no influence on the shear capacity in the LR-plane ($\tau_{RL,u}$) (Figure 44). The shear capacity in the LT-plane is clearly higher than the tension capacity in the radial direction and also higher than the capacity in the compression radial. Grosse [37] therefore concludes that the Mohr theory is not valid for timber.

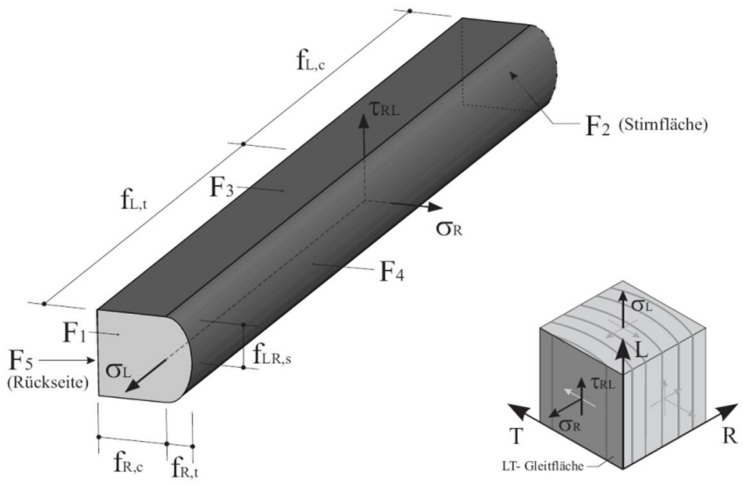

Figure 44: *Multi-surface plasticity criterion for softwood for plan stress in the LR-plane [37]*

The interaction between shear capacity in the LT-plane ($\tau_{TL,u}$) and tension or compression (σ_T) in the tangential direction are different, as shown above. The tension tangential leads to a reduction of the shear capacity, while the compression tangential leads to an increase of the shear capacity in the LT-plane (Figure 45).

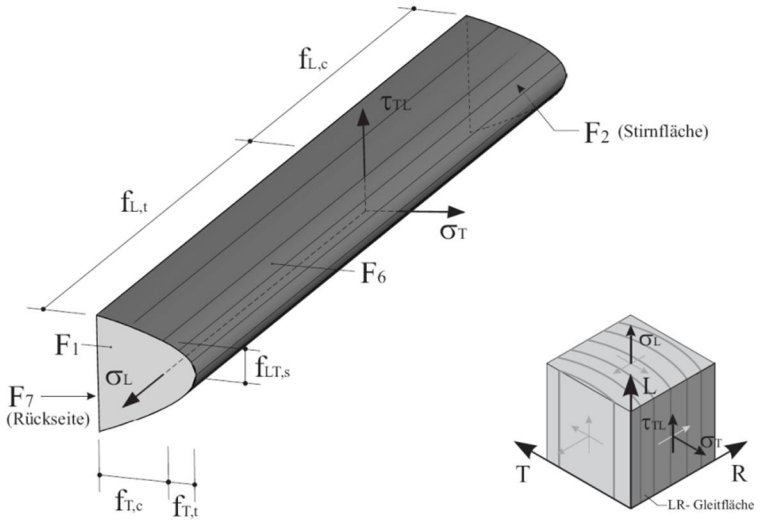

Figure 45: *Multi-surface plasticity criterion for softwood for plan stress in the LT-plane [37]*

For the different failure modes Grosse implemented softening and hardening functions in his numerical timber model. The more or less brittle tension and shear softening is expressed by an exponential function based on the dissipated fracture energy. The softening and hardening functions for the ductile compression failure are more complex. The compression stress in longitudinal direction reaches a local maximum followed by a slight decrease, which leads to a plateau. After the timber is completely crushed, a rapidly rising branch represents the behaviour of the compacted cell material (Figure 46).

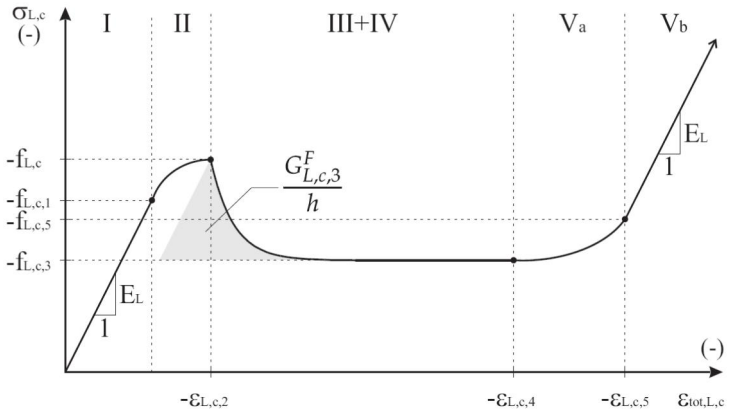

Figure 46: *Stress-strain relationship for compression longitudinal [37]*

For compression perpendicular to the grain, Grosse used qualitative the same function for radial and tangential direction. Timber does not have a clear maximum in transversal compression but goes smoothly from elastic over to a slightly rising branch that represents the buckling, and finally the crushing of the cell walls. After the timber is completely crushed, a rapidly rising branch represents the behaviour of the compacted cell material (Figure 47).

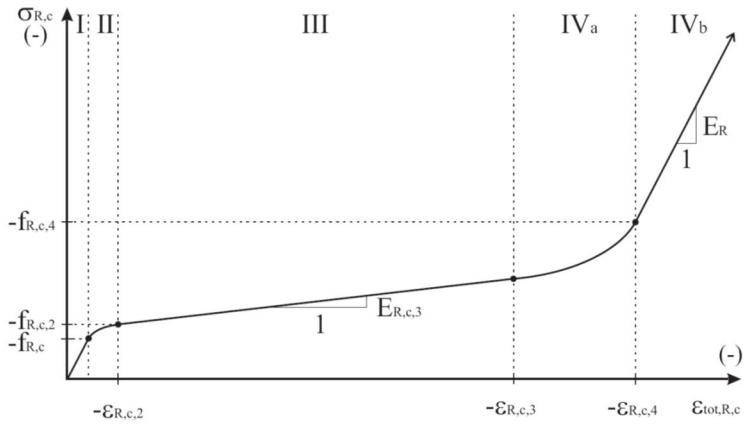

Figure 47: *Stress-strain relationship for perpendicular compression (example of radial compression) [37]*

Dynardo made a multi-surface plasticity model for timber commercially available. The model is based on the dissertation of Grosse [37]. In order to enhance the convergence of the material model, the softening functions are simplified to linear functions. Otherwise, the model is identical to the model developed by Grosse [37].

2.7 Conclusion

The overview of the state of the research demonstrated that comprehensive work in the field of non-linear numerical modelling of timber has already been done. Furthermore, multi-surface plasticity models for timber are commercially available, and therefore, developing a further model could not be justified. The existing models allow the numerical investigation of local stress and strain distribution in the anchorage zone.

On the other hand, no comprehensive analytical calculation model considering the prestressing of CFRP-reinforcement of timber-bending members could be found. In particular, no easily applicable design equation for timber beams prestressed using the camber method was found.

Therefore, the focus of the presented dissertation is to develop and verify a simple routine for prestressing timber-bending members using the camber method.

3 Analytical Calculation Model

The analytical calculation model was developed in order to analyse the influence of the camber and the material properties on the prestressing using the camber method. In addition, simplified equations for structural design are presented.

The calculation model was developed using MathCAD®. The resulting file should allow parametric studies and also the structural design of single-span timber beam with various configurations.

The calculation of the deflection in the model excludes (ultimate limit state) or estimates (service limit state) the deflection before the intervention. In order to include the exact deformation prior to intervention, it has to be measured and added to the values of the calculation model respectively the estimated values have to be replaced with the measured ones. The presented model is only valid in the elastic domain. Bilinear models allow considering the crushing on the compression side but require an iterative approach, which is unacceptable for engineering models. However Schnüriger, Brunner and Lehmann [98] show that the use of a linear-elastic stress-strain relationship instead of considering the crushing on the compression side by using a bilinear stress distribution has no significant influence on the calculated load-bearing limit for low prestress forces. Furthermore, the non-elastic deformation in the timber on the compression side is considered in Chapter 5 using the finite element method. The deflection curve is regarded as constant along the height of the cross section, which introduces an insignificant error. The prestress force (P) is treated as a tension force in the CFRP, and therefore its value is positive. In the equations presented below, distances and eccentricities are regarded as positive values.

The calculation model is illustrated using an example of a single-span bending beam. The configuration prior to intervention of the example is taken from a residential building located in Opfikon, Switzerland that is about 200 years old. The loading conditions after intervention are estimated using the hypothetical case that the multistorey building will be renovated and used for offices. The floor construction and the suggested materials are chosen in order to achieve an acceptable level of sound insulation. The table below shows the load configuration for the example (Table 4). The single-span timber beam has a nearly rectangular cross section of about 120mm (width) by 160mm (height) and a span of 4m.

Table 4: *Load configuration of the example used, to illustrate the calculation model*

Prior intervention		**After intervention**	
floor structure	[kN/m^2]	**floor structure**	[kN/m^2]
beam	0.13	beam	0.13
boards	0.14	OSB	0.22
carpet	0.02	paving slab	1.15
		impact sound insulation	0.03
		OSB	0.16
		parquet	0.12
sum	**0.28**	sum	**1.81**
live loads		**live loads**	
living	**2.00**	office	**3.00**
creep relevant loads		**creep relevant loads**	
dead loads	0.28	dead loads	1.81
0.3*live loads	0.60	0.3*live loads	0.90
sum	**0.88**	sum	**2.71**

3.1 Determination of the prestress force

The force applied during cambering of the beam is limited both by the quality of the beam and the ability to hold down its ends. The force present in the prop needs to be controlled by adequate measures. This can be done by using a load cell or by measuring the deformation and the MOE of the beam. The MOE of the timber is also needed for the calculation of the prestress force. The MOE can be determined on-site by using ultra-sonic measuring equipment, or experimentally by applying a known force in midspan and taking an accurate measurement of the deformation. The experimental method leads to an underestimation of the MOE except the shear deformation is estimated and considered. After determining the desired bending stress present in the timber during the bonding of the CFRP-lamella, the necessary force in the adjustable prop can be calculated using equation (31).

$$F_{pr} = \frac{q_{dl,1} \cdot sp}{2} + \frac{8 \cdot \sigma_{1,ti} \cdot \left(EI_{y.ti} + EI_{y.cf}\right)}{MOE_{ti} \cdot h_{ti} \cdot sp} \qquad (31)$$

Where:

F_{pr} = force in the adjustable prop during the reinforcement (State 1)
$q_{dl,1}$ = distributed dead load during the reinforcement
sp = span of the beam
$\sigma_{1,ti}$ = desired bending stress in the timber during bonding the CFRP-lamella to the timber beam
$EI_{y,ti}$ = bending stiffness of the timber beam is regarded as constant over the beam length
$EI_{y,cf}$ = bending stiffness of the CFRP-lamella
MOE_{ti} = modulus of elasticity of the timber
h_{ti} = height of the timber beam

In order to calculate the prestress force (P_0) and its distribution over the length, the equilibrium of the internal forces after the intervention needs to be calculated. The desired infor-

mation is gained by introducing three calculation states. *State 1* represents the system before bonding the CFRP-lamella but after the installation of the adjustable prop (Figure 48). In *State 2*, the effect of removing of the prop after bonding the CFRP-lamella to the timber (Figure 50) is modelled. *State 0* represents the prestressed system after intervention (Figure 52). Creep due to the prestress and permanent loads and the effect of moister variations are discussed later in this chapter. For the determination of the prestress force, the moments present in the system and its reaction, the deflection curve, needs to be calculated for each state.

In State 1 (Figure 48), the moment due to dead loads and the moment introduced by the prop are both present. The CFRP is not bonded to the timber and therefore the load is mainly supported by the timber. In order to get the exact distribution, the load has to be divided between the CFRP and the timber, considering the ratio between the bending stiffness of the materials. The adhesive is not cured in this state and its stiffness is considered as equal to zero.

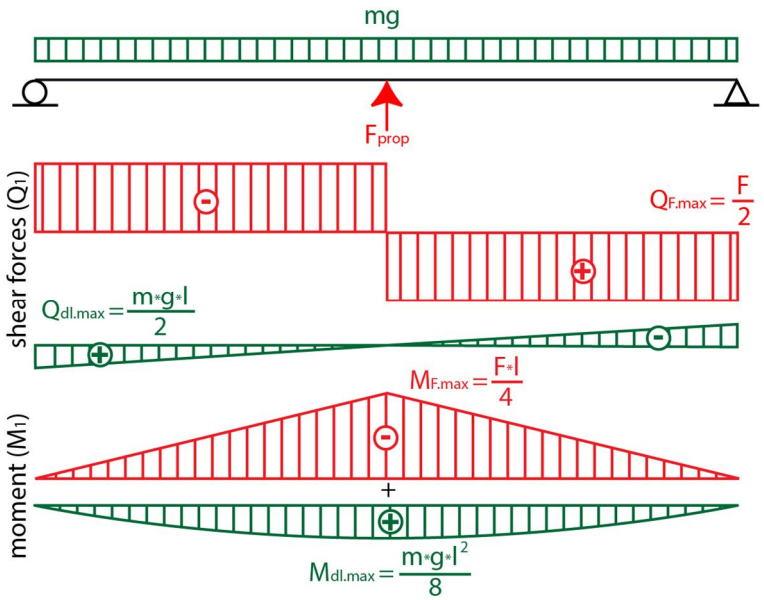

Figure 48: *State 1 in the calculation model, representing the system after setting up the prop but before the bonding of the CRFP-lamella (mg = mass multiplied by the gravitation constant g (-9.81 m/s²))*

The second integration of the moment yields the deformation curve of the timber beam, which represents the reaction of the system to the loads in State 1. The bending curve caused by the moments can be calculated using equation (32). It is not necessary to consider the shear deformation in the calculation of the prestress. The moment introduced by the adjustable prop does not have a continuous function over the beam length. Therefore, two equations or the *Föppel-symbol* are needed to describe the moment as a function of x over the whole length. In this work, the Föppel-symbol is not used because it is sufficient to calculate only half of the beam, due to the symmetry. For the sake of completeness, in this dissertation the equations for the whole length are presented.

$$w_{m,1}(x) = \iint \frac{M_{dl,1}(x) + M_{pr,1}(x)}{-\left(EI_{y,ti} + EI_{y,cf}\right)} dx\, dx \qquad (32)$$

Where:

$w_{m.1}$ (x) = deflection due to moments present in State 1 as a function of x
$M_{dl,1}$(x) = moment due to dead loads during reinforcement as a function of x equation (33)
$M_{pr,1}$(x) = moment introduced by the adjustable prop as a function of x (34)
$EI_{y,ti}$ = bending stiffness of the timber beam is regarded as constant over the beam length
$EI_{y,cf}$ = bending stiffness of the CFRP-lamella
x = position over the beam length

The functions of the moments in equation (32) are presented below in equations (33) and (34):

$$M_{dl,1}(x) = \frac{q_{dl,1} \cdot x(sp - x)}{2} \qquad (33)$$

Where:

$M_{dl,1}$(x) = moment due to dead loads during reinforcement as a function of x
$q_{dl,1}$(x) = distributed dead load during the reinforcement (State 1)
sp = span of the beam
x = position over the beam length

$$M_{pr,1}(x) = \begin{cases} \frac{-F_{pr}}{2} \cdot x & if\ 0 \le x \le \frac{sp}{2} \\ \frac{F_{pr}}{2} \cdot x - \frac{F_{pr} \cdot sp}{2} & if\ \frac{sp}{2} \le x \le sp \end{cases} \qquad (34)$$

Where:

$M_{pr,1}$(x) = moment introduced by the adjustable prop as a function of x
F_{pr} = force in the adjustable prop during the bonding
sp = span of the beam
x = position over the beam length

The insertion of equations (33) and (34) in equation (32) yields the deflection curve of State 1 (Figure 49).

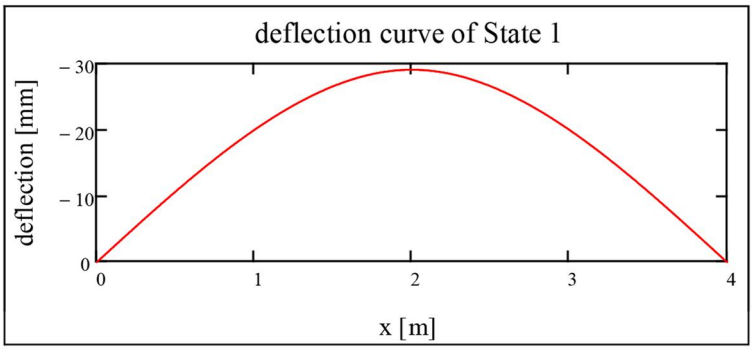

Figure 49: *Deflection curve due to the moments present in state one*

In State 2, the removal of the adjustable prop is considered. This is modelled by applying the force present in the prop during the bonding of the CFRP-lamella on the top of the beam (Figure 50).

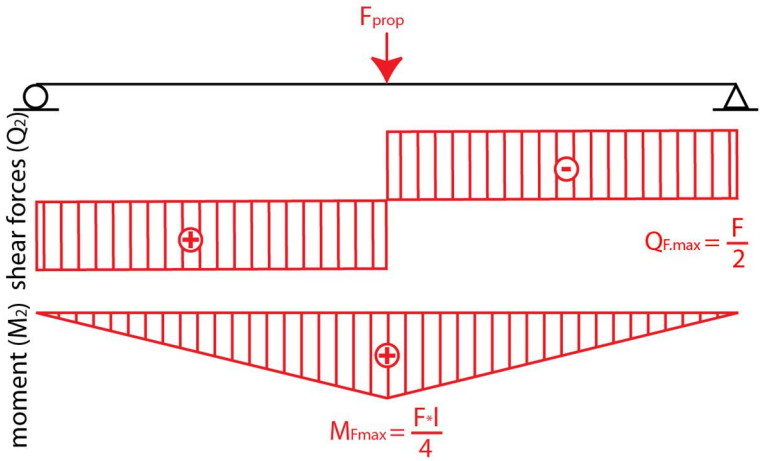

Figure 50: *State 2 in the calculation model, representing the effect of removing the prop after bonding the CRFP-lamella to the timber beam*

Again, the deflection curve is calculated. Because the CFRP-lamella is already bonded to the timber in this state, the bending stiffness of the composite section is used.

$$w_{m,2}(x) = \iint \frac{M_{pr,2}(x)}{-EI_{y,co}} dx\, dx \qquad (35)$$

Where:

$w_{m.2}(x)$ = deflection due to moments present in State 2 as a function of x
$M_{pr,2}(x)$ = moment induced by the removal of the adjustable prop as a function of x (36)
$EI_{y,co}$ = bending stiffness of the composite section is regarded as constant over the beam length
x = position over the beam length

$$M_{pr,2}(x) = -M_{pr,1}(x) = \begin{cases} \frac{F_{pr}}{2} \cdot x & if\ 0 \le x \le \frac{sp}{2} \\ \frac{F_{pr} \cdot sp}{2} - \frac{F_{pr}}{2} \cdot x & if\ \frac{sp}{2} \le x \le sp \end{cases} \qquad (36)$$

Where:

$M_{pr,2}(x)$ = moment induced by the removal of the adjustable prop as a function of x
$M_{pr,1}(x)$ = moment introduced by the in the height adjustable prop as a function of x (34)
F_{pr} = force in the height-adjustable prop during bonding
sp = span of the beam
x = position over the beam length

The bending stiffness of a section is given by the equation below:

$$EI_y = \int_A MOE(z) \cdot z^2 \, dA = \int_{-z_b}^{z_t} b(z) \cdot MOE(z) \cdot z^2 \, dz \qquad (37)$$

Where:

EI_y = bending stiffness of a section
A = area of the cross section
MOE(z) = modulus of elasticity of the material as a function of z
z = position along the height of the section
z_b = distance between the neutral axis and the bottom of the cross section
z_t = distance between the neutral axis and the top of the cross section
b(z) = width of the section as a function of z

The moment of inertia of the composite cross section ($I_{y,co}$) can be calculated using the sentence of Steiner (equation (38)). The different modulus of elasticity (MOE) of the materials is considered, using the factor n_i which is the ratio between the MOE of the material and the reference MOE used to calculate $I_{y,co}$. The multiplication of the moment of inertia ($I_{y,co}$) with the reference modulus of elasticity yields the bending stiffness without solving equation (37).

$$I_{y,co} = \frac{n_{ti} \cdot \left(I_{y,ti} \cdot A_{ti} \cdot {a_{ti}}^2\right) + n_{ad} \cdot \left(I_{y,ad} \cdot A_{ad} \cdot {a_{ad}}^2\right) + n_{cf} \cdot \left(I_{y,cf} \cdot A_{cf} \cdot {a_{cf}}^2\right)}{n_{ti} \cdot A_{ti} + n_{ad} \cdot A_{ad} + n_{cf} \cdot A_{cf}} \qquad (38)$$

Where:

$I_{y,co}$ = moment of inertia of the composite section
n_{ti} = ratio between the MOE of the timber and the reference MOE
$I_{y,ti}$ = moment of inertia of the timber cross section
A_{ti} = cross section area of the timber
a_{ti} = distance between the neutral axis of the timber section and the neutral axis of the composite section
n_{ad} = ratio between the MOE of the adhesive and the reference MOE
$I_{y,ad}$ = moment of inertia of the adhesive cross section
A_{ad} = cross section area of the adhesive
a_{ad} = distance between the neutral axis of the adhesive section and the neutral axis of the composite section
n_{cf} = ratio between the MOE of the CFRP-lamella and the reference MOE
$I_{y,cf}$ = moment of inertia of the CFRP-lamella
A_{cf} = cross section area of the CFRP-lamella
a_{cf} = distance between the neutral axis of the CFRP-lamella and the neutral axis of the composite section

The insertion of equations (36) and (38) in equation (35) yields the deflection curve of State 2.

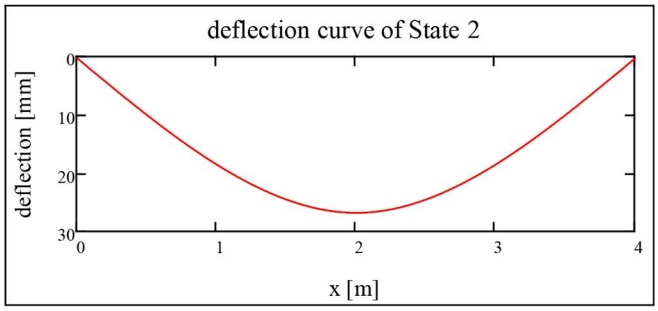

Figure 51: *Deflection curve due to the moments present in State 2*

The addition of the two deflection curves yields the deflection curve of the prestressed system after reinforcing (39) and removing the prop. This represents state 0 in the calculation model (Figure 52).

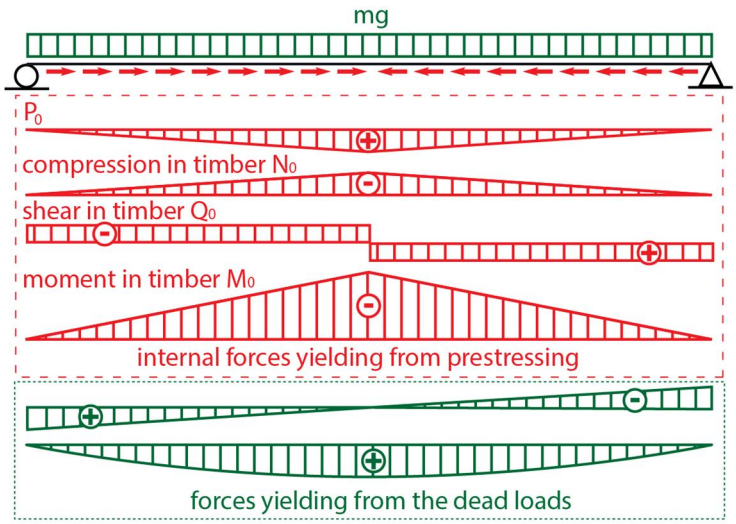

Figure 52: *State 0 in the calculation model represents the system with installed reinforcement and after removal of the prop. The internal forces due to P_0 in the CFRP and the adhesive are not shown. (mg = masse multiplied by the gravitation constant g (-9.81 m/s²)).*

$$w_{m,0}(x) = w_{m,1}(x) + w_{m,2}(x) = \iint \frac{M_{dl,1}(x) + M_{pr,1}(x)}{-(EI_{y,ti} + EI_{y,cf})} dx\, dx + \iint \frac{M_{pr,2}(x)}{-EI_{y,co}} dx\, dx \qquad (39)$$

Where:

$w_{m,0}$ (x) = deflection due to moments present in State 0 as a function of x
$w_{m,1}$ (x) = deflection due to moments present in State 1 as a function of x
$w_{m,2}$ (x) = deflection due to moments present in State 2 as a function of x
$M_{dl,1}$(x) = moment due to dead loads during reinforcement as a function of x (33)
$M_{pr,1}$(x) = moment introduced by the in the height-adjustable prop as a function of x (34)
$EI_{y,ti}$ = bending stiffness of the timber beam is regarded as constant over the beam length
$EI_{y,cf}$ = bending stiffness of the CFRP-lamella
$M_{pr,2}$(x) = moment induced by the removal of the adjustable prop as a function of x (36)
$EI_{y,co}$ = bending stiffness of the composite section is regarded as constant over the beams length
x = position over the beam length

The deflection after reinforcing can also be expressed as a function of the internal moment in the timber due to eccentric prestressing and of the moment due to the dead loads present during reinforcing (40).

$$w_{m,0}(x) = w_{m,P_0}(x) + w_{m,dl,1}(x) = \iint \frac{M_{P_0,ti}(x)}{-EI_{y,ti}} dx\, dx + \iint \frac{M_{dl,1}(x)}{-\left(EI_{y,ti} + EI_{y,cf}\right)} dx\, dx \qquad (40)$$

Where:

$w_{m,0}$ (x) = deflection due to moments present in State 0 as a function of x
$w_{m,Po}$ (x) = deflection due to internal moment due to prestressing as a function of x
$w_{m,dl,1}$ (x) = deflection due to moments present in State 2 as a function of x
$M_{dl,1}$(x) = moment due to dead loads during reinforcement as a function of x (33)
$M_{Po,ti}$(x) = internal moment in timber due to prestressing as a function of x
$EI_{y,cf}$ = bending stiffness of the CFRP-lamella
$EI_{y,ti}$ = bending stiffness of the timber beam is regarded as constant over the beam length
x = position over the beam length

In equation (39), the moment due to the dead loads present during reinforcing can be separated, which yields equation (41).

$$w_{m,0}(x) = \iint \left(\frac{M_{pr,1}(x)}{-\left(EI_{y,ti} + EI_{y,cf}\right)} + \frac{M_{pr,2}(x)}{-EI_{y,co}} \right) dx\, dx + \iint \frac{M_{dl,1}(x)}{-\left(EI_{y,ti} + EI_{y,cf}\right)} dx\, dx \qquad (41)$$

Where:

$w_{m,0}$ (x) = deflection due to moment in State 0 as a function of x
$M_{dl,1}$(x) = moment due to dead loads during reinforcement as a function of x (33)
$M_{pr,1}$(x) = moment introduced by the adjustable prop as a function of x (34)
$EI_{y,ti}$ = bending stiffness of the timber beam is regarded as constant over the beams length
$EI_{y,cf}$ = bending stiffness of the CFRP-lamella
$M_{pr,2}$(x) = moment induced by the removal of the adjustable prop as a function of x (36)
$EI_{y,co}$ = bending stiffness of the composite section is regarded as constant over the beam length
x = position over the beam length

Equation (40) can be set equal with equation (41), yielding equation (42), which is the deformation due to the internal moment yielding from the eccentric prestressing.

$$\iint \frac{M_{P_0,ti}(x)}{-EI_{y,ti}} dx\, dx = \iint \left(\frac{M_{pr,1}(x)}{-\left(EI_{y,ti} + EI_{y,cf}\right)} + \frac{M_{pr,2}(x)}{-EI_{y,co}} \right) dx\, dx = w_{m,P_0}(x) \qquad (42)$$

Where:

$M_{Po,ti}$(x) = internal moment in timber due to prestressing as a function of x
$EI_{y,ti}$ = bending stiffness of the timber beam is regarded as constant over the beam length
$M_{pr,1}$(x) = moment introduced by the adjustable prop as a function of x (34)
$M_{pr,2}$(x) = moment induced by the removal of the adjustable prop as a function of x (36)
$EI_{y,cf}$ = bending stiffness of the CFRP-lamella
$EI_{y,co}$ = bending stiffness of the composite section is regarded as constant over the beam length
$w_{m,Po}$ (x) = deflection due to internal moment due to prestressing as a function of x
x = position over the beam length

Using equations (34) and (36), the deflection curve due to the moment yielding from the eccentric prestressing ($w_{m,Po}$) can be calculated (43).

$$w_{m,Po}(x) = \begin{cases} \dfrac{F_{pr} \cdot \left(EI_{y,ti} + EI_{y,cf} - EI_{y,co}\right)(3sp^2 \cdot x - 4x^3)}{48 \cdot EI_{y,co} \cdot \left(EI_{y,ti} + EI_{y,cf}\right)} & if\ 0 \le x \le \dfrac{sp}{2} \\ \dfrac{F_{pr} \cdot \left(EI_{y,co} - EI_{y,ti} - EI_{y,cf}\right)(sp^3 - 9sp^2 \cdot x + 12sp \cdot x^2 - 4x^3)}{48 \cdot EI_{y,co} \cdot \left(EI_{y,ti} + EI_{y,cf}\right)} & if\ \dfrac{sp}{2} \le x \le sp \end{cases} \qquad (43)$$

Where:

$w_{m,Po}(x)$ = deflection due to moment yielding from eccentric prestressing as a function of x (Figure 53)
F_{pr} = force in the adjustable prop during the bonding
sp = span of the beam
$EI_{y,ti}$ = bending stiffness of the timber beam is regarded as constant over the beam length
$EI_{y,cf}$ = bending stiffness of the CFRP-lamella
$EI_{y,co}$ = bending stiffness of the composite section is regarded as constant over the beam length
x = position over the beam length

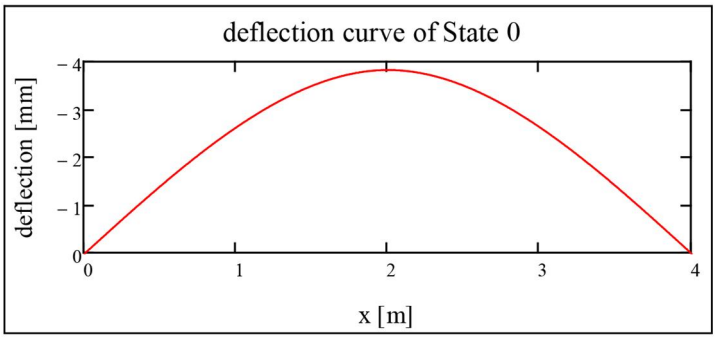

Figure 53: *Deflection curve due to the moment yielding from eccentric prestressing*

The second deviation of the deflection curve yields the negative moment divided by the bending stiffness. This allows the calculation of the internal moment in timber yielding from the eccentric prestressing ($M_{Po,ti}$). Due to the fact that the moment is an internal force of the prestressed beam, the bending stiffness of the timber beam is used in equation (44).

$$M_{P_0,ti}(x) = \frac{d^2}{dx^2} - w_{m,P_0}(x) \cdot EI_{y,ti} \qquad (44)$$

Where:

$M_{Po,ti}(x)$ = internal moment in timber yielding from eccentric prestressing as a function of x (Figure 54)
$w_{m,Po}$ (x) = deflection due to internal moment yielding from eccentric prestressing as a function of x
$EI_{y,ti}$ = bending stiffness of the timber beam is regarded as constant over the beams length
x = position over the beam length

The moment yielding from the eccentric prestressing equals the prestress force multiplied by the eccentricity (Figure 54).

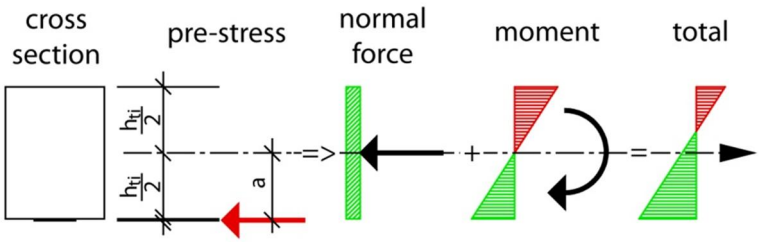

Figure 54: *Reaction of the timber to the eccentric prestressing*

The prestress force shown in the above figure is distributed between the CFRP-lamella and the adhesive. The force is not distributed evenly between the two materials but in ratio to the tensile stiffness (area multiplied by the MOE). The total prestress force can be determined using equation (45).

$$P_0(x) = \frac{M_{P_0,ti}(x)}{-a} = \begin{Bmatrix} \frac{EI_{y,ti} \cdot F_{pr} \cdot x \cdot \left(EI_{y,ti} + EI_{y,cf} - EI_{y,co}\right)}{2 \cdot a \cdot EI_{y,co} \cdot \left(EI_{y,ti} + EI_{y,cf}\right)} & if\ 0 \le x \le \frac{sp}{2} \\ \frac{EI_{y,ti} \cdot F_{pr} \cdot (sp - x) \cdot \left(EI_{y,ti} + EI_{y,cf} - EI_{y,co}\right)}{2 \cdot a \cdot EI_{y,co} \cdot \left(EI_{y,ti} + EI_{y,cf}\right)} & if\ \frac{sp}{2} \le x \le sp \end{Bmatrix} \quad (45)$$

Where:

$P_0(x)$ = addition of the prestress force in the CFRP-lamella and adhesive as a function of x
$M_{Po,ti}(x)$ = internal moment in timber yielding from eccentric prestressing as a function of x (44)
a = eccentricity of the prestress force (Figure 54 and equation (46))
F_{pr} = force in the adjustable prop during the bonding
sp = span of the beam
$EI_{y,ti}$ = bending stiffness of the timber beam is regarded as constant over the beam length
$EI_{y,cf}$ = bending stiffness of the CFRP-lamella
$EI_{y,co}$ = bending stiffness of the composite section is regarded as constant over the beam length
x = position over the beam length

The eccentricity of the total prestress force can be determined using equation (46).

$$a = \frac{h_{ti}}{2} + \frac{EA_{cf} \cdot \left(h_{ad} + \frac{h_{cf}}{2}\right) + EA_{ad} \cdot \frac{h_{ad}}{2}}{EA_{cf} + EA_{ad}} \quad (46)$$

Where:

a = eccentricity of the prestress force (Figure 54)
h_{ti} = height of the timber beam
EA_{cf} = MOE of the CFRP-lamella multiplied by the cross section area of the CFRP-lamella
h_{cf} = height of the CFRP-lamella
EA_{ad} = MOE of the adhesive multiplied by the cross section area of the adhesive layer
h_{ad} = height of the adhesive layer

The prestress in the CFRP-lamella can be determined using equation (47), for the determination of the prestress force in the adhesive. The tension stiffness of the CFRP-lamella (EA_{cf}) has to be replaced by the tension stiffness of the adhesive (EA_{ad}) in the numerator of equation (47).

$$P_{0,cf}(x) = \frac{P_0(x) \cdot EA_{cf}}{EA_{cf} + EA_{ad}} \tag{47}$$

Where:

$P_{0,cf}(x)$ = prestress force in the CFRP-lamella as a function of x
$P_0(x)$ = addition of the prestress force in the CFRP-lamella and adhesive as a function of x
EA_{cf} = MOE of the CFRP-lamella multiplied by the cross section area of the CFRP-lamella
EA_{ad} = MOE of the adhesive multiplied by the cross section area of the adhesive layer

The first deviation of the moment due to eccentric prestressing ($M_{Po,ti}(x)$) yields the shear force due to prestressing in the timber (48).

$$Q_{P_0,ti}(x) = \frac{d}{dx} M_{P_0,ti}(x) = \frac{d^3}{dx^3} - w_{m,P_0}(x) \cdot EI_{y,ti} = \begin{Bmatrix} \frac{EI_{y,ti} \cdot F_{pr} \cdot (EI_{y,ti} + EI_{y,cf} - EI_{y,co})}{2 \cdot EI_{y,co} \cdot (EI_{y,ti} + EI_{y,cf})} & if\ 0 \le x \le \frac{sp}{2} \\ \frac{EI_{y,ti} \cdot F_{pr} \cdot (EI_{y,co} - EI_{y,ti} - EI_{y,cf})}{2 \cdot EI_{y,co} \cdot (EI_{y,ti} + EI_{y,cf})} & if\ \frac{sp}{2} \le x \le sp \end{Bmatrix} \tag{48}$$

Where:

$Q_{Po,ti}(x)$ = internal shear force due to prestressing as a function of x
$M_{Po,ti}(x)$ = internal moment in timber yielding from eccentric prestressing as a function of x
$w_{m,Po}(x)$ = deflection due to internal moment yielding from eccentric prestressing as a function of x
F_{pr} = force in the adjustable prop during the bonding
sp = span of the beam
$EI_{y,ti}$ = bending stiffness of the timber beam is regarded as constant over the beam length
$EI_{y,co}$ = bending stiffness of the composite section is regarded as constant over the beam length
$EI_{y,cf}$ = bending stiffness of the CFRP-lamella
x = position over the beam length

The equations (44), (45) and (48) allow the determination of the stresses in the timber beam due to eccentric prestressing. The stresses in the CFRP-lamella due to prestressing can be approximated by dividing the prestress force ($P_0(x)$) by the area of the CFRP-lamella. In order to get the exact stress distribution in the CFRP, the bending and shear stress due to the deflection also need to be considered. Furthermore, the distribution of the prestress force between the adhesive and CFRP needs to be considered. In order to get the bending stress in the CFRP, the second derivation deflection curve in State 1 has to be taken. The equations to calculate the two internal forces present in the CFRP-lamella are presented in the equations (49) and (50) below. When designing a timber structure, the shear force and the moment in the CFRP-lamella yielding from the deflection at State 0 can be neglected.

$$M_{P_0,cf}(x) = \frac{d^2}{dx^2} - w_{m,P_0}(x) \cdot EI_{y,cf} \tag{49}$$

Where:

$M_{Po.cf}(x)$ = internal moment in the CFRP-Lamella yielding from eccentric prestressing as a function of x
$w_{m,Po}(x)$ = deflection due to internal moment yielding from eccentric prestressing as a function of x

$EI_{y,cf}$ = bending stiffness of the CFRP-lamella
x = position over the beam length

$$Q_{P_0,cf}(x) = \frac{d}{dx} M_{P_0,cf}(x) = \frac{d^3}{dx^3} - w_{m,P_0}(x) \cdot EI_{y,cf} \qquad (50)$$

Where:

$Q_{Po,cf}(x)$ = internal shear force in the CFRP-lamella yielding from eccentric prestressing as a function of x
$M_{Po,cf}(x)$ = internal moment in the CFRP-lamella yielding from eccentric prestressing as a function of x
$w_{m,Po}$ (x) = deflection due to internal moment yielding from eccentric prestressing as a function of x
$EI_{y,cf}$ = bending stiffness of the CFRP-lamella
x = position over the beam length

In order to get the exact stress present at State 0 in the adhesive, the tension force due to prestressing (equation (47) using EA_{ad} in the numerator) and the bending stress due to deflection have to be considered. The bending stress due to deflection in the adhesive can be determined using the second derivation of difference in the deflection curve in State 2 and State 0.

The camber yielding from prestressing can be calculated by adding the deformation due to the moment and shear force yielding from the eccentric prestressing in the timber. The permanent deflection prior to intervention has to be considered in order to get the camber after reinforcing. The part due to the moment can be calculated using equation (43). The deformation due to the shear force yielding from eccentric prestressing can be determined using equation (51).

$$w_{s.Po}(x) = \int \frac{Q_{P_0,ti}(x)}{GA_{ti}} dx = \frac{M_{P_0,ti}(x)}{GA_{ti}}$$
$$= \begin{cases} \dfrac{EI_{y,ti} \cdot F_{pr} \cdot x \cdot \left(EI_{y,ti} + EI_{y,cf} - EI_{y,co}\right)}{2 \cdot EI_{y,co} \cdot GA_{ti} \cdot \left(EI_{y,ti} + EI_{y,cf}\right)} & if\ 0 \le x \le \dfrac{sp}{2} \\ \dfrac{EI_{y,ti} \cdot F_{pr} \cdot (sp - x) \cdot \left(EI_{y,ti} + EI_{y,cf} - EI_{y,co}\right)}{2 \cdot EI_{y,co} \cdot GA_{ti} \cdot \left(EI_{y,ti} + EI_{y,cf}\right)} & if\ \dfrac{sp}{2} \le x \le sp \end{cases} \qquad (51)$$

Where:

$Q_{Po,ti}(x)$ = internal shear force due to prestressing as a function of x
GA_{ti} = shear stiffness of the timber section (regarded as constant over the beam length)
$w_{m,Po}$ (x) = deflection due to internal moment yielding from eccentric prestressing as a function of x
$M_{Po,ti}(x)$ = internal moment in timber yielding from eccentric prestressing as a function of x
F_{pr} = force in the adjustable prop during the bonding
sp = span of the beam
$EI_{y,ti}$ = bending stiffness of the timber beam is regarded as constant over the beam length
$EI_{y,cf}$ = bending stiffness of the CFRP-lamella
$EI_{y,co}$ = bending stiffness of the composite section is regarded as constant over the beam length
x = position over the beam length

The contribution of the shear deformation due to eccentric prestressing to the camber is 4.2% and not significant for engineering purposes compared to the variation of the elastic properties in timber.

3.2 Ultimate-limit state

In the Swiss Timber Construction Standard [51], prestressing is not considered. In the Swiss Basics of Construction Standard [52], it is recommended to apply the guidelines of the Swiss Concrete Construction Standard SIA 262 [50] to all other materials. These guidelines recommend add the characteristic value of the prestress to the system resistance. For the method presented, it is more convenient to add the characteristic stresses due to eccentric prestressing due to the design loads (the direction of the stresses needs to be considered). The sum can be compared to the design values determined in the Swiss Timber Construction Standard [51].

Due to the different creep behaviour of the materials used in the composite section, the long-term effects lead to load redistribution within the cross section. Therefore, the verification of the cross section has to be done twice. Once at time = 0, which represents the time when the timber beam is reinforced, and once at time = ∞, which represents the time when the creeping is terminated.

3.2.1 Short-term design

Figure 55 shows the forces that need to be considered when verifying the resistance of the timber section in the composite beam.

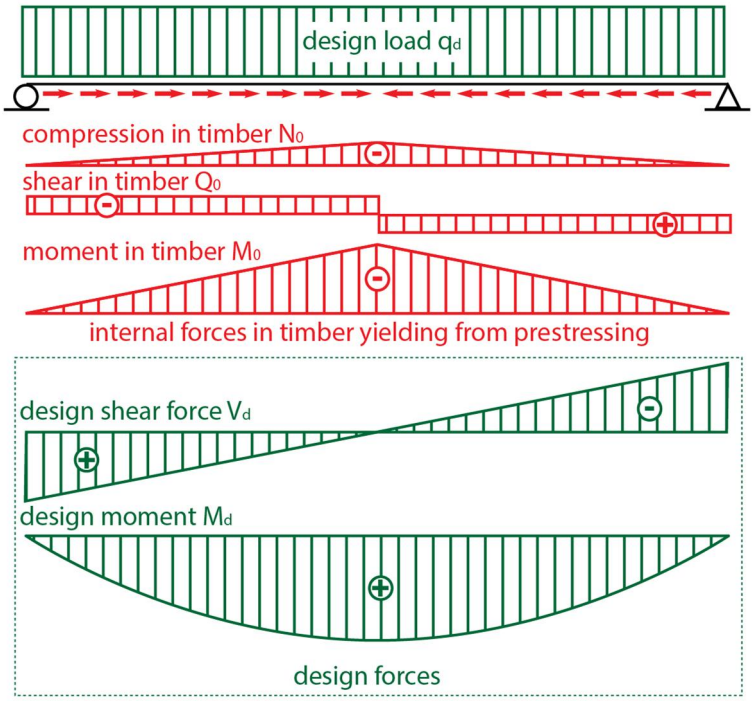

Figure 55: *Prestressed system with design loads. The forces in the CFRP and the adhesive are not shown.*

Adding the internal forces does not yield the correct result. For the design loads, the bending stiffness of the composite section has to be taken into account, and for the internal forces only the bending stiffness of the timber section is taken. The summation of the normal stresses (stresses yielding from moments and normal forces) yields the following stress dis-

tribution at the bottom and top face of the timber over the beam length (Figure 56 and Figure 57).

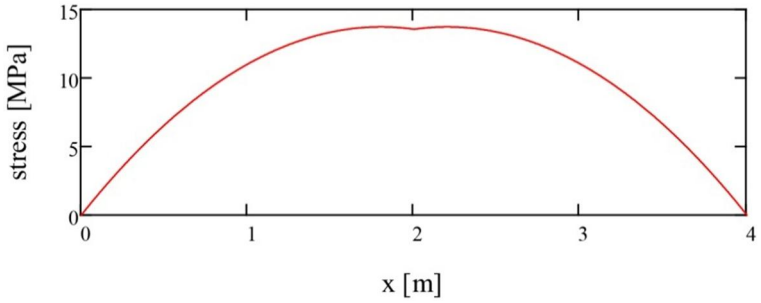

Figure 56: *Tension stress distribution at the lower face of the timber over the length of the beam*

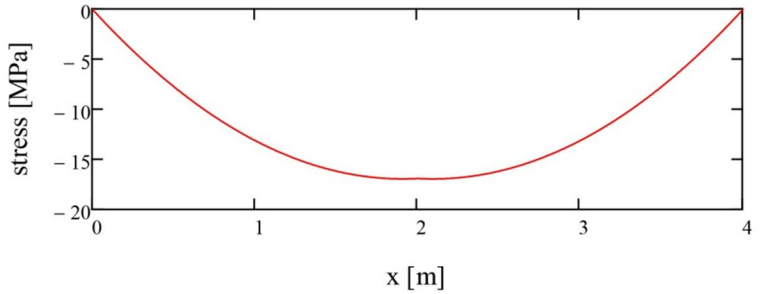

Figure 57: *Compression stress distribution at the top face of the timber* over the length of the beam

For single-span beams with distributed loads (commonly found in buildings), the maximal-design moment (M_d) is in the midspan of the beam, and the maximal-design shear force (V_d) is near the support. The Swiss Timber Construction Standard [51] recommends using the shear force, which is the height of a beam, apart from the support. After adding the stresses from prestressing and design loads, the maximal-shear stress is still near the support but the maximal-bending stress is no longer in midspan (Figure 56 and Figure 57). Due to the symmetry, only one of the two peaks needs to be calculated. The locations of the maximal-tension stress in the timber can be determined using equation (52).

$$x_{\sigma,d,0,max} = \frac{sp}{2} \pm \frac{F_{Pr} \cdot \left(EI_{y,co} - EI_{y,ti} - EI_{y,cf}\right)}{2 \cdot q_d \cdot z_{b,ti} \cdot \left(EI_{y,ti} + EI_{y,cf}\right)} \cdot \left(\frac{h_{ti}}{2} + \frac{I_{y,ti}}{a \cdot A_{ti}}\right) \qquad (52)$$

Where:

$x_{\sigma,d,0,max}$ = location of the maximal-tension stress in the timber, based on the loading rules of the SIA standard
sp = span of the beam
F_{pr} = force in the adjustable prop during the bonding
$EI_{y,co}$ = bending stiffness of the timber beam is regarded as constant over the beam length
$EI_{y,ti}$ = bending stiffness of the timber beam is regarded as constant over the beam length
$EI_{y,cf}$ = bending stiffness of the CFRP-lamella
q_d = distributed design load
$z_{b.ti}$ = distance between the neutral axis of the composite section and the lower face of the timber
h_{ti} = height of the timber beam

$I_{y,ti}$ = moment of inertia in the timber cross section
a = eccentricity of the prestress force (Figure 54 and equation (46))
A_{ti} = cross section area of the timber

The building codes require verifying the compression and the tension stress resulting from bending. In this particular case, the Swiss Timber Construction Standard (SIA 265) [51] recommends considering the bending in combination with the compression resulting from prestressing. This verification is done using equation (53) [51].

$$\left(\frac{\sigma_{c,0,d}(x)}{f_{c,0,d}}\right)^2 + \frac{\sigma_{m,d}(x)}{f_{m,d}} \leq 1 \qquad (53)$$

Where:

$\sigma_{c,0,d}(x)$ = design stress in compression parallel to the grain as a function of x
$f_{c,0,d}$ = design value in compression parallel to the grain according to SIA 265 [51]
$\sigma_{m,d}(x)$ = design stress in bending as a function of x
$f_{m,y,d}$ = design value in bending according to SIA 265 [51]

The verification of the compression side of a reinforced bending beam leads in timber construction to a very conservative approach. The experiments described in Chapter 4 as well as by other authors [14-17, 19, 20, 23, 94, 98, 100, 114] show that a beam reinforced with one CRFP-lamella fails because of tension failure. Furthermore, a violation of the design value at the compression side leads to crushing of the timber fibres and larger deformation but not to a complete failure, which is similar to the behaviour of reinforced concrete. Eurocode 5 [27] takes into consideration the ductile behaviour of timber in compression. Unfortunately, this factor is not explicitly mentioned in the Swiss standard, however. Therefore, the author suggests using the tension stress at the bottom of the timber to verify the reinforced timber beam. The verification is done using equation (54).

$$\frac{\sigma_{d,b,ti}(x)}{f_{m,d}} \leq 1 \qquad (54)$$

Where:

$\sigma_{d,b,ti}(x)$ = design normal stress at the bottom of the timber section due to prestressing and loading as a function of x
$f_{m,d}$ = design value in bending according to SIA 265 [51]

The use of equation (54) leads to a significantly higher design-bending capacity than the use of the conservative method recommended by SIA 265 [51]. Figure 58 shows the wide difference between the two methods of verifying a reinforced timber beam.

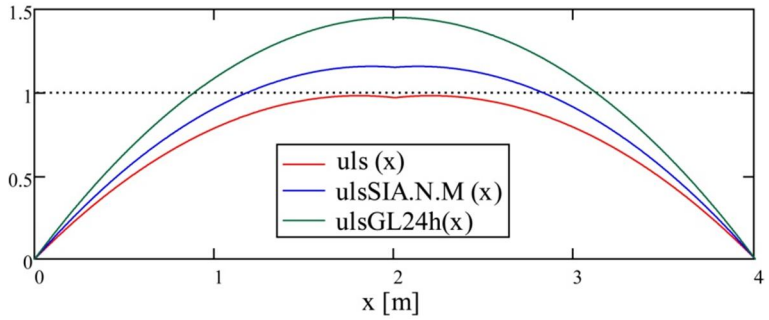

Figure 58: *Results of equation (53) (**blue**) and (54) (**red**) for a reinforced beam at time = 0 (160mm x 120mm GL24h reinforced with one 1.2mm-thick, 50mm-wide CFRP-lamella); unreinforced glulam beam (160mm x 120mm) (**green**). A value of one means the design capacity of the beam is reached. (All beams are equally loaded.)*

The location of the maximal-shear stress does not change over the length of the beam; however, the neutral axis of the section does change due to reinforcing, and therefore stress distribution along the height of the beam as well. The shear stress distribution is usually calculated according to the neutral fibre of the beam. In order to be able to add the stress due to prestressing to the stresses due to design loads, the shear stress distribution in the timber due to prestressing is determined with reference to the neutral axis of the composite section. The summation of the shear stresses yields equation (55).

$$\tau_{d,0}(z) = \frac{q_d \cdot S_{co}(z) \cdot \left(\frac{sp}{2} - h_{ti}\right)}{b_{co}(z) \cdot I_{y,co}} + \left\{ \begin{array}{ll} \dfrac{F_{pr} \cdot MOE_{ti} \cdot \left(EI_{y,ti} + EI_{y,cf} - EI_{y,co}\right) \cdot (z - z_t) \cdot (h_{ti} + z - z_t)}{4 \cdot EI_{y,co} \cdot \left(EI_{y,ti} + EI_{y,cf}\right)} & if - z_{b,ti} \le z \le z_t \\ 0 & if - z_b \le z \le -z_{b,ti} \end{array} \right\} \quad (55)$$

Where:

$\tau_{d,ti}$ (z) = design shear stress in timber as a function of z
F_{pr} = force in the adjustable prop during the bonding
$EI_{y,ti}$ = bending stiffness of the timber beam is regarded as constant over the beam length
$EI_{y,co}$ = bending stiffness of the composite section is regarded as constant over the beam length
$EI_{y,cf}$ = bending stiffness of the CFRP-lamella
MOE_{ti} = modulus of elasticity of the timber
h_{ti} = height of the timber section
z_t = distance between the neutral axis and the top of the composite section
$z_{b,ti}$ = distance between the neutral axis of the composite section and the bottom of the timber section
q_d = distributed design loads
$S_{co}(z)$ = = first moment of area of the composite section as a function of z
sp = span of the beam
$b_{co}(z)$ = breadth of the composite section as a function of z
$I_{y,co}$ = moment of inertia of the composite section
z_b = distance between the neutral axis and the bottom of the composite section
z = position over the beam height

Equation (55) yields the following shear stress distribution over the composite beam height (Figure 59).

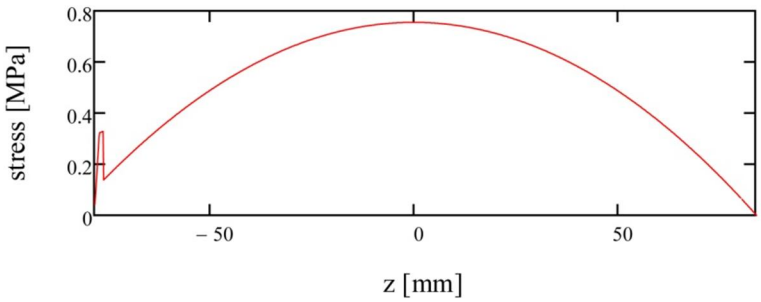

Figure 59: *Design shear-stress distribution over the composite beam height at time zero.*

The locus of the maximal-design shear stress over the beam height can be determined using equation (56) below. The theoretical maximum shear stress is located over the support. For determining the locus of the theoretical maximum, sp, instead of (sp - $2h_{ti}$) has to be used in the last term of the denominator.

$$z_{\tau,d,0,max} = \frac{F_{Pr} \cdot (h_{ti} - 2z_t) \cdot \left(EI_{y,co} - EI_{y,ti} - EI_{y,cf}\right)}{2 \cdot F_{Pr} \cdot \left(EI_{y,ti} + EI_{y,cf} - EI_{y,co}\right) + 2 \cdot q_d \cdot \left(EI_{y,ti} + EI_{y,cf}\right) \cdot (sp - 2h_{ti})} \qquad (56)$$

Where:

$z_{\tau,d,0,max}$ = location of the maximal-shear stress over the beam height
F_{pr} = force in the adjustable prop during the bonding
h_{ti} = height of the timber beam
z_t = distance between the neutral axis and the top of the composite section
$EI_{y,co}$ = bending stiffness of the timber beam is regarded as constant over the beam length
$EI_{y,ti}$ = bending stiffness of the timber beam is regarded as constant over the beam length
q_d = distributed design load

The simplified equation presented below (57) leads to a slight underestimation of the maximal-design shear stress; in the presented example it as less as 0.02%. This error is not significant for structural design purposes.

$$\tau_{d,simply} = \frac{Q_d(x = h_{ti}) \cdot S_{co}(0)}{b_{ti} \cdot I_{y,co}} + 1.5 \cdot \frac{Q_{P,ti}(x = h_{ti})}{A_{ti}} \qquad (57)$$

Where:

$Q_d(x = h_{ti})$ = design shear force as relevant for designing a timber structure along the SIA 265 [51]
b_{ti} = width of the timber section
S_{co} (0) = first moment of area of the composite section at time = 0 at the position of the neutral axis
$I_{y,co}$ = moment of inertia of the composite section at time = 0 can be calculated using equation (38) and $n_{ti\infty}$ instead of n_{ti}
$Q_{P,ti}(x = h_{ti})$ = shear force in timber yielding from eccentric prestressing as relevant for designing a timber structure along the SIA 265 [51]
h_{ti} = height of the timber cross section
A_{ti} = area of the timber cross section

The Swiss standard for externally-bonded reinforcement (SIA 166) [11] recommends verifying the anchorage zone and the tension stress in the reinforcement. The anchorage zone of a beam reinforced with the camber method is equal to the length of the reinforcement, and therefore not critical. The design stress in the CFRP-lamella is determined by adding the stresses yielding from prestressing to the stresses yielding from the design forces.

$$\sigma_{d,0,cf}(x) = n_{cf} \cdot \frac{M_d(x) \cdot z_b}{I_{y,co}} + \frac{P_{0,cf}(x)}{A_{cf}} + \frac{M_{P_0,cf}(x) \cdot h_{cf}}{2 \cdot I_{y,cf}} \quad (58)$$

Where:

$\sigma_{d,0,cf}(x)$ = design stress in CFRP-lamella at time = 0 as a function of x
x = position over the length of the beam
n_{cf} = ratio between the MOE of the CFRP-lamella and the reference MOE
$M_d(x)$ = design moment as a function of x
z_b = distance between the neutral axis and the bottom of the composite section
$I_{y,co}$ = moment of inertia of the composite section
$P_{0,cf}(x)$ = prestress force in the CFRP-lamella as a function of x
A_{cf} = area of the CFRP-lamella
$M_{Po.cf}(x)$ = moment in CFRP-lamella yielding from prestressing
h_{cf} = height of the CFRP-lamella
$I_{y,cf}$ = moment of inertia of the composite section

The last term in equation (58) represents the stress yielding from the camber, due to eccentric prestressing. Its contribution is quite small (0.3 MPa for the calculated example) and not significant. The maximum-tension stress in the CFRP is located at midspan.

3.2.2 Long-term design

Long-term loads lead to creep in timber, whereas CFRP-lamellas and the epoxy adhesive used are not prone to creep. In designing timber structures, creep is regarded as an increase of strain and usually considered only in the service-limit state. In a composite composed of materials with different creep behaviour, the creeping leads to a strain increase in all materials, and therefore in case of different creep behaviour, to load redistribution over time.

In cases of retrofitting, the load history must be taken into account for long-term design and calculation. According to Navi and Heger [81], creep can be regarded as linear viscoelastic behaviour for loads up to 40% of the short-term load-bearing capacity. Therefore, the long-term loads that were already present in the timber beam prior to intervention[1] do not contribute to the long-term effects that occur after intervention.

The creep-relevant loads in buildings are the dead loads, the near-permanent part of the live loads and the forces due to prestressing. Normally, creep leads to an elevated strain. On the lower side of the timber where the CFRP-lamella is bonded to the beam strain, differences in the timber also lead to strain differences in the CFRP, which leads to a difference in the forces present in the CFRP. The creep due to prestressing leads to an increase of the compres-

[1] It is assumed that the creep of the long-term loads present prior to intervention has already reached its limit at the time the retrofitting takes place, which is regarded as time = 0.

sion strain in the timber, and therefore leads to a reduction of the prestress. This reduction reduces the stress in the timber, and therefore also reduces the strain. The internal forces must always be in equilibrium. The permanent and near-permanent loads also lead to creep in the timber. Therefore, the strain on the tension side of the timber increases, leading to higher strain and stress in the CFRP-lamella, a load redistribution from the timber to the CFRP, and a movement of the neutral axis of the section. This shift is only valid for additional permanent and near-permanent loads[2]. Therefore, the composite section has two different neutral axes: one for creep-relevant external loads and one for the other external loads. Again, the action and the reaction of the composite beam are always in equilibrium. The two effects described above take place at the same time and place but move in opposite directions. Figure 60 below presents a sketch of the different creeping strains present in a prestressed timber beam. The long-term prestress force (P_∞) can be expressed by equation (59) below.

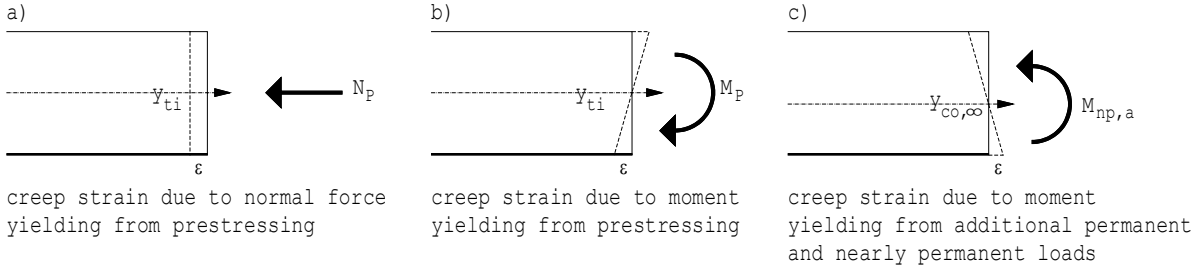

Figure 60: *Systematic sketch of the creep-relevant forces and the yielding strain of the composite section*

$$P_\infty(x) = P_0(x) + \Delta P_\infty(x) \qquad (59)$$

Where:

$P_\infty(x)$ = prestress force present in the system after the long-term effect have taken place (time = ∞) as a function of x

$P_0(x)$ = prestress force after removing the adjustable prop (time = 0) as a function of x (equation (45))

$\Delta P_\infty(x)$ = difference in prestress force due to long-term effects as a function of x

In order to determine the long-term prestress force, the equilibrium of forces in the prestressed system at time = ∞ has to be calculated. In this calculation, only the creep relevant loads for the prestressed beam need to be considered. Therefore, in the equations below, only the prestress force, the additional permanent and near-permanent loads are considered.

The stress present in the timber at the interface with the adhesive due to additional creep relevant loads at time = ∞ ($\sigma_{\infty,b,ti}$) can be determined using equation (60) - (63).

$$\sigma_{\infty,b,ti}(x) = \sigma_{P_\infty,b,ti}(x) + \sigma_{M_{np,a},b,ti}(x) \qquad (60)$$

[2] Additional permanent and near-permanent loads stand for the difference between those permanent and near-permanent loads that are present in the system prior to intervention and after renovation.

$$\sigma_{P_\infty,b,ti}(x) = \frac{-\left(P_0(x) + \Delta P_\infty(x)\right)}{A_{ti}} + \frac{-\left(P_0(x) + \Delta P_\infty(x)\right) \cdot a \cdot \frac{h_{ti}}{2}}{I_{y,ti}} \quad (61)$$

$$\sigma_{M_{np,a},b,ti}(x) = n_{ti\infty} \frac{\left(\psi_2 \cdot M_{ll}(x) + M_{dl}(x) - M_{np,pi}(x)\right) \cdot z_{b,ti\infty}}{I_{y,co\infty}} \quad (62)$$

$$n_{ti\infty} = \frac{MOE_{ti}}{(1+\varphi) \cdot MOE_{ref}} \quad (63)$$

Where:

$\sigma_{\infty,b,ti}(x)$ = stress due to additional creep relevant loads at the bottom of the timber at time = ∞ as a function of x

$\sigma_{P\infty,b,ti}(x)$ = stress due to prestressing at the bottom of the timber at time = ∞ as a function of x

$\sigma_{Mnp,a,b,ti}(x)$ = stress due to additional permanent and nearly permanent loads at the bottom of the timber at time = ∞ as a function of x

$P_0(x)$ = prestress force after removing the adjustable prop (time = 0) as a function of x (equation (45))

$\Delta P_\infty(x)$ = difference in prestress force due to long-term effects as a function of x

A_{ti} = area of the timber cross section

a = eccentricity of the prestress force (Figure 54 and equation (46))

h_{ti} = height of the timber

$I_{y,ti}$ = moment of inertia of the timber section

$n_{ti\infty}$ = ratio between the long-term MOE of the timber and the reference MOE

ψ_2 = reduction factor for the near-permanent value of a variable action as defined in SIA 260 [52]

$M_{ll}(x)$ = moment due to live loads after intervention as a function of x

$M_{dl}(x)$ = moment due to dead loads after intervention as a function of x

$M_{np,pi}(x)$ moment due to dead loads prior intervention as a function of x

$z_{b,ti\infty}$ = distance between the neutral axis of the composite section at time = ∞ and the bottom of the timber

$I_{y,co\infty}$ = moment of inertia of the composite section at time = ∞ can be calculated using equation (38) and $n_{ti\infty}$ instead of n_{ti}

MOE_{ti} = modulus of elasticity of the timber

φ = creep factor

MOE_{ref} = reference MOE

Dividing the stress by the modulus of elasticity yields the elastic strain. Multiplying the elastic strain with the creep factor (φ) yields the creep strain (ε_φ); the sum of the elastic strain and the creep strain is the total strain after creeping at time = ∞. The creep strain at the lower face of the timber can be calculated using equations (64) - (67).

$$\varepsilon_{\varphi,b,ti}(x) = \varepsilon_{\varphi,N_{P\infty},b,ti}(x) + \varepsilon_{\varphi,M_{P\infty},b,ti}(x) + \varepsilon_{\varphi,M_{np,a},b,ti}(x) \quad (64)$$

$$\varepsilon_{\varphi,N_{P\infty},b,ti}(x) = \varphi \cdot \frac{-\left(P_0(x) + \Delta P_\infty(x)\right)}{A_{ti} \cdot MOE_{ti}} \quad (65)$$

$$\varepsilon_{\varphi,M_{P\infty},b,ti}(x) = \varphi \cdot \frac{-\left(P_0(x) + \Delta P_\infty(x)\right) \cdot a \cdot \frac{h_{ti}}{2}}{I_{y,ti} \cdot MOE_{ti}} \quad (66)$$

$$\varepsilon_{\varphi,M_{np,a},b,ti}(x) = \varphi \cdot n_{ti\infty} \cdot \frac{\left(\psi_2 \cdot M_{ll}(x) + M_{dl}(x) - M_{np,pi}(x)\right) \cdot z_{b,ti\infty}}{I_{y,co,\infty} \cdot MOE_{ti}} \quad (67)$$

Where:

$\varepsilon_{\varphi,b,ti}(x)$ = strain due to additional creep relevant loads at the bottom of the timber at time = ∞ as a function of x

$\varepsilon_{\varphi,NP\infty,b,ti}(x)$ = strain due to the normal force yielding from prestressing at the bottom of the timber at time = ∞ as a function of x

$\varepsilon_{\varphi,MP\infty,b,ti}(x)$ = strain due to the moment yielding from prestressing at the bottom of the timber at time = ∞ as a function of x

$\varepsilon_{\varphi,Mnp,a,b,ti}(x)$ = strain due to additional permanent and near-permanent loads at the bottom of the timber at time = ∞ as a function of x

φ = creep factor

$P_0(x)$ = prestress force after removing the adjustable prop (time = 0) as a function of x (equation (45))

$\Delta P_\infty(x)$ = difference in prestress force due to long-term effects as a function of x

A_{ti} = area of the timber cross section

MOE_{ti} = modulus of elasticity of the timber

a = eccentricity of the prestress force (Figure 54 and equation (46))

h_{ti} = height of the timber

$I_{y,ti}$ = moment of inertia of the timber section

$n_{ti\infty}$ = ratio between the long-term MOE of the timber and the reference MOE

ψ_2 = reduction factor for the near-permanent value of a variable action as defined in SIA 260 [52]

$M_{ll}(x)$ = moment due to live loads after intervention as a function of x

$M_{dl}(x)$ = moment due to dead loads after intervention as a function of x

$M_{np,pi}(x)$ moment due to dead loads prior intervention as a function of x

$z_{b,ti\infty}$ = distance between the neutral axis of the composite section at time = ∞ and the bottom of the timber

$I_{y,co\infty}$ = moment of inertia of the composite section at time = ∞ can be calculated using equation (38) and $n_{ti\infty}$ instead of $n_{ti.}$

The creep strain at the lower face of the timber and the strain in the CFRP-lamella can be regarded as proportional as long as the adhesive is sufficiently rigid. Therefore, the creep in the timber leads to a strain increase or decrease in the CFRP-lamella, resulting in a different stress in the CFRP. This stress increase or decrease occurs without any adjustment of the loads; so the stress difference is regarded as a decrease or increase of the prestress. The adhesive layer also experiences a strain increase or decrease due to the creep of timber. In order to determine the difference in the prestress force, the strain difference at the centre of gravity of the prestress force is determined using equation (68).

$$\Delta\varepsilon_{\varphi,P}(x) = \varepsilon_{\varphi,N_{P\infty},b,ti}(x) + \varepsilon_{\varphi,M_{P\infty},b,ti}(x) \cdot \frac{2 \cdot a}{h_{ti}} + \varepsilon_{\varphi,M_{np,a},b,ti}(x) \cdot \frac{z_{P\infty}}{z_{b,ti\infty}} \qquad (68)$$

Where:

$\Delta\varepsilon_{\varphi,P}(x)$ = strain difference due to additional creep relevant loads at centre of gravity of the prestress force at time = ∞ as a function of x

$\varepsilon_{\varphi,NP\infty,b,ti}(x)$ = strain due to the normal force yielding from prestressing at the bottom of the timber at time = ∞ as a function of x

a = eccentricity of the prestress force (Figure 54 and equation (46))

h_{ti} = height of the timber

$\varepsilon_{\varphi,MP\infty,b,ti}(x)$ = strain due to the moment yielding from prestressing at the bottom of the timber at time = ∞ as a function of x

$\varepsilon_{\varphi,Mnp,a,b,ti}(x)$ = strain due to additional permanent and near-permanent loads at the bottom of the timber at time = ∞ as a function of x

$z_{P\infty}$ = distance between the neutral axis of the composite section at time = ∞ and the centre of gravity of the prestress force

$z_{b,ti\infty}$ = distance between the neutral axis of the composite section at time = ∞ and the bottom of the timber

Knowledge of the strain difference allows the determination of the difference of the prestress force which is presented in equation (69).

$$\Delta P_{\infty}(x) = \Delta\varepsilon_{\varphi,P}(x) \cdot \left(EA_{cf} + EA_{ad}\right) \tag{69}$$

Where:

$\Delta P_{\infty}(x)$ = difference in prestress force due to long-term effects as a function of x

$\Delta\varepsilon_{\varphi,P}(x)$ = strain difference due to additional creep relevant loads in centre of gravity of the prestress force at time = ∞ as a function of x

EA_{cf} = MOE of the CFRP-lamella multiplied with the cross section area of the CFRP-lamella

EA_{ad} = MOE of the adhesive multiplied by the cross section area of the adhesive layer

In order to solve equation (69), equations (65) to (67) are inserted in equation (68) and then (68) is inserted in equation (69). Finally, inserting equation (69) in equation (59) yields the prestress force at time = ∞ (P_{∞}). The solution is presented in equation (70).

$$P_{\infty}(x) = P_0(x) + \frac{n_{ti\infty} \cdot \frac{\left(\psi_2 \cdot M_{ll}(x) + M_{dl}(x) - M_{np,pi}(x)\right) \cdot z_{P\infty}}{I_{y,co,\infty}} - P_0(x) \cdot \left(\frac{1}{A_{ti}} + \frac{a^2}{I_{y,ti}}\right)}{\frac{MOE_{ti}}{\varphi \cdot \left(EA_{cf} + EA_{ad}\right)} + \frac{1}{A_{ti}} + \frac{a^2}{I_{y,ti}}} \tag{70}$$

Where:

$P_{\infty}(x)$ = long-term prestress force as a function of x

$n_{ti\infty}$ = ratio between the long-term MOE of the timber and the reference MOE

ψ_2 = reduction factor for the near-permanent value of a variable action as defined in SIA 260 [52]

$M_{ll}(x)$ = moment due to live loads after intervention as a function of x

$M_{dl}(x)$ = moment due to dead loads after intervention as a function of x

$M_{np,pi}(x)$ moment due to dead loads prior intervention as a function of x

$z_{P\infty}$ = distance between the neutral axis of the composite section at time = ∞ and the centre of gravity of the prestress force

$I_{y,co\infty}$ = moment of inertia of the composite section at time = ∞ can be calculated using equation (38) and $n_{ti\infty}$ instead of n_{ti}

$P_0(x)$ = prestress force after removing the adjustable prop (time = 0) as a function of x (equation (45))

A_{ti} = area of the timber cross section

a = eccentricity of the prestress force (Figure 54 and equation (46))

$I_{y,ti}$ = moment of inertia of the timber section

φ = creep factor

MOE_{ti} = modulus of elasticity of the timber

EA_{cf} = MOE of the CFRP-lamella multiplied with the cross section area of the CFRP-lamella

EA_{ad} = MOE of the adhesive multiplied by the cross section area of the adhesive layer

As mentioned above, the creeping of the timber leads to a shift of the neutral axis. This shift is valid only for the additional permanent and near-permanent loads. For all other loads, the neutral axis calculated at time = 0 is still valid. Therefore, the ultimate-limit state design at time = ∞ is done using the neutral axis at time = 0 and at time = ∞. Furthermore, the internal and external forces cannot just be added at time = ∞ but the stresses have to be added in order to validate the cross section. The maximal-tension stress at the bottom of the timber is calculated using equation (71).

$$\sigma_{b,ti,\infty}(x) = \frac{\left(M_d(x) - M_{np,a}(x)\right) \cdot z_{b,ti}}{I_{y,co}} + \frac{M_{np,a}(x) \cdot z_{b,ti,\infty}}{I_{y,co,\infty}} + \frac{M_{P\infty,ti}(x) \cdot h_{ti}}{2 \cdot I_{y,ti}} \qquad (71)$$

Where:

$\sigma_{b,ti,\infty}(x)$ = normal stress at the bottom of the timber due to loading and prestressing at time = ∞

$M_d(x)$ = design moment as a function of x

$M_{np,a}(x)$ = moment due to additional permanent and near-permanent loads as a function of x

$I_{y,co}$ = moment of inertia of the composite section at time = 0 can be calculated using equation (38)

$z_{b,ti}$ = distance between the neutral axis of the composite section and the bottom of the timber section at time = 0

$z_{b,ti,\infty}$ = distance between the neutral axis of the composite section and the bottom of the timber section at time = ∞

$I_{y,co,\infty}$ = moment of inertia of the composite section at time = ∞ can be calculated using equation (38) and $n_{ti\infty}$ instead of n_{ti}

$M_{P\infty,ti}(x)$ = internal moment in timber yielding from eccentric prestressing as a function of x at time = ∞

h_{ti} = height of the timber section

$I_{y,ti}$ = moment of inertia of the timber section

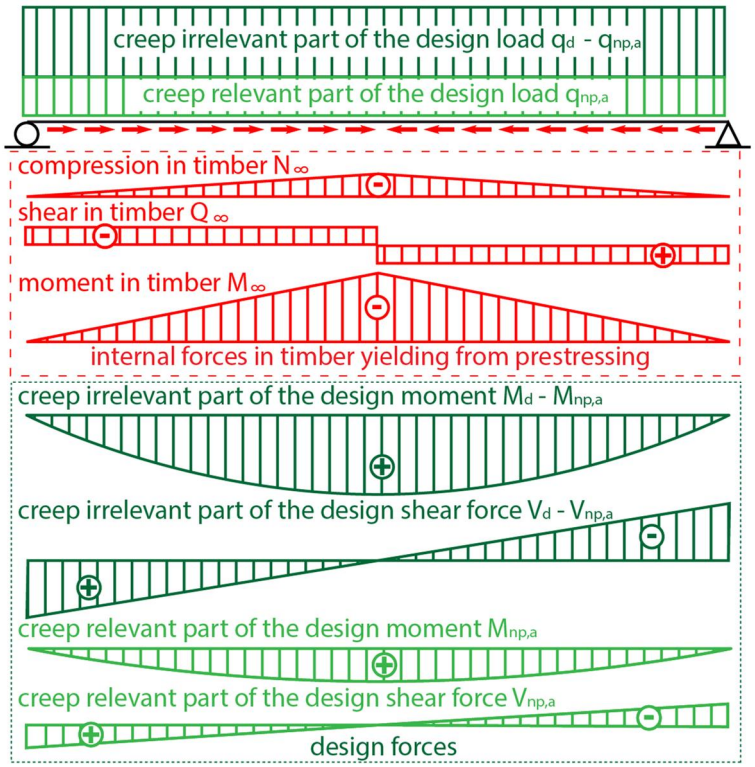

Figure 61: *Prestressed system with design loads including the effect of creep at time = ∞. For the internal forces, the neutral axis of the timber is valid; for the creep-irrelevant forces, the neutral axis at time = 0 is valid; and for creep-relevant forces, the neutral axis at time = ∞ is valid.*

The verification on the compression side of the prestressed bending beam can be done using equation (53), where $\sigma_{m,d}$ is the sum of the bending stresses yielding from the creep-relevant and creep-irrelevant loads. Again, the verification of the compression side of the timber is a conservative approach (Figure 62) and should be questioned. Unfortunately, not many long-term bending tests with adjacent determination of the ultimate load have been carried out so far. Lehmann [62] presents the mechanical properties of an historic timber beam where the properties were determined using small clear specimens cut from one beam. The results allow the assumption that historic timber also has extended non-linear behaviour in compression parallel to the grain. Failure on the tension side led to complete failure of the bending specimen. Not all bending specimens showed extensive non-linear behaviour towards the end, however. The results presented by Lehmann [62] emphasise that verification of the tension side only should at least be considered.

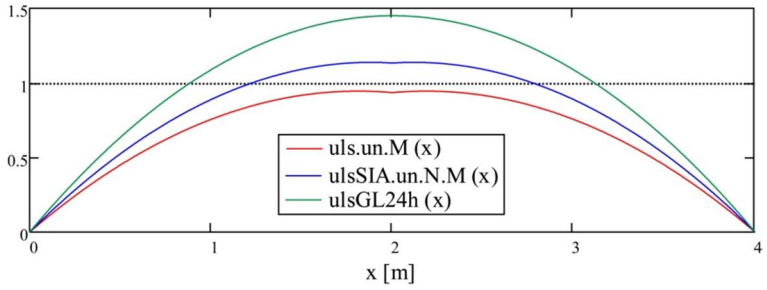

Figure 62: *Results of equations (53) (**blue**) and (54) (**red**) for a reinforced beam at time = ∞ (160 x 120mm GL24h, reinforced with one 1.2mm thick, 50mm wide CFRP-lamella); an unreinforced glulam beam (160mm x 120mm) (**green**). A value of one means the design capacity of the beam is reached. (All beams are equally loaded.)*

The locus of the maximum-tension stress on the lower side of the timber is found by inserting the functions of the forces in equation (72) below, and solving it for x. The difference between the local maximum und the tension stress in midspan is quite small (1% for the section presented in Chapter 1) and not significant for building purposes.

$$\frac{d}{dx}\cdot\frac{\left(M_d(x)-M_{np,a}(x)\right)\cdot z_{b,ti}}{I_{y,co}}+\frac{M_{np,a}(x)\cdot z_{b,ti,\infty}}{I_{y,co,\infty}}+\frac{M_{P\infty,ti}(x)\cdot h_{ti}}{2\cdot I_{y,ti}}=0 \qquad (72)$$

Where:

$M_d(x)$ = design moment as a function of x

$M_{np,a}(x)$ = moment due to additional permanent and nearly permanent loads as a function of x

$I_{y,co}$ = moment of inertia of the composite section at time = 0 can be calculated using equation (38)

$z_{b,ti}$ = distance between the neutral axis of the composite section and the bottom of the timber section at time = 0

$z_{b,ti,\infty}$ = distance between the neutral axis of the composite section and the bottom of the timber section at time = ∞

$I_{y,co,\infty}$ = moment of inertia of the composite section at time = ∞ can be calculated using equation (38) and $n_{ti\infty}$ instead n_{ti}

$M_{P\infty,ti}(x)$ = internal moment in timber yielding from eccentric prestressing as a function of x at time = ∞

h_{ti} = height of the timber section

Iy,ti = moment of inertia of the timber section

As for the bending actions, as well as for the shear forces, three neutral axes are considered,. In order to be able to add the shear stresses, the stresses have to be calculated in respect to one neutral axis (in this work it is done in respect to the neutral axis of the composite section at time = ∞). The last term in equation (73) is the shear stress yielding from the eccentric prestress force and is present in the timber only.

$$\tau_{d,\infty}(x,z)=\frac{\left(Q_d(x)-Q_{np,a}(x)\right)\cdot S^*_{co}(z)}{b(z)\cdot I_{y,co}}+\frac{Q_{np,a}(x)\cdot S_{co,\infty}(z)}{b(z)\cdot I_{y,co,\infty}}+\frac{Q_{P\infty,ti}(x)\cdot(z_{t,\infty}-z)\cdot\left(h_{ti}+z-z_{t,\infty}\right)}{2\cdot I_{y,ti}} \qquad (73)$$

Where:

$Q_d(x)$ = design shear force as a function of x

x = position over the beam length

$Q_{np,a}(x)$ = shear force due to additional permanent and near-permanent loads as a function of x

$S^*_{co}(z)$ = first moment of area of the composite section at time = 0 as a function of z in respect to the neutral axis at time = ∞

b(z) = width of the composite section as a function of z

$S_{co,\infty}(z)$ = first moment of area of the composite section at time = ∞ as a function of z

$I_{y,co}$ = moment of inertia of the composite section at time = 0 can be calculated using equation (38)

$z_{t,\infty}$ = distance between the neutral axis and the top of the composite section at time = ∞

$I_{y,co,\infty}$ = moment of inertia of the composite section at time = ∞ can be calculated using equation (38) and $n_{ti\infty}$ instead of n_{ti}

$Q_{P\infty,ti}(x)$ = shear force in timber yielding from eccentric prestressing as a function of x at time = ∞

h_{ti} = height of the timber section

z = position over the cross section height

$I_{y,ti}$ = moment of inertia of the timber section

The maximum-shear stress is not exactly at the location of the neutral axis. In order to determine the locus of the maximum, the values of the shear forces and function of the first section modulus is inserted in equation (73). Then, the first derivation is set equal to zero and solved for z. The yielding equation is quite complicated and too long to be presented here. However, the difference of the local maximum and the shear stress at the neutral axis is 0.02%, which is quite small and not relevant to the calculated example.

The use of the simplified equation (74), which is presented below for the calculation of the maximal-shear stress at time = ∞, leads to an underestimation of about 1.5% for the calculated example. This error can be accepted for building purposes.

$$\tau_{d,\infty,simply} = \frac{Q_d(x = h_{ti}) \cdot S_{co,\infty}(0)}{b_{ti} \cdot I_{y,co,\infty}} + 1.5 \cdot \frac{Q_{P.\infty,ti}(x = h_{ti})}{A_{ti}} \qquad (74)$$

Where:

$Q_d(x=h_{ti})$ =.design shear force as relevant for designing a timber structure along the SIA SIA 265 [51]

b_{ti} = width of the timber section

$S_{co,\infty}(0)$ = first moment of area of the composite section at time = ∞ at the position of the neutral axis

$I_{y,co,\infty}$ = moment of inertia of the composite section at time = ∞ can be calculated using equation (38) and $n_{ti\infty}$ instead of n_{ti}

$Q_{P\infty,ti}(x=h_{ti})$ = shear force in timber yielding from eccentric prestressing at time = ∞ as relevant for designing a timber structure along the SIA 265 [51]

h_{ti} = height of the timber cross section

x = position over the beam length

A_{ti} = area of the timber cross section

The creeping of the timber leads to an elevated design stress in the CFRP-lamella. The design stress present at time = ∞ can be calculated using equation (75) below. The last term represents the stress yielding from the camber, due to eccentric prestressing. The contribution of this stress is quite small (0.5 MPa for the calculated example or 0.5%) and not signifi-

cant for structural purposes. The maximum-tension stress in the CFRP-lamella is located at midspan.

$$\sigma_{d,\infty,cf}(x) = n_{cf} \cdot \left(\frac{\left(M_d(x) - M_{np,a}(x)\right) \cdot z_b}{I_{y,co}} + \frac{M_{np,a}(x) \cdot z_{b,\infty}}{I_{y,co,\infty}} \right) + \frac{P_{\infty,cf}(x)}{A_{cf}} + \frac{M_{P_\infty,cf}(x) \cdot h_{cf}}{2 \cdot I_{y,cf}} \qquad (75)$$

Where:

$\sigma_{d,\infty,cf}(x)$ = design stress in CFRP-lamella at time = ∞ as a function of x
x = position over the length of the beam
n_{cf} = ratio between the MOE of the CFRP-lamella and the reference MOE
$M_d(x)$ = design moment as a function of x
$M_{np,a}(x)$ = moment due to additional permanent and nearly permanent loads as a function of x
z_b = distance between the neutral axis and the bottom of the composite section at time = 0
$I_{y,co}$ = moment of inertia of the composite section at time = 0
$z_{b,\infty}$ = distance between the neutral axis and the bottom of the composite section at time = ∞
$I_{y,co,\infty}$ = moment of inertia of the composite section at time = ∞
$P_{0,cf}(x)$ = prestress force in the CFRP-lamella as a function of x
A_{cf} = area of the CFRP-lamella
$M_{Po.cf}(x)$ = moment in CFRP-lamella, yielding from prestressing
h_{cf} = height of the CFRP-lamella
$I_{y,cf}$ = moment of inertia of the composite section

3.3 Service-limit state

The Swiss standard, Basics of Structural Design SIA 260 [52] recommend verifying different situations for the service-limit state. Three different load cases (near-permanent, frequent and occasional) with different consequences (reversible or irreversible) are given. Only the 'occasional' load case leads to irreversible consequences, and constructional measures are recommended rather than upgrading the stiffness. Furthermore, three limit states are given: functionality, comfort and appearance. Functionality is again divided into three sub-categories: fittings with brittle behaviour, fittings with ductile behaviour and use and operation. The long-term effects have only to be considered for three limit states: fittings with brittle behaviour, fittings with ductile behaviour and appearance. For the two limit states considering the fittings only, the deformation taking place after the installation of the relevant equipment or non-loadbearing component has to be considered. In the presented example it is assumed that all dead loads are installed prior to installing the fittings with ductile behaviour.

Identifying the deformation prior and due to intervention (equations (43) and (51)) allows the calculation of the deformation due to service loads at time zero. The elastic-bending deformation due to service loads can be calculated using well-known equations [36], and the bending stiffness of the composite section ($EI_{y,co}$ equation (38)). According to Heuer [42], the shear stiffness of the composite section (GA_{co}) can be calculated using equation (76) below. The knowledge of the composite shear stiffness allows the determination of the shear deformation at time zero using well-known [36] equations.

$$GA_{co} = \frac{EI_{y,co}{}^2}{\int_{-z_b}^{z_t} \frac{\left(\int_{-z_b}^{z} MOE(\chi) \cdot \chi \cdot b(\chi)\ d\chi\right)^2}{G(z) \cdot b(z)}\ dz} \tag{76}$$

Where:

GA_{co} = shear stiffness of the composite section is regarded as constant over the beam length
$EI_{y,co}$ = bending stiffness of the composite section is regarded as constant over the beam length
G = shear modulus of the relevant material
MOE = modulus of elasticity of the relevant material
b = width of the section
z_t = distance between the neutral axis and the top of the composite section
z_b = distance between the neutral axis of the composite section and the bottom of the timber section
z = position over the beam height

The deformation at time zero is the sum of the deformation due to prestressing at time = 0, the elastic deformations due to service loads and the creep deformations prior to intervention. The deformation due to shear is less than 3% of the deformation due to bending, and therefore, not significant for building purposes if one is considering the variation in the elastic properties of timber.

For long-term deformation, the different creep behaviour of the material have to be considered. As mentioned above in the example, timber only is prone to creep which results in a load redistribution and increasing deformation due to long-term effects. Furthermore, according to Navi and Heger [81], it is assumed that the creep deformation prior to intervention stayed within its linear elastic limit. In order to determine the deformation, the load history has to be considered (Table 4). Therefore, the creep relevant loads are only the additional near-permanent loads and the additional dead loads. The creep deformation of the loads prior to intervention is the permanent deformation at the time of reinforcing, and can be measured on-site. In the presented example, the permanent deformation is assumed to be equal to 60% of the elastic deformation of the permanent and near-permanent loads prior to reinforcing, and calculated using the bending stiffness of the timber section. The long-term deflection due to bending loads of a reinforced beam can be assumed using equation (77).

$$\begin{aligned} w_{m,np}(x) = & \frac{q_{np,a} \cdot sp^3 \cdot x - 2 \cdot q_{np,a} \cdot sp \cdot x^3 + q_{np,a} \cdot x^4}{24 \cdot EI_{y,co,\infty}} \\ & + \frac{q_{np,pi} \cdot sp^3 \cdot x - 2 \cdot q_{np,pi} \cdot sp \cdot x^3 + q_{np,pi} \cdot x^4}{24 \cdot EI_{y,co}} \\ & + \frac{q_{np,pi} \cdot sp^3 \cdot x - 2 \cdot q_{np,pi} \cdot sp \cdot x^3 + q_{np,pi} \cdot x^4}{24 \cdot EI_{y,ti}} \cdot \varphi + \iint \frac{P_\infty(x) \cdot a}{-\frac{EI_{ti}}{(1+\varphi)}}\, dx\, dx \end{aligned} \tag{77}$$

Where:

$w_{m,np}$ =
$EI_{y,co}$ = bending stiffness of the composite section at time = 0
$EI_{y,co,\infty}$ = bending stiffness of the composite section at time = ∞
$EI_{y,ti}$ = bending stiffness of the timber section

sp = span of the beam

$q_{np,a}$ = creep relevant loads after intervention

$q_{np,pi}$ = creep relevant loads prior to intervention

φ = creep factor

P_{∞} = prestress force at time = ∞

a = eccentricity of the prestress force

x = position over the beam length

The deflection due to shear forces can be determined in a similar way to that for bending moments. The shear stiffness of the composite section at time = ∞ can be estimated using equation (78).

$$GA_{co,\infty} = \frac{EI_{y,co,\infty}{}^{2}}{\int_{-z_{b,\infty}}^{z_{t,\infty}} \frac{\left(\int_{-z_{b,\infty}}^{z} MOE(\chi) \cdot \chi \cdot b(\chi)\ d\chi\right)^{2}}{G(z) \cdot b(z)}\ dz} \qquad (78)$$

Where:

$GA_{co,\infty}$ = shear stiffness of the composite section at time = ∞ is regarded as constant over the beam length

$EI_{y,co,\infty}$ = bending stiffness of the composite section at time = ∞

G = shear modulus of the relevant material (for timber G is divided by 1+φ)

MOE = modulus of elasticity of the relevant material (for timber MOE is divided by 1+φ)

b = breadth of the section

$z_{t,\infty}$ = distance between the neutral axis and the top of the composite section at time = ∞

$z_{b,ti,\infty}$ = distance between the neutral axis of the composite section and the bottom of the timber section at time = ∞

z = position over the beam height

The deformation due to shear is less than 4% of the deformation due to bending. This is not significant for building purposes if one is considering the variation in the elastic properties of timber.

In the example presented, the service-limit state for appearance is not fulfilled. However, the estimation of the deformation is only 8% higher than the limit, and the deformation could be accepted for an historic building. The service-limit state for use and operation is reached without any discussions; and the same is true for a case where the timber beam has not been reinforced. The service limit for fittings with ductile behaviour is not reached by 6%, and in cases where there are such fittings, construction measures need to be taken to avoid damage. The service-limit state for fittings with brittle behaviour is not possible to reach, and therefore construction measures must be taken. The comparison of the reinforced section with the timber beam only shows a large improvement due to strengthening using the camber method (Figure 63).

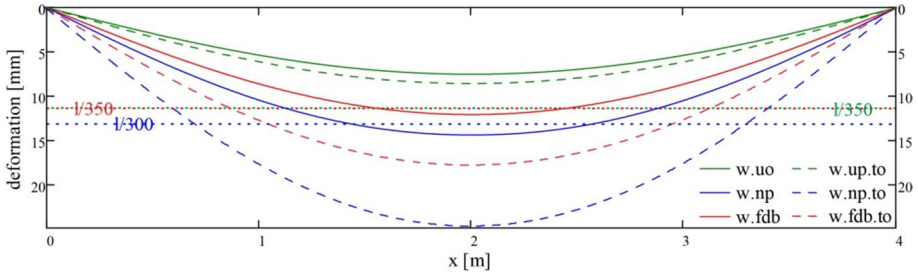

Figure 63: *Service-limit state of the reinforced beam (solid lines) and the timber beam only (dashed lines). The dotted lines represent the limit given in the SIA 260 [52]. The green lines show the limit state for use and operation (uo), the blue lines for near-permanent loads, regarding appearance (np) and the red lines for fittings with ductile behaviour.*

3.4 Discussion and conclusion

The model presented above allows the engineering design and calculation of a retrofitted timber beam. The position of the adjustable prop is, in the example presented, always placed in midspan. For other load configurations, the prop can be placed at other positions or even two props at the third points of the span could be used. In the case of a different load configuration or different placement of the prop, the equations for the position of the maximal-normal stress are no longer valid. Nevertheless, the model allows the calculation of the internal moment, and this, together with the external moment, allows the calculation of the maximal-normal stress and its position.

If the verification of the cross section is done as recommended in the Swiss Standard for Timber Construction (SIA 265) [51], the method loses its efficiency. Although the experiments show that a failure on the compression side of the timber leads to crushing and larger deformation, this factor is not relevant for structural safety. Therefore the author suggests verifying only the critical tension side of the timber. In cases where the compression side needs to be considered, the second-order analytical equations for the interaction of bending and compression presented in the doctoral thesis of Hörsting [45] are recommended.

The presented example demonstrates the efficiency of the camber method for reinforcing single span timber beams. In the ultimate-limit state, the calculated gain is 48%; and in the service-limit state concerning the appearance, the gain is 72% (including the camber). Concerning the limit state for fittings with ductile behaviour, the gain is 48%. Furthermore, the prestressing allows the verification of structural safety. If no prestressing is applied, the timber beam will be overloaded by 20% on the tension side. The prestressed composite beam nearly fulfils the service-limit state for the appearance; if the timber beam is reinforced without prestressing the deflection will overpass the limit by 50%. The utilisation regarding the design strain of the CFRP is improved from 24 to 40 % by prestressing. The presented example shows the efficiency of the camber method in reinforcing ancient timber beams.

The long-term effects have only a small influence (below 5%) on the design stress in timber. The additional near-permanent loads lead to load redistribution from timber to the CFRP-lamella. Therefore, the long-term effects for the ultimate-limit state in the timber can be dis-

regarded, and need only be considered if a high modulus CFRP-lamella is used (see also Chapter 5.3).

The equations presented for shear deformation show it to be less than 5% of the total deformation and therefore, if the variation of the elastic timber properties is considered, not significant for building purposes. The equations presented for the deflection due to bending allow estimating the deflection of a reinforced single span timber beam with adequate accuracy.

The 2% difference in the bending-tension stress in timber at midspan and the maximum is quite small in the calculated example. The author presented in an earlier paper [64] an easy to apply engineering model for the camber method. In this model, only the stresses due to prestressing in midspan are determined and added to the stresses due to design load. This approach leads to a slight underestimation of the stresses. If one considers this underestimation during design, the simpler engineering model can be used for the safe design of reinforced timber beams.

4 Experimental Work

The experimental work included prestressing the beams and subsequently testing the specimen in bending. The work was divided into two parts: Series 1 and 2. Series 1 was done using nearly clear and relatively small specimens. In this series the applied level of bending stress in the timber during bonding of the CFRP-lamella was varied, and three different adhesives were tested. In Series 2, large scale specimens were produced using GL24h[3] and the most promising parameters of Series 1.

The cambering method was used to prestress the specimens for the bending tests. The aim of the experimental work was to verify the analytical calculation model and prove the feasibility of the method. The test results were also used to verify the numerical analyses and the analytical calculation model which are presented in chapters 5 and 3 respectively.

4.1 Series 1

In Series 1, the feasibility and influence of the stress level during cambering prior to the bonding was tested. In this series, three different adhesives were used to produce small prestressed timber specimens.

4.1.1 Material and methods

Series 1 was manufactured using the relatively clear and small specimen of *picea abies*. There were no knots present in the specimens but some minor slope of grain was present in some specimens. The timber had a cross section of 40 x 53mm and was tested with a span of 1m. The CFRP-lamellas were Sika CarboDur lamellas with a section of 15 x 1.2mm. The mechanical properties are presented in the table below (Table 5):

Table 5: *Mechanical properties of the CarboDur S CRFP-lamellas used in this research (all values are according to Sika [5])*

MOE [GPa]				Tensile strength [MPa]				Strain	
mean	min.	5% percentile	95% percentile	mean	min.	5% percentile	95% percentile	**design**	**failure**
165	160	162	180	3100	2800	3000	3600	0.85%	1.70%

The CFRP-lamellas for Series 1 were cut out of lamellas with a cross section of 50 x 1.2mm. Three different resins were tested (Table 6). SikaDur-30 is a stiff epoxy resin that is normally used for CFRP-lamella reinforcement in concrete constructions. Quartz sand is used as filler in this resin. The MOE of SikaDur-30 is similar to the one of timber. The MOE of SikaDur-330 is 4.5GPa and significantly lower. This resin is used for CFRP-sheet impregnation and is therefore not filled with quartz sand. SikaDur-331W is a low cost and ecologically interesting water-based epoxy resin. For all the epoxy adhesives used in this research, it was important to ensure a good wetting of the timber. To avoid any difficulties with the wetting, a thin epoxy layer was spread onto the timber with high pressure, using a wallpaper scraper. This process was done immediately before the CFRP-Lamella was bonded to the timber.

[3] Glue-laminated timber of the grade GL24h as defined in SIA 265 [51].

Table 6: *Resins used in Series 1*

Resin	MOE* [MPa]	Comment
SikaDur-30	11'200	Solvent-free epoxy adhesive used for CFRP-lamella application in concert structures.
SikaDur-330	4'500	Solvent-free epoxy adhesive used to impregnate CFRP-sheet in concrete structures.
SikaDur-331W	3'500	Water-based epoxy impregnation resin used in tunnelling.

*Measured in tension according to Sika [8-10].

Four different levels of prestressing were tested using SikaDur-30 (Table 7). According to Kucera and Gfeller [57], the MOR of *Picea Abies* is between 65 and 77 MPa. As this is stated for small clear specimens, the MOR of the specimens used in Series 1 was estimated to be 65 MPa, which is the lower-end value. This value was chosen due to size effects and the slope of grain that was present in certain of the specimens used in Series 1. The estimated MOR allows the assumption that the chosen stress level during the bonding of the CFRP-lamella is well below the elastic limit of the timber. In order to define the MOR of the timber, a control sample consisting of five specimens without reinforcement were tested. Series 1 consisted in total of seven samples with five specimens each.

Table 7: *Samples tested in Series 1*

Sample	Number of specimens*	Adhesive	Induced stress** [MPa]	Timber section [mm]	CFRP section [mm]
Control	5 (1–5)	-	-	40 x 53	-
A	5 (6–10)	SikaDur-331W	20	40 x 53	1.2 x 15
B	5 (11–15)	SikaDur-330	20	40 x 53	1.2 x 15
C	5 (16–20)	SikaDur-30	20	40 x 53	1.2 x 15
D	5 (21–25)	SikaDur-30	10	40 x 53	1.2 x 15
E	5 (26–30)	SikaDur-30	30	40 x 53	1.2 x 15
F	5 (30–35)	SikaDur-30	0	40 x 53	1.2 x 15

*The figures in brackets represent the numbering of the specimens.
**Bending stress in timber during the bonding of the carbon lamella.

After machining, the timber specimens were stored at 20°C / 65%rh until constant weight was reached. Prior to the reinforcement with CRFP-lamellas, the local and global MOE of all timber specimens was determined (Figure 64). This was done according to SN EN 408:2003 [26] using the same equipment as for the bending tests after prestressing. For the determination of the MOE, the deflection at 10 and 40% of the estimated failure load of the timber was taken.

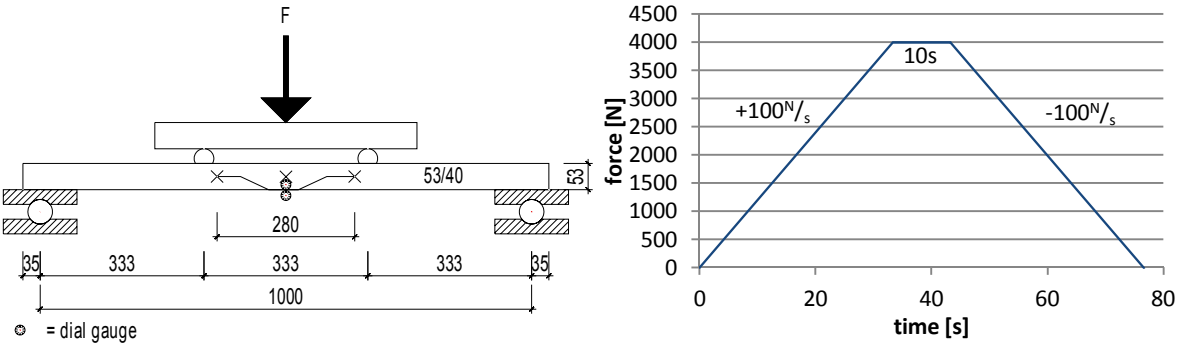

Figure 64: *Testing setup and cycle of the MOE measurement in Series 1*

Some 30 out of the 35 specimens were reinforced with CFRP-lamellas. The production of the specimens was done upside down. The battens were loaded with suspended steel weights. The curing of the resin was done in a drying kiln at 50°C and 73%rh, which results, according to Niemz [85], in an equilibrium moister content (EMC) of 12%. The specimens were left in this climate for 20 hours. In order to estimate the influence of elevated temperature and humidity on the MOE of the timber, the control specimens were also exposed to this climate for 20 hours. The deflection of the specimens was measured before and after the reinforcement. Strain-gauges were used to determine the prestress force and its distribution in the CFRP-lamella. Two gauges per specimen were glued to the CFRP before bonding the lamella to the timber. One was situated in midspan and the other, 50mm from the end of the lamella (Figure 65).

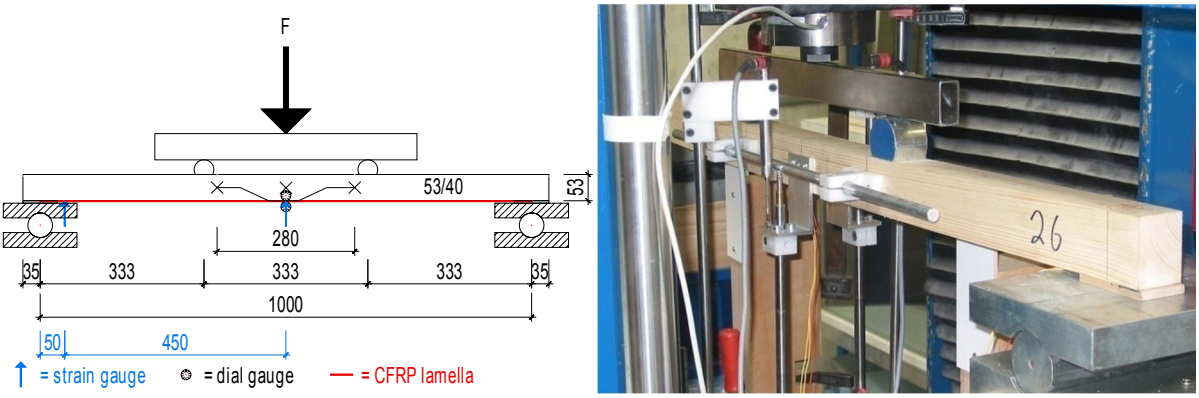

Figure 65: *Four-point bending setup as used for Series 1 to test the reinforced specimens*

In order to get an accurate measurement, the CRFP-lamella was situated on the timber specimen, and the zero point of the gauge was determined before the specimens were prestressed. After prestressing, the specimens were stored for one week in an air-conditioned storage room at 20°C / 65%rh and then tested in four-point bending. Prior to testing, the strain gauges were measured and the prestress was determined. A beach-spacer (Figure 65) was used to guarantee that the CFRP-lamella did not have any contact with the support, and therefore all forces had to be transmitted by the adhesive into the timber. In order to prevent damaging the deflection-measuring device, it was removed at 6kN reinforced specimens and at 5kN for the controls. The MOE was calculated using the deflection at 10 and 40% of the failure load. The loading cycle is presented in Figure 66.

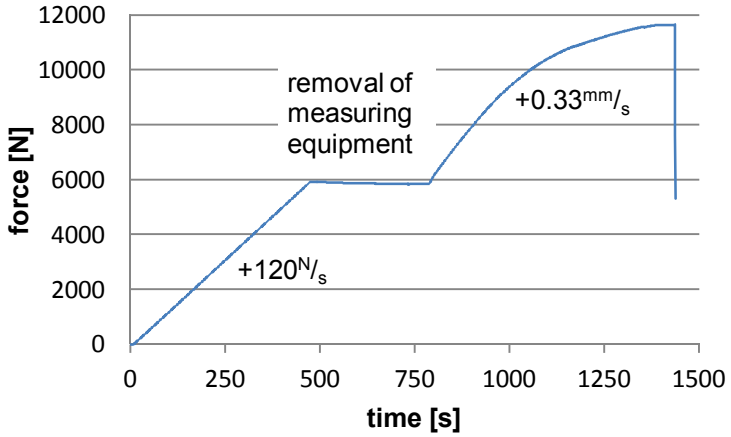

Figure 66: *Testing cycle of the reinforced specimens in Series 1*

All bending tests were done on a Schenk Trebel Universal testing machine with a load capacity of 250kN. The deflection was measured on both sides of the specimen and averaged. Two inductive standard displacement transducers with a nominal displacement of 10mm were used to measure the local deflection. For the global deflection, transducers with a nominal displacement of 50mm were used. One load cell (Burster 8524-6050) with the capacity of 50kN was used to monitor the force. The software Catman®[4] was used to log and monitor the different measuring devices during the bending tests. One Spider 8 of HBM was used for the PC-based data acquisition. The recording frequency was set to 10 Hz. Excel® was used to progress and evaluate the numerical data of the Schenk-Trebel universal testing machine and Catman®.

Strain gauges were used to monitor the strain and to allow the calculation of stress. On the CRFP-LY41-6/120, strain gauges of HBM were used. The gauges were connected in a three-wire circuit. All strain gauges were connected with a bridge completion resistor in a half-bridge circuit. The temperature in the laboratory during the tests was always around 23°C (± 2°C). Therefore it was not necessary to consider strain due to temperature, and gauges compensated for steel could be used. Prior to the installation of the gauges on the CFRP, the lamella was grinded locally using a scotch pad and then cleaned using the cleaning solvent RMS1 of HBM. The adhesive Z70 of HBM was used to bond the strain gauges to the CFRP-lamella.

4.1.2 Results

The measurements of the residual camber and the strain gauges on the CFRP-lamella show that the cambering method is suitable for prestressing timber-bending beams (Table 8).

[4] Data acquisition software of HBM (Hottinger Baldwin Messtechnik GmbH, Darmstadt, Germany).

Table 8: *Overview of the results of Series 1 (presented is the average of the five specimens in each sample and the coefficient of variation (COV))*

Sample	MOE timber		Prestress measured		Camber		Increase EI	Cross head movement at failure		M_{max}		Increase of M_{max}
	[MPa]	COV	[MPa]	COV	[mm]	COV		[mm]	COV	[kNm]	COV	[%]
Control	15054	10%	-	-	-	-	-	36	29%	1.49	9%	-
A	13915	13%	141	17%	3.31	27%	34%	40	16%	1.9	7%	28
B	15328	9%	154	7%	1.92	27%	30%	48	24%	1.83	9%	23
C	14345	11%	144	11%	1.83	30%	32%	33	17%	1.85	11%	24
D	15126	17%	79	13%	0.93	22%	29%	38	11%	1.76	5%	18
E	14132	12%	205	12%	2.67	38%	34%	30	15%	1.71	6%	15
F	14090	6%	4	66%	0	-	32%	27	26%	1.77	15%	19

There was no significant difference in the remaining prestress force between the different adhesives. However the difference between the various levels of prestressing was significant at a confidence level of 99%.

The residual camber of sample A, produced using the water-based epoxy adhesive (SD-331W), was significantly higher than the one produced using solvent-free epoxy adhesives (SD-30 and SD-331) (Figure 67).

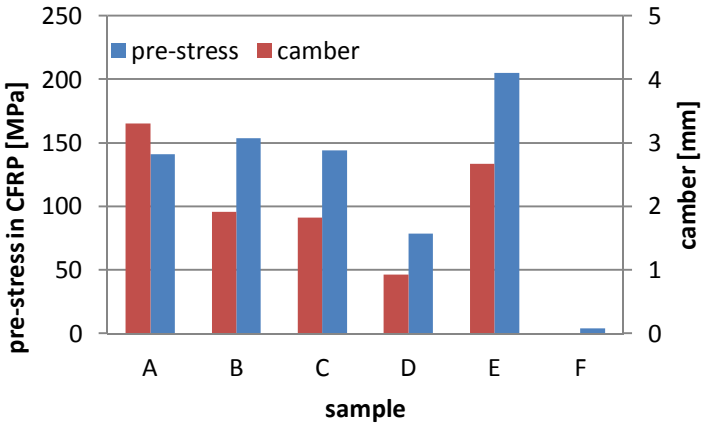

Figure 67: *Residual prestress and camber determined prior to four-point bending tests*

There is a correlation between the residual camber and the prestress of samples C to F (Figure 68). The residual camber is significantly different between these samples at a confidence level of 95%.

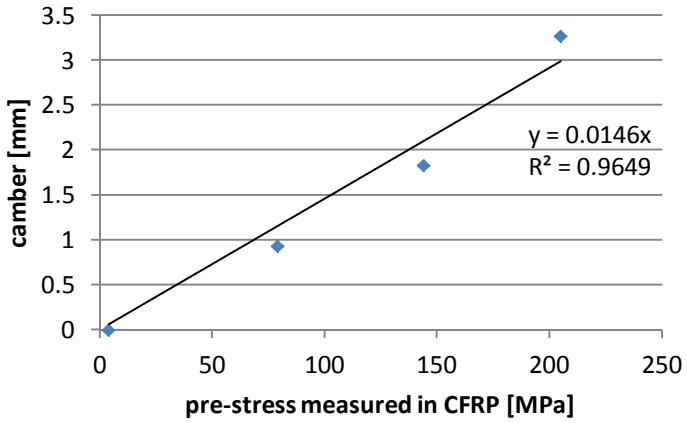

Figure 68: *Residual camber as a function of the residual prestress prior to four-point bending (only the samples C to F, using different levels of prestressing but the same adhesive, are presented in this graph)*

There was no significant difference in the increase of the bending stiffness due to reinforcing between the different samples. The average increase over all reinforced specimens was 32%. This increase is a geometrical effect that takes place as long as the lamella is properly bonded to the timber and the prestressing has no influence on it. As expected, a higher MOE of the timber resulted in a lower increase of the bending stiffness, leading to a reduction of the variation in the bending stiffness (Figure 69). A comparison of the coefficient of variation between the local EI of the timber and the local bending stiffness of the reinforced battens proved this reduction. The COV of the bending stiffness of the timber was 11% over all reinforced specimens (samples A to F) and the COV of the EI of the composite was 8% over the same specimens.

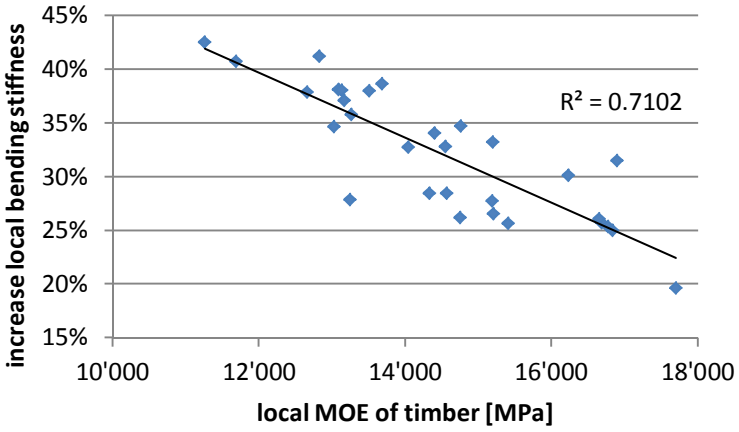

Figure 69: *Increase of the local bending stiffness due to reinforcement with CFRP as a function of the local MOE of the timber measured prior to reinforcement*

The MOE measurements of the control sample before and after the heat treatment showed no visible influence of the evaluated temperature during the adhesive curing on the MOE of the timber. There was also no significant difference found between the local MOE of the various samples.

The specimens produced using SD-330 (sample B) had a tendency to a longer non-linear part in the load to crosshead displacement graph of the four-point bending test (Figure 70). This tendency is more prominent if sample B is compared with sample C as if sample B is compared with sample A (Figure 70). In order to quantify this tendency, the ductility index was calculated (Table 9). The calculation was done according to the SIA 265 [51] using equation (79), which is used for the calculation of the ductility index of connections.

$$\text{ductility index} = \frac{w_u}{w_y} \qquad (79)$$

where:

F_u = maximal load

F_y = yield load as shown in the figure right

w_y = elastic deformation at F_y

w_u = maximal deformation or deformation at 0.8 F_u (the smaller value was taken)

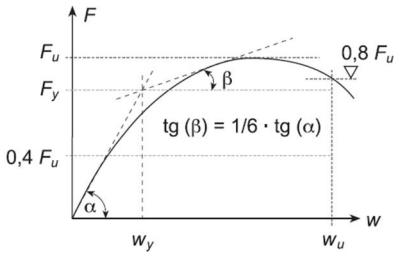

Due to the fact that the deflection of the specimens was not measured up to failure, the determination of the ductility index was done using the crosshead displacement of the testing machine. Therefore the values presented can only be used for comparison within Series 1 (Table 9).

Table 9: *Ductility index for the different samples (the index is calculated with the crosshead displacement instead of the deflection)*

	Control	Sample A	Sample B	Sample C	Sample D	Sample E	Sample F
average	1.73	1.91	2.34	1.63	1.94	1.57	1.34
COV	25.1%	23.7%	20.4%	9.5%	13.5%	16.6%	10.4%

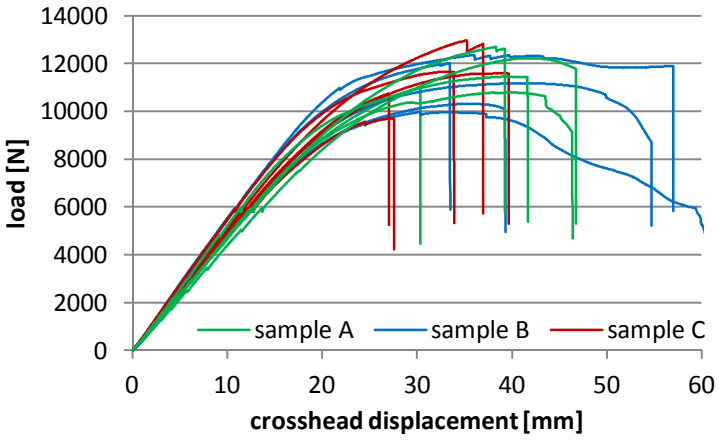

Figure 70: *Load as a function of the crosshead movement (only the specimens of the three samples using different adhesives are presented in this graph)*

At failure, the lamella did partly delaminate, and it was assumed that this delamination was caused by the splitting of the timber. Figure 71 shows that the lamella is still attached to the timber at both ends, and that the delamination does not go past the timber failure.

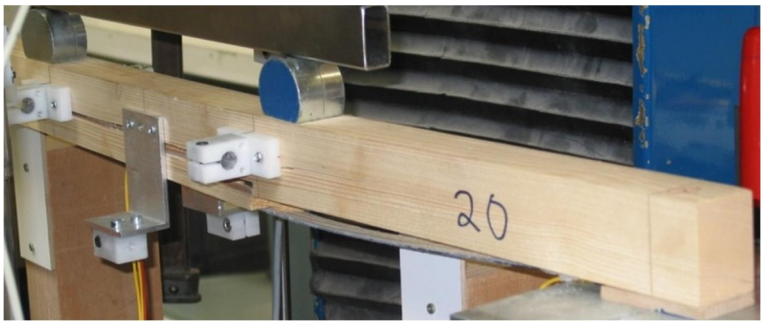

Figure 71: *Specimen with a partly delaminated lamella, where the lamella is still attached to the timber at both ends*

In samples B to F, which were produced using a solvent-free epoxy adhesive (SD-30 or SD-330), the timber started to fail in the middle, due to bending tension stress. In some cases, the CFRP bridged the failure for a short time, and this is clearly visible in Figure 72 and Figure 73. The first small partial failure occurred at 10.4kN, after which strong crushing on the compression side became visible and continued until complete failure occurred. The second partial failure, which came after the crushing started, would have led to complete failure without the CRFP-lamella.

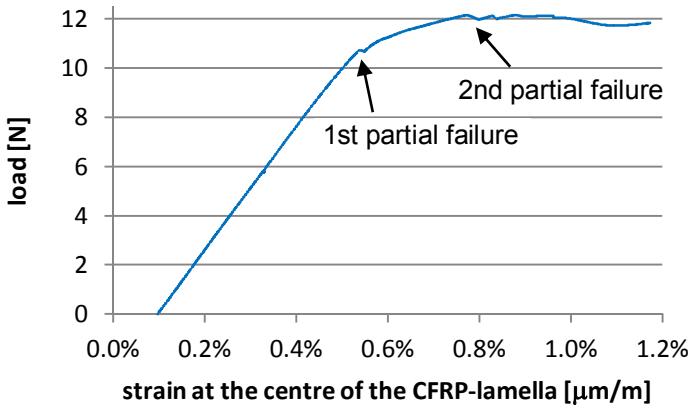

Figure 72: *Load as a function of the strain at the centre of the CRFP-lamella (the specimen is shown in Figure 73), the strain at zero force was due to the prestressing*

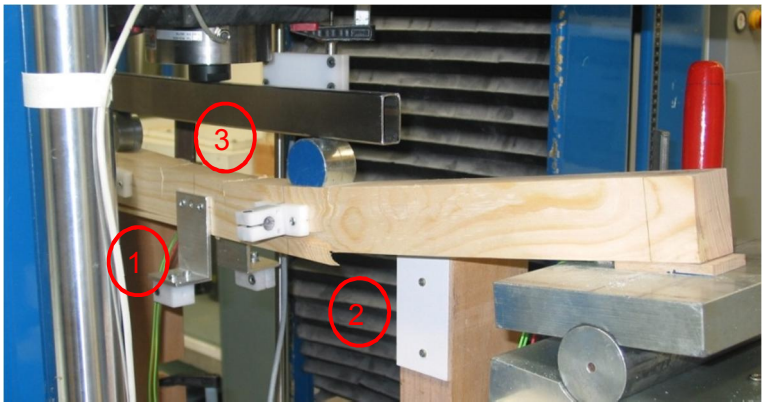

Figure 73: *Specimen 14 shortly before complete failure (the force strain graph is presented in Figure 72**) 1:** first partial failure, **2:** second partial failure, **3:** strong crushing*

The load-bearing capacity of the reinforced specimens was clearly higher than the one of the controls. No significant difference could be found in the maximal-bending moment between the samples with the different adhesives (samples A to C). There was also no significant difference between the different levels of prestressing (samples C to F) (Figure 74).

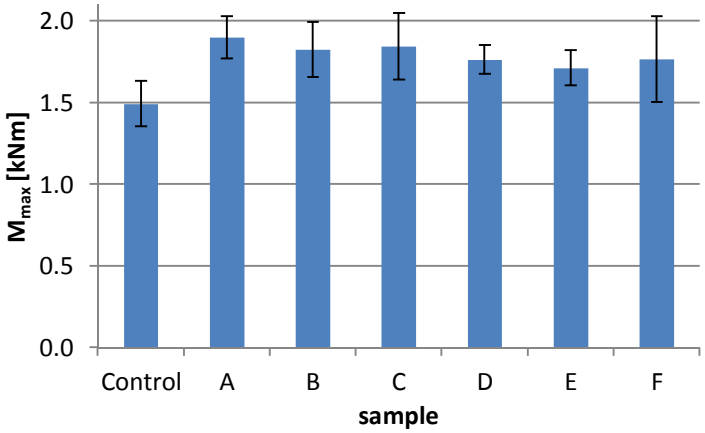

Figure 74: *Maximal-load-bearing capacity of each sample in Series 1 (the column represents the average and the error-bars indicate the standard deviation of each sample)*

The prestress level had some influence on the stress in the CFRP at failure. The sample reinforced without prestressing (sample F) compared with the two higher levels of prestress (samples C and E) had a significant difference at a confidence level of 95% (Table 10). Due to a recording error during the bending test of specimens 7 to 13, the recording of the strain did not work until the failure of the specimen. Therefore no data is available for the comparing of the different adhesives.

Table 10: *Stress in CFRP at failure of the battens*

	Sample C	Sample D	Sample E	Sample F
average	1174 MPa	1052 MPa	1183 MPa	895 MPa
COV	12.3%	8.3%	13.8%	24.3%

4.1.3 Discussion and conclusion

The determination of the prestress force, introduced with the camber method, verified the feasibility of the system. No clear influence of the prestress level on the bending capacity could be determined. However, the prestressing led to a significant cambering of the battens (Figure 67). Therefore prestressing has a significantly positive effect on the service-limit state. Considering that deflection mainly governs the design for single span beams, and taking into account the simplicity of the method, the prestressing can be regarded as a success.

The adhesive type had no significant influence on the load-bearing capacity or the residual prestress of the reinforced specimens. However, it did have an influence on the residual camber after prestressing. The water-based epoxy adhesive (sample A) yielded a significantly higher camber than the other two adhesives. The water-based epoxy (SD-331W) is more prone to shrinkages than solvent-free epoxy resins. After curing, the shrinkage of the water-

based adhesive was clearly visible and it is assumed that this shrinkage led to the difference in the camber due to prestressing.

Only in the sample produced using SD-331W did the delamination go past the timber failure, and in one case the CFRP-lamella completely delaminated. The strain-gauge measurements did not show any evidence that the CFRP delaminated before the timber failed. Therefore it cannot be determined if the failure started in the adhesive or the timber. The delamination was partly a cohesion failure in the adhesive, and an adhesion failure on the interface with the timber or the CFRP. In some cases of this interface failure, some timber fibres were still on the adhesive. Only in the sample produced with the water-based epoxy, could failure in the adhesive or adhesions be detected. As mentioned above, SD-331W showed significant shrinkage during curing. It is assumed that the stress resulting from shrinkage was responsible for the failure of the resin. Considering that the CFRP-lamella in Series 2 would be wider and therefore the shrinkage even greater, it was decided not to use the water-based adhesive for the production of the large specimens.

The two solvent-free adhesives displayed good bonding behaviour and can be regarded as suitable for this method. The SD-330 had a tendency to a longer non-linear part in the force deflection graph. This factor, together with the tendency to a stronger ability than the very stiff SD-30 in bridging partial failure in the timber, led to the decision to use SD-330 for Series 2.

Considering that in Series 1 the prestress force had to be anchored over a relatively short distance of 500mm, no delaminating should be expected in structural-sized beams, where the ratio of the prestress to anchoring length is much smaller, and therefore the shear stress in the anchorage zone is lower.

4.2 Series 2

In Series 2, beams in structural size were tested using the most promising parameters from Series 1. The induced bending stress during the bonding of the CFRP-lamella was set to 20 MPa. With this level it can be expected that the timber is still in its elastic range and no crushing will occur. This factor is important in the load-bearing situation as crushing would be in the zone with the highest bending tension, and would therefore lead to a considerable weakening of the timber.

4.2.1 Material and methods

The specimens in Series 2 had a cross section of 120 x 160mm and a span of 4m, similar to the beams usually found in old buildings. In order to reduce the variability of the timer, glulam of the class GL24h was chosen. For the reinforcement, Sika CarboDur lamellas S512/80 with a cross section of 50 x 1.2mm were used (for mechanicl properties see Table 5). SikaDur-330 was used to bond the CFRP-lamella to the timber. The MOR of GL24h used for the prestress level determination was estimated at 40 MPa. This estimation is based on experience at the BFH-AHB [98].

Table 11: *Sample tested in Series 2*

Sample	Number of specimens*	Resin	Induced stress** [MPa]	Induced stress** in % of estimated MOR	Timber section [mm]	CFRP section [mm]
G	10 (41-50)	SikaDur-330	20	50	120 x 160	1.2 x 50

*The figures enclosed in brackets represent the numbering of the specimens.
**Bending stress in timber during the bonding of the carbon lamella.

Prior to the reinforcement, the global and local MOE of each timber beam was determined using the same four-point bending test setup as for the bending tests after prestressing (Figure 76). The loading rate was ± 300N/s the maximal force of 12kN was held for 10 seconds.

For prestressing, the large specimens were cambered using a Schenk-Trebel universal-testing machine. Two beams were produced together and to ensure equal loading, a bridge with two pin joints was used (Figure 75). After reinforcing, the specimens were stored for a week in the laboratory and afterwards tested in four-point bending, according to the SN EN 408-2003 [26] using the Schenk-Trebel universal tester. The loading rate was 20mm per minute, and the measuring equipment for the bending stiffness was removed at 16kN. The same measuring equipment was used for the bending stiffness as for Series 1 (section 4.1.1). Two load cells (Burster 8524-6050) with a capacity of 50kN were used to monitor the force during the tests. The software Catman® was used to log and monitor the different measuring devices during the bending tests. Three Spider 8 of HBM were used for the PC-based data acquisition. The recording frequency was set to 10 Hz. Excel® was used to process and evaluate the numerical data of the Schenk-Trebel universal testing machine and Catman®. The camber of the specimens was measured at the centre of the beam both prior to and following prestressing. The measurement was done using a ruler and a straight steel beam.

Strain gauges were used to monitor the strain and allow the calculation of stress. On the CFRP, the same strain gauges and bonding process were used as in Series 1 (section 4.1.1). On the timber LY41-10/120 and LY41-20/120, strain gauges of HBM were used. For all strain gauges, the same wiring technique as in Series 1 was used. The climate in the testing laboratory was quite constant; therefore the strain due to humidity and temperature did not need to be considered. The strain gauges were bonded to the timber using the adhesive X60 of HBM. The beams were ordered half a metre longer than needed so it was possible to place the strain gauges in an area with relatively straight fibres and without knots or finger joints. Prior to bonding no special treatment of the timber was necessary except blowing off the dust. The strain gauges on the timber were covered with the protective coating SG-250 of HBM.

Figure 75: *Cambering of two beams in Series 2 with the cables of the carboheater clearly visible on the left*

For more efficient curing, the CFRP-lamellas were heated using the carboheater system of Sika [4]. This system sends a current through the carbon lamella and, due to its electrical resistance, the lamella is heated. The temperature in the adhesive layer is monitored using a k-wire. The amount of current sent through the lamella was controlled by the adhesive temperature. Meier [75] documented using this heating system for reinforcing a timber bridge. The described application involved using a sand-filled epoxy resin and curing at 70°C. Meier reported no obstacles using the carboheater in combination with timber.

The resin was cured at 90°C for 60 minutes. In order to prevent over rapid heating of the timber near the resin layer, which would lead to high vapour pressure, the temperature was raised at a constant rate over 30 min. During the production of the first two specimens, it was seen that the vapour pressure was still too high, which led to gas bubbles in the resin layer. In order to prevent this, screw clamps were used to apply a little pressure on the CFRP-lamella. After curing, the specimens were kept loaded until the temperature in the adhesive layer had fallen to below 40°C, which is below the heat distortion temperature (HDT) [9], and this took about 45 minutes.

On strain-gauge position five (Figure 76) gauges were also installed on both the top and bottom sides of the timber beam. Two different strain gauges were bonded on each side. One had a wide measuring grid of 10 by 6mm and the other, a long and narrow measuring grid of 20 by 0.7mm. The strain gauges were installed parallel to the fibre direction. The aim was to see if there was a significant difference between the two different measuring grids and to gain information about the strain and stress distribution in the timber. Due to the fact that the MOE varies quite widely within one timber beam, the local MOE under the strain gauges needed to be determined for stress calculations. This was done during the MOE measurement of the timber specimen before its reinforcement. Identifying the stress state of the timber in its elastic domain as well as identifying the strain measurement, allowed the calculation of the MOE under the strain gauges, using Hooks Law.

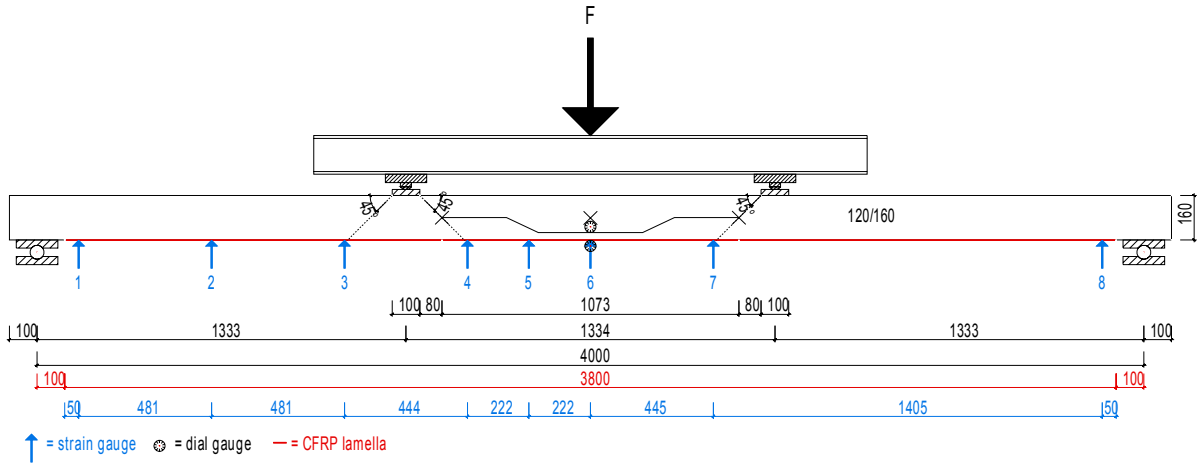

Figure 76: *Four-point bending setup as used for the bending tests in Series 2*

In order to determine the prestress distribution over the length of the lamella, eight strain gauges were placed along its length. Three were placed between the loading point and the end of the lamella, and another three between the loading point and the middle of the beam. The last two were placed between the middle and the other end of the lamella in order to verify the symmetry (Figure 76). After the failure of the specimens, the strain gauges were once more controlled to verify the bond quality. The moving around involved, together with the number of strain gauges used, did not allow for the constant monitoring of the gauges throughout the production of the specimen. Therefore the zero point was determined after installing the strain gauges, and the strain gauges on the CFRP were monitored both before and during the bending test. The strain gauges on the timber were also monitored during the MOE determination of the timber beams. These measurements allowed the reconstruction of the strain for each step.

4.2.2 Results

The residual camber and strain measurements done in Series 2 proved the feasibility of the method for structural-sized specimens (Table 12).

The average camber measured after prestressing was 4.1mm, which represents a thousandth of the span, and just under a third of the allowable deformation recommended in SIA 260 [52].

Table 12: *Overview of the four-point bending test results*

#	MOE*	EI local	EI global	Gain EI local	Ductility index	Camber	Prestress measured	M_{max}	Gain load-bearing**
	[MPa]	[Nmm^2]	[Nmm^2]	[%]	[-]	[mm]	[MPa]	[kNm]	[%]
41	9907	437.3E+9	425.6E+9	13.8	1.04	5	263	17.44	31
42	11761	533.1E+9	478.6E+9	16.9	1.07	3	253	22.82	22
43	14640	625.2E+9	536.9E+9	10.1	1.72	2	221	35.91	12
44	12955	577.4E+9	515.4E+9	14.9	1.10	3	240	25.69	41
45	12093	525.8E+9	475.8E+9	12.1	1.20	6	d.l.***	24.15	36
46	11673	508.3E+9	461.4E+9	12.3	1.23	3	233	27.80	d.l.***
47	10750	479.5E+9	443.5E+9	15.0	1.05	5	278	22.64	36
48	11049	482.9E+9	445.6E+9	12.7	1.38	3	268	27.76	16
49	11086	501.6E+9	468.3E+9	16.7	1.06	4	273	22.48	71
50	13032	563.2E+9	495.1E+9	11.4	1.10	7	246	27.67	16
average	11895	523.4E+9	474.6E+9	13.6	1.19	4.1	253	25.44	31.2
COV	11%	10%	7%	17%	18%	39%	8%	19%	58.4%

*MOE stands for the local MOE of the timber beam before reinforcement.

**M_{max} without reinforcement was estimated using the stress in the timber at the first significant partial failure with load redistribution from timber to CFRP.

***d.l. stands for data lost.

The prestress introduced is not constant over the length of the beam. As expected, the prestress has a triangular shape with the maximum at the centre of the beam where it is mostly used for bending beams with a constant load (Figure 77).

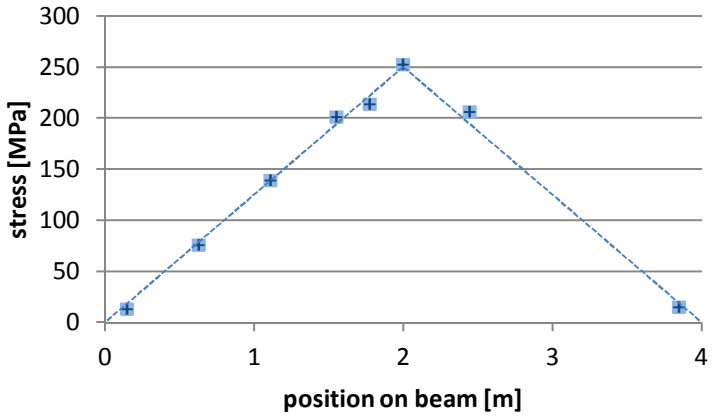

Figure 77: *Prestress distribution over the length of the beam. The markers represent the average prestress calculated using the strain measurements on the CFRP. The dotted line represents the expected qualitative prestress distribution.*

The average measured strain in the CFRP-lamella at strain-gauge position six (at midspan) after prestressing was 0.15%, which results in 253 MPa stress.

The residual prestress determined in the CFRP-lamella at strain-gauge position six (at midspan) showed a tendency to decrease with higher MOE of the timber beam (Figure 78).

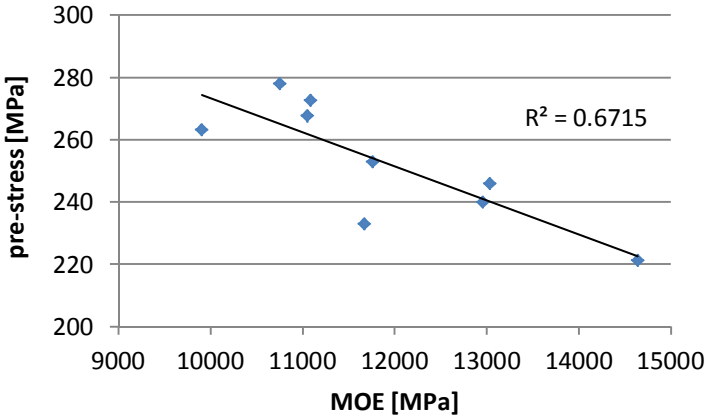

Figure 78: *Prestress at the centre of the CFRP-lamella as a function of the local MOE of the timber beam*

After prestressing, a negative moment and a compression force were present in the timber. The average compression stress on the lower side of the beam was -3.5 MPa, which represents 22% the design-bending stress stated in SIA 265 [51]. On the top side of the beam, the average tension stress was 2.2 MPa (Figure 79).

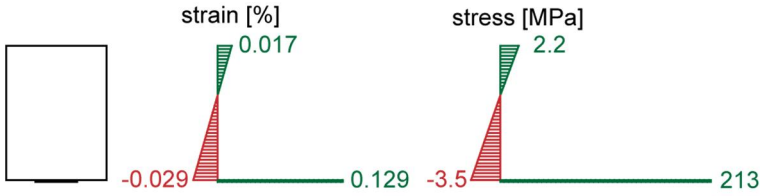

Figure 79: *Strain and stress distribution in the composite beam after prestressing at strain-gauge position five*

Identifying the strain after prestressing and the strain measurements during the four-point bending test did allow the calculation of the effective strain in the timber and the CRFP-lamella (Figure 80). The presented strain distribution along the height of the section is only valid for the elastic range of the beams. Afterwards the assumption of plane sections is not valid anymore.

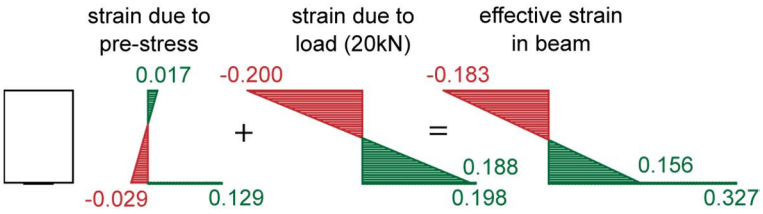

Figure 80: *Measured strain distribution in the composite beam during four-point bending at strain-gauge position five. The values are given in % and represent the average of all specimens at 20 kN load, which is within the elastic limit of the beams.*

The tendency for a higher MOE of the timber to lead to a lower gain in local bending stiffness due to the reinforcement was not as clear in Series 2 as in Series 1 (Figure 81 and Figure 69). The reduction of the coefficient of variation in the local bending stiffness (from 11 to 10%) was not very distinct.

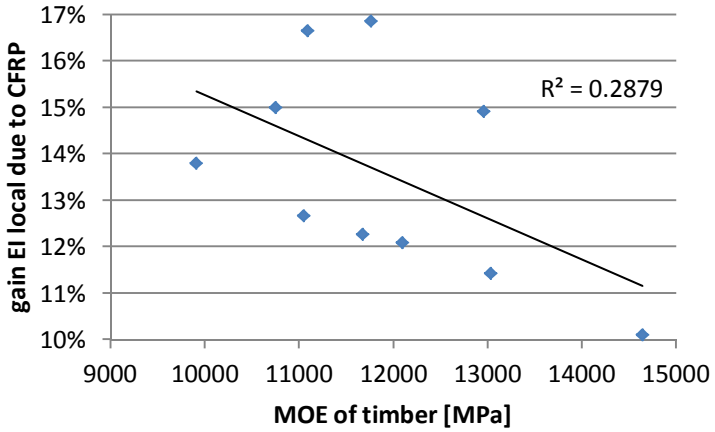

Figure 81: *Gain in local bending stiffness due to the reinforcement using CFRP-lamellas as a function of the local MOE of the timber beam only*

Some specimens had a clear non-linear section towards the end of the bending test in the force-crosshead displacement graph. The tested sample was not large enough to define the influence of the CFRP-lamella on the non-linear behaviour in a bending test. Nonetheless, some knowledge can be gained from the results. The ductility index of the clear specimens is significant larger than the one using glue-laminated beams. This outcome could be expected when the stress at failure is much higher in a clear specimen, and therefore crushing on the compression side is more likely and extended. Crushing normally leads to a continuous change of the slope of the force-crosshead displacement graph (Figure 83). Figure 82 shows that for specimen 48, significant crushing started at 30 kN. After 35 kN, the force still increased but the measured strain kept its level, and therefore no further strain occurred at the very top part of the timber at the position of the strain gauge, but there was a high level strain at the location of the crushing. In the case of strong crushing in specimen 43, a reduction of the strain under the strain gauge, combined with an increase of the load could be observed. If the crushing was not in the region of the strain gauge, the measured force-strain graph was linear. In all specimens, the crushing occurred in areas with knots (Figure 84).

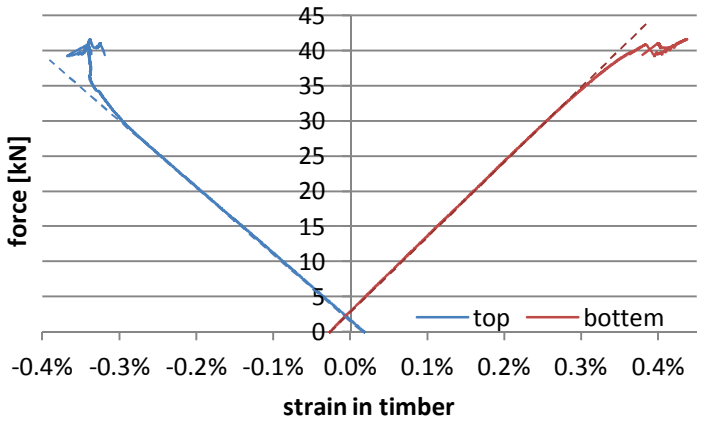

Figure 82: *Force as a function of strain measured on the timber during the bending test (specimen 48). The strain at zero force is due to prestressing. The dotted lines represent the elastic behaviour.*

Figure 82 shows how an over-proportional increase of the strain on the tension side of the timber beam starts with the crushing. This indicates that the neutral axis of the beam moves towards the lower side. According to Kollmann [48], this shift also happens in a timber beam without reinforcement.

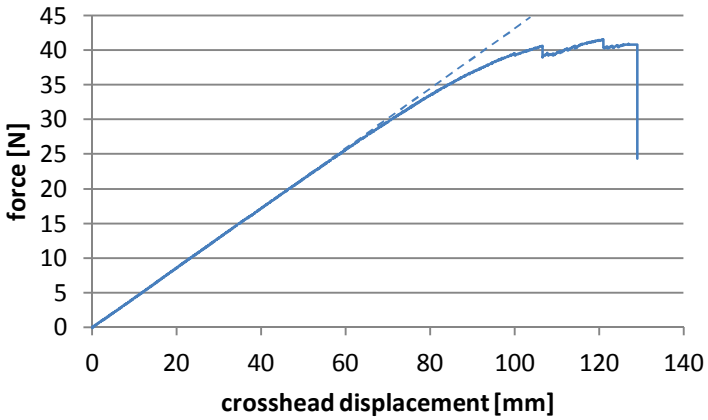

Figure 83: *Force as a function of the crosshead displacement during the bending test (specimen 48). The dotted line represents the elastic behaviour.*

The step down in the force-crosshead displacement graph was due to a partial failure in the tension side of the timber (Figure 83). A partial failure on the tension side usually starts near a knot or in a finger joint, and appears as a crack in the longitudinal direction of the timber. Such partial failures were usually in combination with load redistribution from timber to CFRP (Figure 85). If the partial failure did not damage the timber underneath the strain gauges but was still in the region of the gauges, increasing strain in the timber and CFRP, combined with decreasing force could be observed.

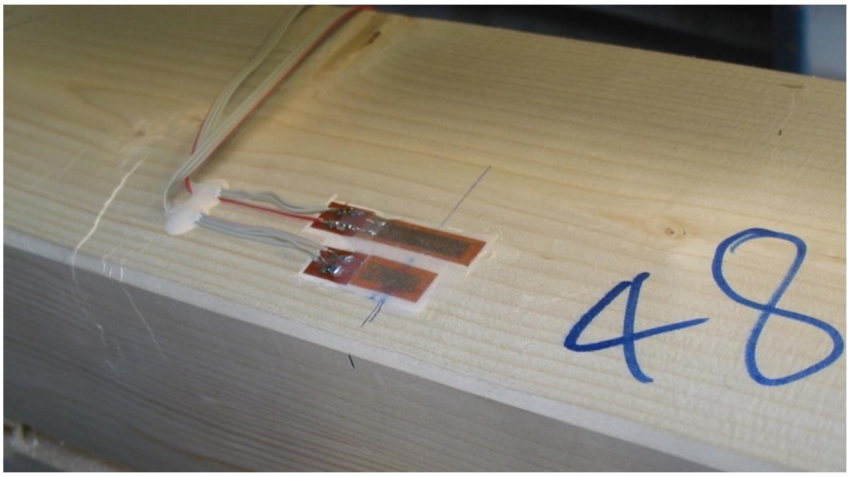

Figure 84: *Specimen 48 after complete failure and unloading. The crushing is clearly visible on the left side of the image. In the centre, the two strain gauges are visible (the shorter one has a measuring grid of 10 by 6mm and the longer one, a grid of 20 by 0.7mm).*

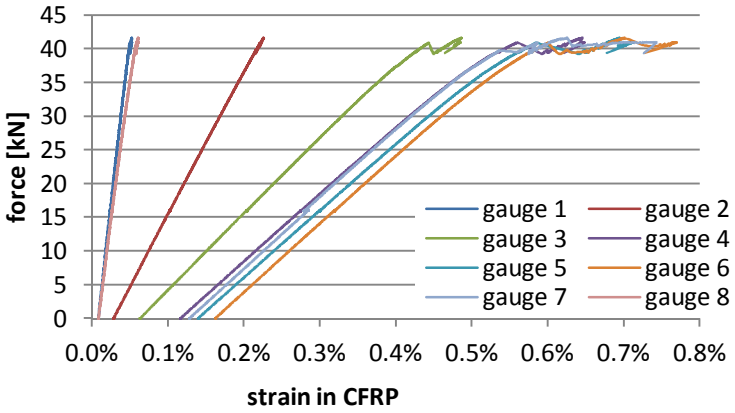

Figure 85: *Force as a function of strain measured on the CFRP during the bending test. The strain at zero force is due to prestressing.*

Specimen 43 had an exceptionally high MOE of the timber and also a very high failure load. Overall, the specimens show tendency that a higher MOE of the timber leads to a higher load-bearing capacity (Figure 86).

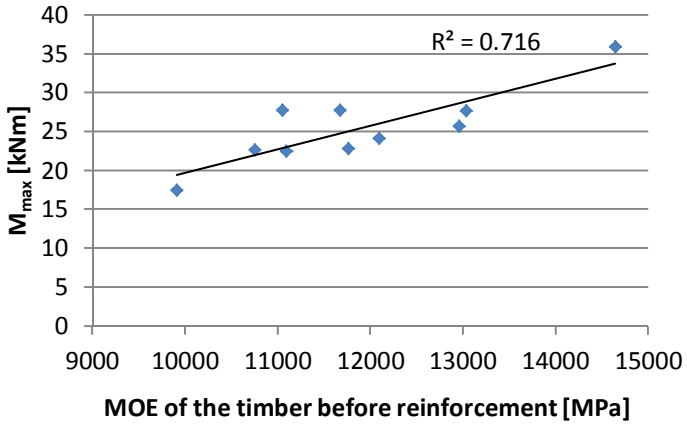

Figure 86: *M_{max} as a function of the MOE of the timber before reinforcing*

Figure 87 shows MOE as a function of the stress in the timber at the first partial failure with significant load redistribution from the timber to the CFRP. For specimens without partial failure, the maximal stress in the tension zone of the timber was taken. Again, the stress at gauge position five was taken for the analysis.

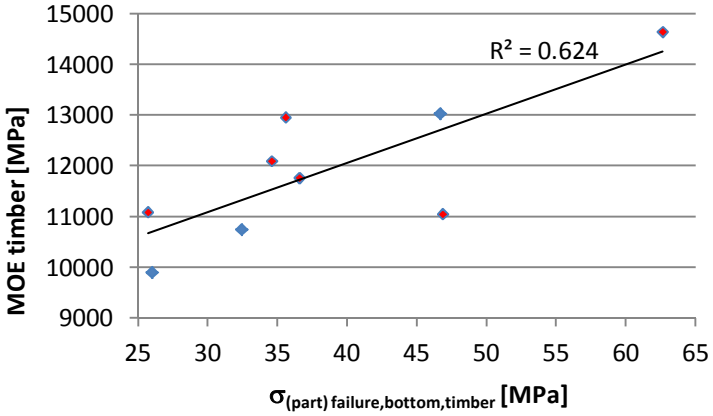

Figure 87: *MOE as a function of the maximal-bending tension stress in timber at the first (partial) failure with significant load redistribution form timber to CFRP. The red markers indicate specimens with partial failure, which occurred at less than the maximum strain.*

The increase in the load-bearing capacity shown in Table 12 is based on an elastic stress distribution in the timber, and was calculated using equation (80) below. For the calculation, the strain in the lower zone at the first partial failure with significant load redistribution form the timber to the CRFP-lamella was taken.

$$M_{u,ti} = \varepsilon_{ti} \cdot E_{ga} \cdot \frac{w_{ti} \cdot {h_{ti}}^2}{6} \qquad (80)$$

Where:

$M_{u,ti}$ = estimated failure moment of the timber beam without reinforcement
ε_{ti} = measured strain due to applied bending moment on the lower face of the timber
E_{ga} = module of elasticity of the timber underneath the strain gauge
w_{ti} = width of the timber beam
h_{ti} = height of the timber beam

A correlation of the modulus of elasticity of the timber with the maximal stress in the tension zone at gauge position five indicates that a higher MOE leads to higher stress in the lower zone of the timber beam at failure (Figure 88 and Figure 87). An inspection of the strain gauges on the tension side of specimen 46 showed that they were not properly bonded to the timber. Therefore, the measurements of these gauges are not included in the analysis. For the other specimens, the stress was determined using the strain measurements on timber and the determined MOE underneath the gauge. Kollmann [48] describes the same tendency for *Picea Abies* and also the strength grades in SIA 265 [51] show the same tendency for structural timber.

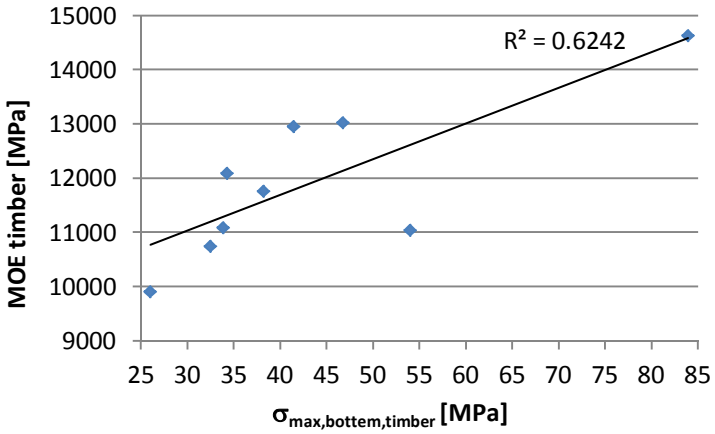

Figure 88: *MOE as a function of the maximal-bending tension stress in timber (not taking partial failure into account)*

4.2.3 Discussion and conclusion

The measured average camber after prestressing was 4.1mm, which represents a thousandth of the span. The SIA 160 [52] requests a maximum deformation of span divided by three hundred for the quasi-permanent load case in buildings. Therefore the residual camber is over 30% of the limit. In combination with the increase of the bending stiffness due to the CFRP-lamella, the presented method for reinforcing has a significant contribution of about 45% to the service-limit state.

The design strain in the CFRP-lamella, calculated using equation (81), is around 0.3%, which indicates that the CFRP is not used to its full capacity. In the Swiss preliminary standard for externally-bonded reinforcement SIA 166 [11], the design strain of the FRP is limited to 0.8% for concrete structures. According to Sika [5], the minimal strain at failure for the used CFRP-lamellas is 1.7%, and the design strain is limited to 0.85%.

$$\varepsilon_{u,d,CF} = \varepsilon_{P_0,CF} + \frac{f_d}{MOE} \qquad (81)$$

Where:

$\varepsilon_{u,d,CF}$ = design strain of the CRFP-lamella

$\varepsilon_{Po,CF}$ = strain in CFRP due to prestressing

f_d = design stress for GL24h, according to SIA 265 [51] (16 MPa)

MOE = modulus of elasticity for GL24h, according to SIA 265 [51] (11 GPa)

Hammer, Müller and Bücheler [39] present an example where the applied strain in CFRP-lamellas, during the retrofitting of a concrete bridge, equals 0.68% and allows the CFRP to be used more efficiently. They also report that the prestressing of externally-bonded CFRP-lamellas, due to the high-installation costs, is only economical feasible in cases where the service-limit state requires it. In order to reach such high design strains in timber beams other methods for prestressing than those used in the presented study have to be applied, leading to increased installation work and costs, and thereby questioning economic feasibility. Schnüriger Brunner and Lehmann [98] present a method for prestressing timber beams that

reaches an applied strain of 0.53%. They used heavy equipment, however, which is difficult to use in cases of on-site reinforcement.

Theoretically, the unsymmetrical distribution of the stress in the prestressed but unloaded beam leads to more prone crushing on the compressions side of the beam during loading, and therefore to higher deformation at failure. As stated above, the tested sample allows no established prediction about the influence of the reinforcement on the ductility of the beam.

The strain measurements on the timber provide some information about the strain distribution in the timber at partial failure and failure. The variation of the maximal-compression strain is lower than the one of the maximal-tension strain. It should be remembered that no visible crushing or splitting occurred under the strain gauges. This and the plots of the strain measurements allow the assumption that the timber stayed within its elastic domain under the gauges. This assumption allows a calculation of the maximal stress in the timber at gauge position five, using Hooks Law and the MOE of the timber under the strain gauge (Table 13).

Table 13: *Effective strain on the timber at partial and complete failure*

	Maximal				**Partial failure**			
	tension		**compression**		**tension**		**compression**	
	strain [%]	stress [MPa]	strain [%]	stress [MPa]	strain [%]	stress [MPa]	strain [%]	stress [MPa]
average	0.339	43.44	-0.353	-45.01	0.303	38.57	-0.323	-41.13
COV	27.2	39.8%	19%	17%	20.6	30.5%	19	17%

The variance of the determined tension stress is larger than that of the tension strain. On the compression side, the stress has a slightly lower variance than the strain. The maximal-compression stress shows a good correlation with the maximal moment (Figure 89). The correlation with the MOE of the timber is less prone but still clearly visible (Figure 90).

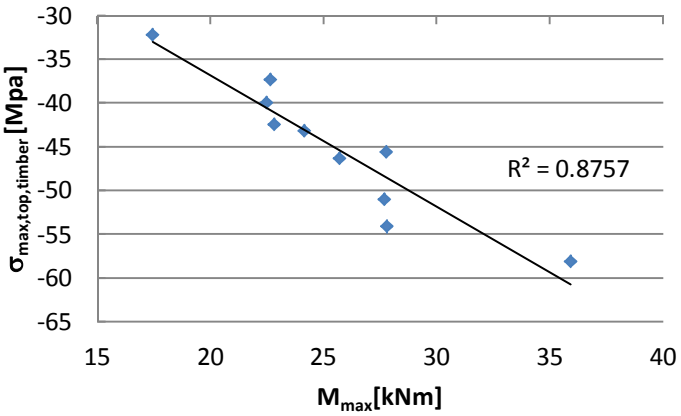

Figure 89: *Maximal-compression stress in timber at strain-gauge position five as a function of the load-bearing capacity*

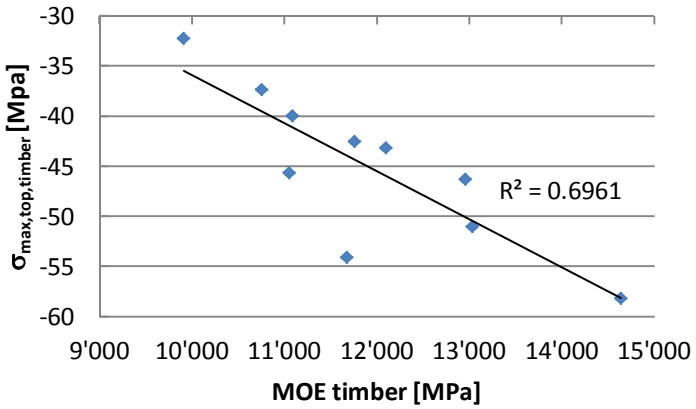

Figure 90: *Maximal-compression stress in timber at strain-gauge position five as a function of the local MOE of the timber*

There is a tendency for a lower load-bearing capacity to lead to a lower compression strain in the timber (Figure 91) but the correlation is much lower than for the stress and the load-bearing capacity. No correlation can be found in the specimens between maximal compression strain and the MOE of the timber. This is mainly due to the strain measurements of the specimens 46 and 48, which differ from all the other specimens. No evidence for a measurement error could be found and the strain measurements on the tension side of these two specimens also showed high readings. (As already mentioned the strain gauges on the tension side of specimen 46 failed; therefore the strain of the timber was estimated using the strain measurement on the CFRP-lamella at position five.) It is assumed that the high-strain values are due to the local variability of the elastic properties within one lumber.

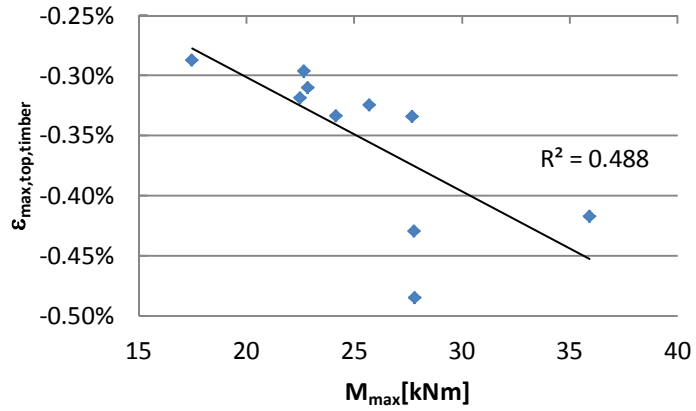

Figure 91: *Maximal-compression strain in timber at gauge position five as a function of the load-bearing capacity*

In some cases of a partial failure, a comparison of the strain in timber and CFRP indicates a possible local failure of the bond between CFRP and timber (Figure 94). There is no clear evidence that this local failure led to the delamination of the CFRP-lamella, but it cannot be ruled out either. The CFRP-lamellas were partly delaminated after complete failure of the composite beams. Two possible reasons for the delamination could be determined:

- Large stress perpendicular to the adhesive layer was introduced by a complete bending failure of the timber. This stress was due to the downward movement of one part of the timber. In this case, delamination was caused by the complete failure of the specimen and was not the reason for it (Figure 92).
- A local partial failure of the timber in the tension zone forced a local failure of the bond between the timber and the CFRP-lamella. This local failure led to a complete delamination and caused the complete failure of the specimens (Figure 93). According to Ulaga [116], this failure mode is also known in concrete structures that are reinforced using externally bonded CFRP-lamellas.

The data collected during the bending test does not allow for an exact distinction between these two factors but it is assumed that both did occur. The delamination was mostly an interface failure as carbon or wood fibres were found on the adhesive. The proportion of cohesion failure in the adhesive was very little.

Figure 92: *Specimen 45 after complete failure and unloading. The delamination of the CFRP-lamella was most likely forced by the failure of the timber.*

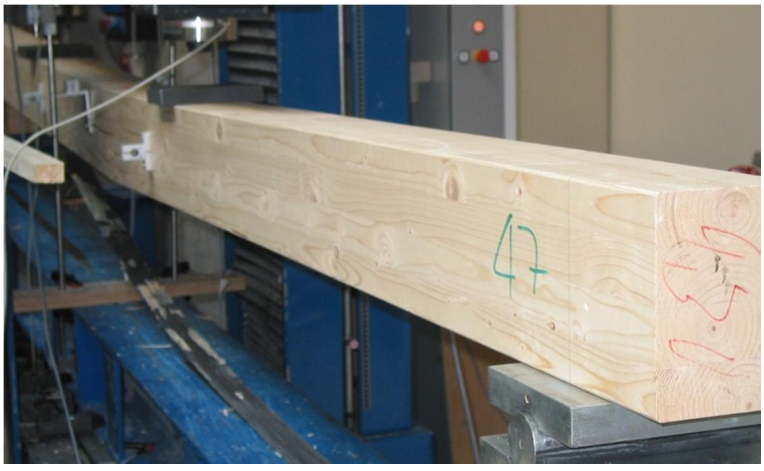

Figure 93: *Specimen 47 after complete failure and unloading. The delamination of the CFRP-lamella was possibly the result of a partial failure.*

A comparison between the different strain gauges used on the timber showed that the gauges with the shorter and wider measuring grid (10 x 6mm) had a tendency to detect lower

strain then the long and narrow (20 x 0.7mm) gauges (Figure 94). The calculated stress using Hooks law and the local MOE of the timber underneath the strain gauge showed almost no difference between the two gauge types. A comparison of the strain measured on the tension side of the timber and on the CFRP-lamella showed that the strain measured on the timber was slightly underestimated based on an elastic strain distribution over the composite section (Figure 80). Therefore, for strain measurements, gauges with a long but narrow grid should be preferred on timber.

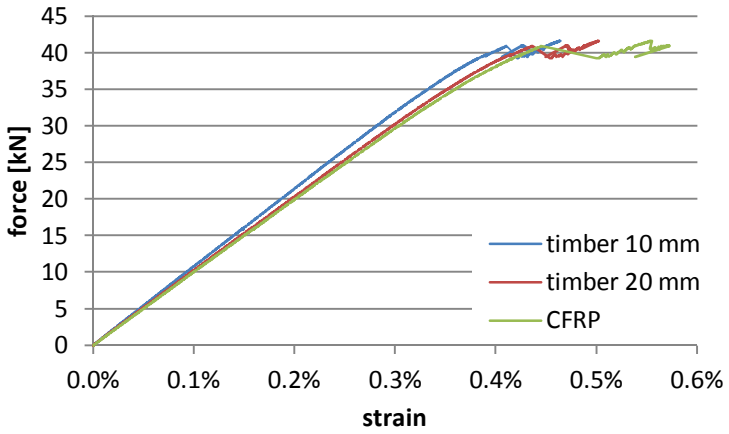

Figure 94: *Force as a function of strain measured on the CFRP during the bending test (specimen 48). The strain due to prestressing is excluded.*

The failure always started in the tension zone of the timber, and no early delamination of the CFRP-lamella could be observed. Therefore the proposed method to prestress timber beams is a solution to tackle the delamination. The strain measurements on the timber and the CFRP-lamella showed that until the first significant partial failure of the timber, there was no slippage between the materials, thereby demonstrating the efficacy of the adhesive. Some specimens did have an abrupt failure, and so an elevated ductility index could not be determined for the structural-sized specimen.

The prestress level reached was quite low compared to other methods. According to Schnüriger, Brunner and Lehmann [98], it is possible to prestress CRFP-lamellas on timber structures successfully with up to 800 MPa after elastic losses. In order to reach and anchor such high prestress, heavy and sophisticated equipment is necessary, making the installation economically unviable. The cambering method allows prestressing very simply and quickly, while significantly increasing the load-bearing capacity in this study by more than 50% and the serviceability by about 50%.

In order to avoid complete debonding after timber failure, the composite beam could be wrapped with CFRP fabrics, towards the end of the CFRP-lamella. If the CFRP-lamella were slotted into the timber, not only would the debonding at complete failure be reduced, but the impact on the appearance of the structure would be minimised.

5 Numerical Modelling

The analytical calculation model presented in Chapter 3 allows the safe design of a structure reinforced using the camber method. The equations are quite simple, and no special software is required. In order to understand the load-bearing behaviour of a reinforced beam after its proportional limit is reached, the true stress-strain relationship of timber has to be considered. This is done using numerical modelling and the software ANSYS, including the MultiPlas material library provided by Dynardo. The timber model implemented in MultiPlas is based on the multi-surface plasticity model developed by Grosse [37]. The exponential softening functions of Grosse are replaced by linear functions that lead to better convergence of Ansys. Using MultiPlas and the mechanical properties for small clear specimens as described in the section below (Table 15), the following stress-strain relationship of timber can be calculated (Figure 95 to Figure 97).

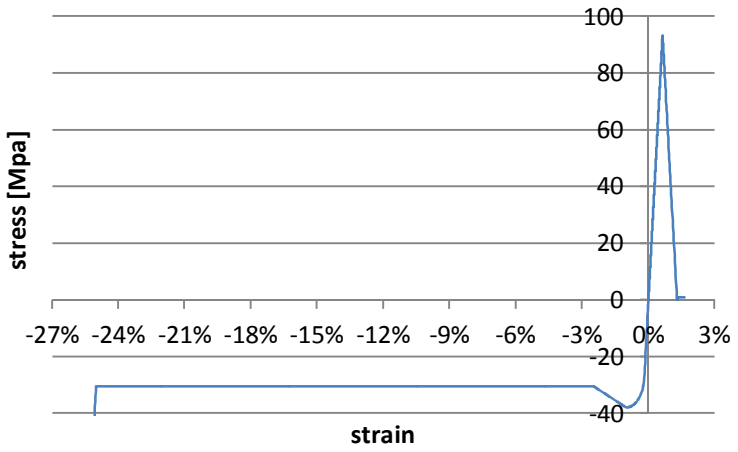

Figure 95: *Stress – strain relationship for clear Picea Abies in longitudinal direction. This graph was calculated using Ansys and the MultiPlas timber model.*

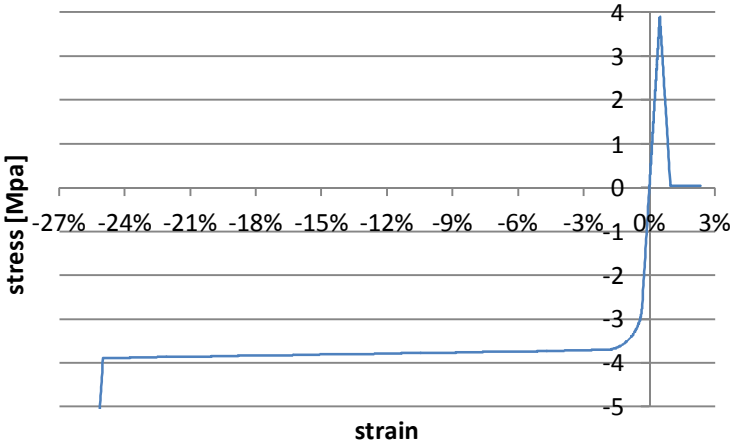

Figure 96: *Stress–strain relationship for clear Picea Abies in radial direction. This graph was calculated using Ansys and the MultiPlas timber model.*

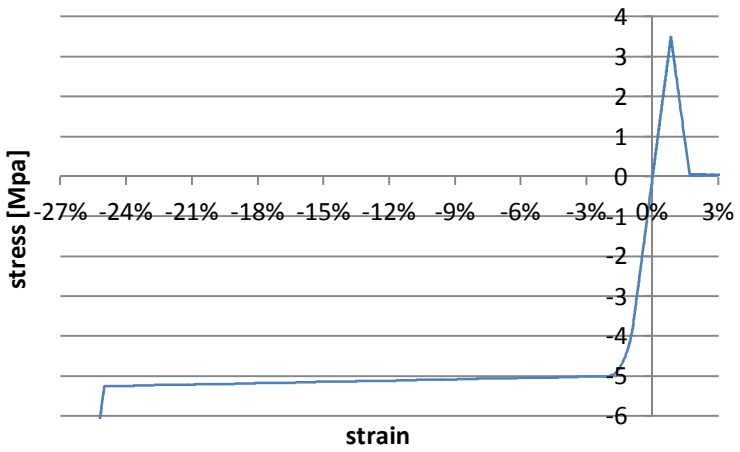

Figure 97: *Stress–strain relationship for clear Picea Abies in tangential direction. This graph was calculated using Ansys and the MultiPlas timber model.*

5.1 Material properties

The used material properties are derived from literature, material data sheets or measured during the experiments.

As timber is modelled as an orthotropic material, its compliance tensor contains nine independent elastic coefficients. The coefficients used in this work are taken from Neuhaus [84] (Table 14). As the modulus of elasticity parallel to the grain was determined of each timber specimen prior to reinforcing, the average local-bending MOE was used for the corresponding sample during the modelling (Table 8 and Table 12).

Table 14: *Elastic coefficients for Picea Abies according to Neuhaus [84] for a moister content of 12%*

MOE		**Shear modulus**		**Minor Poisson's ratio**	
[MPa]		[MPa]		[-]	
longitudinal (L)	11'990	RL	623	TL	0.0352
radial (R)	817	RT	42	RT	0.3107
tangential (T)	419	TL	722	RL	0.0553

The multi-surface plasticity material model used in this work requires the input of the ultimate strength in the various directions. The author had already determined the strength of *Picea Abies* in the frame of previous research [62]. The results are presented in the Table 15 below. As these values are for small clear specimens, the tension and compression parallel to the fibres are reduced for the numerical calculations considering structural-sized specimens.

Table 15: *Strength of Picea Abies according to Lehmann [62]*

Tension [MPa]		Compression [MPa]		Shear [MPa]	
longitudinal (f_{Lt})	93.4	longitudinal (f_{Lc})	37.9	f_{RLs}	11.7
radial (f_{Rt})	3.9	radial (f_{Rc})	3.7	f_{RTs}	3.5
tangential (f_{Tt})	3.5	tangential (f_{Tc})	5	f_{TLs}	11.2
				f_{TRs}	2.7

The CRFP-laminates are modelled as orthotropic, linear-elastic material. The modulus of elasticity in longitudinal direction was set as specified by the producer [5]. The modulus of elasticity across, the shear modulus (across/longitudinal) and Poisson's ratio of the CFRP-lamellas were determined by using the mixing rules according to Meier [76]. The *rolling-shear modulus* was set to the shear modulus of the matrix. The elastic constants for the CFRP-lamella used in the experiments (CarboDur type S) are presented in Table 16.

Table 16: *Elastic constants used in numerical modelling for the CFRP-lamella (type S)*

MOE [MPa]		Shear modulus [MPa]		Minor Poisson's ratio [-]	
longitudinal (L)	165'000	L/P	6698	L/P	0.0196
perpendicular (P)	10'816	rolling (P/P)	1185	P/P	0.3

For the high modulus CRFP-lamellas (types M and H), the modulus of elasticity and shear modulus were adjusted (Table 17).

Table 17: *Selected mechanical properties used to model the CFRP-lamellas*

Type	MOE longitudinal (L) [MPa]	MOE perpendicular (P) [MPa]	shear modulus (L/P) [MPa]
S	165'000	10'816	6698
M	210'000	11'094	6632
H	300'000	10'569	5930
UH	400'000	12'356	7074

All lamellas considered in this study are produced using the same matrix. The matrix is composed of 52.1% resin (Sika Biresin CR 141), 46.9% hardener (Sika Biresin CH 141) and 1% accelerator (Sika Biresin CA 141). Selected mechanical properties of the matrix are presented below (Table 18) [6].

Table 18: *Selected mechanical properties of the matrix according to [6]*

Density [kg/cm^3]	MOE [MPa]	$f_{t,u}$ [MPa]	$f_{c,u}$ [MPa]	$\varepsilon_{t,u}$ [%]
1.2	3200	78	122	3.3

The four CFRP-lamella types considered in the presented study are produced using different carbon fibres. Selected mechanical properties of the carbon fibres are shown in the table below (Table 19).

Table 19: *Selected mechanical properties of the carbon fibres and the CFRP-lamellas produced using these fibres according to [5, 13]*

Carbon fibres				**CFRP-lamella**		
MOE	$f_{t,u}$	$\varepsilon_{t,u}$	lamella type	MOE	$f_{t,u}$	$\varepsilon_{t,u}$
[GPa]	[MPa]	[%]		[GPa]	[MPa]	[%]
230	4900	2.1	S	165	3100	1.7
294	5490	1.9	M	210	3200	1.35
437	2100	0.42	H	300	1500	0.45

According to de Castro San Román [29], the epoxy-based adhesives were modelled as isotropic linear elastic materials. Therefore, only two elastic constants are needed to describe the material (Table 20).

Table 20: *Modulus of elasticity and Poisson's ratio used for the different adhesives*

Adhesive type	**MOE**	**Minor Poisson's ratio**
	[MPa]	[-]
SD 30	11'200	0.35
SD 330	4'500	0.35
SD 331W	3'500	0.35

5.2 Modelling of the experiments

The aim of modelling the experiments was to develop a numerical model that allows the stress and strain distribution in the bond area to be investigated, in function of the mechanical properties of the materials used (e.g. MOE of the CFRP, MOE of the adhesive). As timber-bending failure was the governing failure mode during the experiments (Chapter 4), no special measures concerning delaminating were taken during the finite element modelling. However, the multi-surface plasticity model used includes softening functions that allow for modelling failure to a certain degree [37]. Therefore, one can assume that the calculated stress distribution would clearly indicate the beginning of a delamination.

In order to reduce the model-size, two symmetrical planes were used, and therefore only a quarter of the beam was modelled (Figure 98).

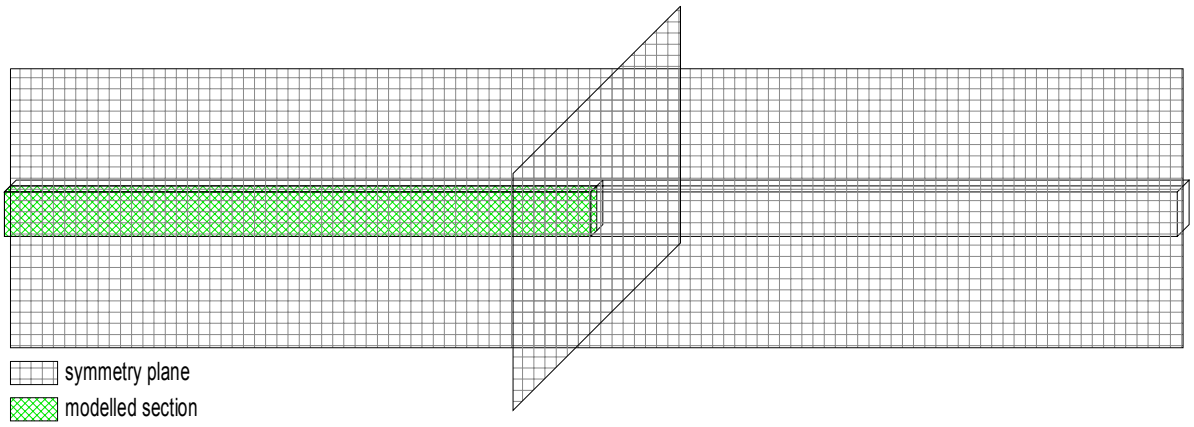

Figure 98: *Symmetry planes used and resulting model*

The multi-surface plasticity model used allows the description of spruce timber with easy to measure parameters. Contact elements and other elements requiring input parameters that are not related to the mechanical properties of the material were avoided as far as possible. Contact elements were used between the timber and the loading/support plates. The modelling of the prestressing also required the use of contact elements that were set inactive after prestressing. This strategy allowed the result governing input parameters to be all well-known material parameters; therefore no *curve fitting* was needed to determine the contact stiffness parameter. Consequently, the adhesive layer was modelled as a solid with at least three elements in its smallest dimension. The nodes between timber and adhesive and also between adhesive and CFRP were merged so no slippage could occur. The ratio between the edge lengths in one element was limited to ten. These restrictions led to a large but still reasonably-sized model.

The cambering was modelled as previously done in the experiments. Therefore, the first load step was introducing the camber into the timber while keeping the elements of the adhesive layer inactive. The elements of the CFRP-lamella were connected to the timber using a dummy material layer with a very low MOE as can be expected of uncured adhesive. Contact elements with a tangential contact stiffness of nearly zero were used between the timber and the dummy material, and also between the dummy material and the CFRP. At the end of load step one, the timber was cambered and the CRFP-lamella had the same curvature as the beam. The stress and stress distribution in the timber and the CFRP were equal to the stress resulting from the curvature. This proves that the dummy material and its contact element did not transmit any forces but still ensured that the CFRP had the same camber as the timber.

During the second load step, no deformations or forces were introduced but the elements of the dummy material and its contact elements were set inactive, and the elements of the adhesive, set active. These actions yielded an adhesive layer with the MOE of cured adhesive, and the same camber as the timber but with no stress present in the material. The stress and its distribution in the timber and CFRP did not change during this load step. This behaviour of the model corresponds with the material behaviour expected during the bonding process.

Load step three involves the removal of all external forces and results in a prestressed composite beam. The composite beam contains no contact or interface elements. Only at the supports and the loading plates were contact elements used.

Lastly, the four-point bending was modelled. In this step, a deformation was applied on the loading plates. Complete failure of the beam was assumed at the point where Ansys no longer converted. The last converted solution showed significant plastic strain on the tension side, which was evident in cracks and starting failure. The timber model used does not convert if a large number of elements have passed its elastic limits in tension. Therefore, the post-failure behaviour of a beam cannot be investigated with the multi-surface plasticity model used.

During the experiments, the specimen showed a quite abrupt failure; therefore the deformation measuring devices had to be removed before complete failure. Consequently, the crosshead displacement was taken for comparison with the numerical modelling. The deformation of the testing equipment was considered for theses comparisons.

For verification of the multi-surface plasticity timber model in its elastic domain, the four-point bending of a glulam beam was modelled using orthotropic elasticity in one run and the multi-surface plasticity model in the other. Then the same was done for reinforced beams. The two models yielded the same deformation for a glulam beam in its elastic domain (Figure 99). Furthermore, the importance of considering the non-linear behaviour of timber could be seen. The failure load is overestimated by approximately 10% if tension strain in midspan is regarded as the failure criterion for the calculations using only orthotropic elasticity.

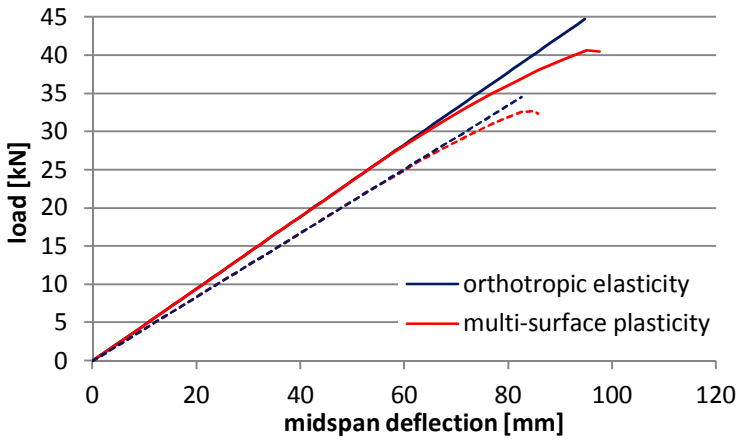

Figure 99: *Comparison of orthotropic elasticity with the multi-surface plasticity model for timber (solid lines: reinforced beams; dotted lines: glulam GL24h)*

5.2.1 Modelling of Series 1

The model for the small specimens contains only regular-shaped brick elements with eight nodes. The adhesive layer was modelled with three elements in its thickness; and over the height of the CRFP-lamella, four elements were used. The element size was varied over the height of the timber beam. In the region where high strain and active yield criteria were expected, small elements were selected. In regions with low strain, larger elements were used (Figure 100).

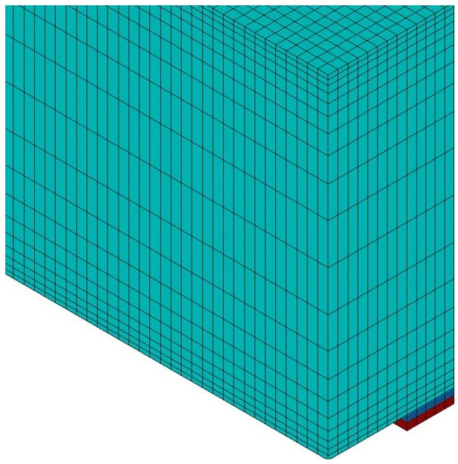

Figure 100: *Element-size distribution of the finite element model for the small specimen (the dummy material and loading plates are not shown)*

All seven samples of Series 1 were modelled. The MOE for timber in the fibre direction was set for each sample as the measured average bending MOE. All other elastic constants were set as defined in section 5.1. The ultimate strengths of the timber were initially set to the values given above (Table 15).

5.2.1.1 Comparison with the Experiments

The load-crosshead displacement graphs show that in the numerical calculation, and using the strength presented above (Table 15), the timber begins to yield at a significant lower load than in the experiments. The graph below shows the comparison for the sample control with to calculated results (Figure 101).

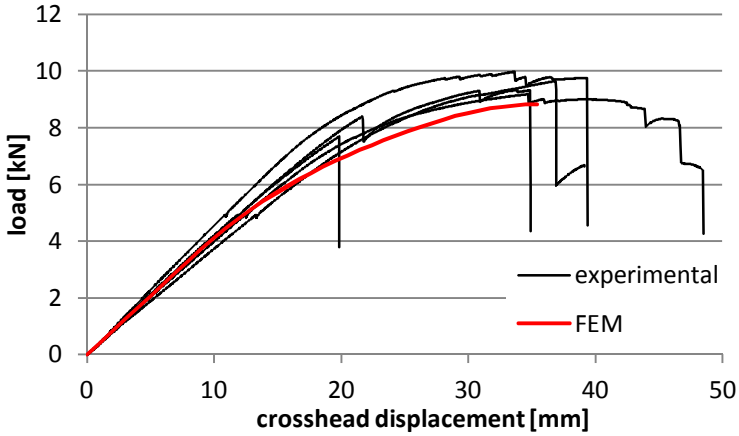

Figure 101: *Load as a function of the crosshead displacement of the control specimens (**black**: experimental measurements; **red**: FEM)*

According to Kollmann [48], the compression strength determined by the author [62] is quite low. Kollmann [48] specifies between 31.8 MPa and 34.5 MPa for air-dried clear spruce, depending on the specimen geometry. For room-dried small clear specimens, values between 56.2 MPa and 60 MPa depending on the specimen geometry are given. As the timber used for the experimental part of this dissertation had a moister content of 12%, the compression strength can be expected to be between the values given by Kollmann.

The ultimate load-bearing capacity was generally overestimated by the finite element calculation. This can be explained by the slope of grain that was present in some timber specimens. According to Vallée, Tannert, Lehmann et al. [118], a slope of grain of 10 degrees leads to a reduction in the tensile strength from 98.2 to 43.7 MPa, which represents more than 50% for quite a small deviation of the fibres in the loading direction. Therefore, it can be assumed that the minor slope of grain present in some specimens led to a significant reduction in the failure load. A reduction in the tensile strength to 85 MPa showed, in combination with a compression strength of 45.6 MPa, quite a good correlation with the control specimens (Figure 102). The graphs of the other samples in Series 1 can be found in the Appendix. Generally the numerically calculated graph starts to yield earlier than the graph measured in the experiments. However, a good agreement was detected for sample A. During the experiments, sample B showed a more pronounced non-linear branch than the other samples, although this could not be seen in the numerical calculations.

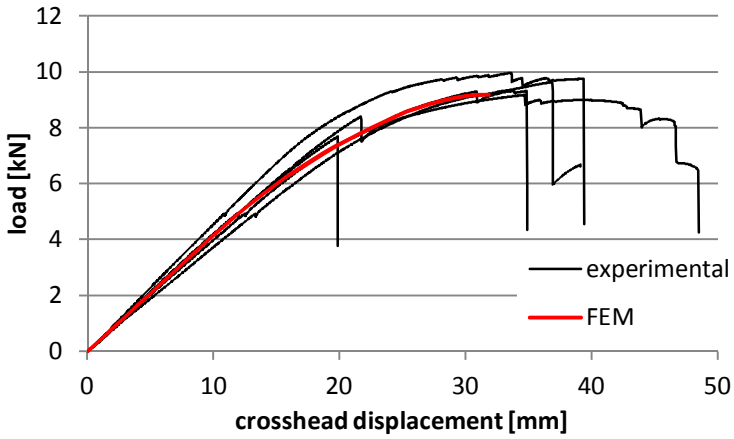

Figure 102: *Load as a function of the crosshead displacement (**black**: experimental measurements of the control specimens; **red**: FEM)*

The numerically-determined load-bearing capacity of the controls was only 1.8 % higher than the average determined during the experiments (Table 21).The failure load for the reinforced specimens was generally overestimated in the numerical calculation. Generally, the calculated failure load was in the range of the strongest specimen within the sample. One possible explanation could be the variation of timber or the slope of grains present in the experiments, which led to an overestimation of the tensile strength in the model. The fracture in tension parallel to the fibres in the multi-surface plasticity model used is described with a linear softening function. The angle of the softening function has a significant influence on the failure propagation: in the model used, the angle was set to the negative value of the module of elasticity. As this angle is very difficult to determine experimentally, no additional literature was found, and therefore no justification for reducing it was found. A steeper softening function leads to a more brittle failure and therefore reduces the crack-bridging capability of the CFRP, thereby reducing the ultimate load-bearing capacity.

Table 21: *Comparison of the load-bearing capacity and the prestress between the experiments and numerical calculation of Series 1*

	Load-bearing capacity		**Prestress in CFRP**	
	experimental [kNm]	FEM [kNm]	experimental [MPa]	FEM [MPa]
Control	1.49	1.52	-	-
Sample A	1.9	2.12	141	173
Sample B	1.83	2.1	154	162
Sample C	1.85	2.13	144	168
Sample D	1.76	2.12	79	81
Sample E	1.71	2.14	205	254
Sample F	1.77	2.1	4	-

The governing parameters of the material model allow adjustment until nearly perfect agreement with the experiments. However, the aim is to use the input parameters given by the literature or measured experimentally, and therefore no curve fitting was undertaken. All samples were modelled using the same material parameters except for the comparison with the experiments. The module of elasticity parallel to the grain was set for each sample to the bending MOE determined during the experiments.

The zones with active non-linearity in the numerical model do correspond with the observations made during the experiments. In the experiments, some compression wrinkles occurred between loading point and support, which corresponds with the large zone behind the loading points (Figure 103). The grey zone in the figure shows the loading points, and represents the compression yielding perpendicular to the fibre. Some yielding is also visible in the support region. The active non-linearity in the tension zone represents the cracks that occurred before failure of the specimen.

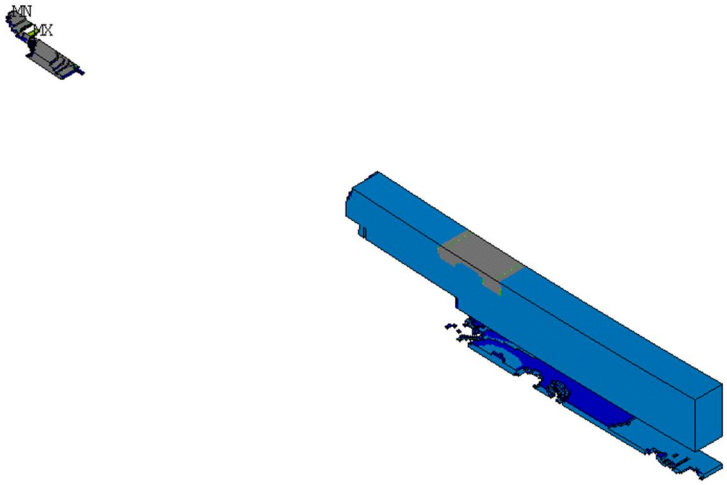

Figure 103: *Elements with active non-linearity at maximum load*

5.2.1.2 Results

For the comparison of the numerically-calculated results between the different samples, the modulus of elasticity of timber was set to the average of the control specimens for all samples. This allowed the influence of the adhesive and the prestress level on calculated results to be determined. In order to compare the influence of the studied parameters on the stress distribution towards the end of CFRP-lamella, this region was meshed using smaller elements.

The different load level during the bonding of the lamella can be clearly seen in the force deflection graph (Figure 104). Higher stress in timber during bonding leads to a larger camber and therefore to less deflection at a given load.

The computed stress distribution after prestressing indicates a fairly regular distribution of the shear stress in the adhesive layer. Towards the end of the lamella, a slightly higher stress level was observed.

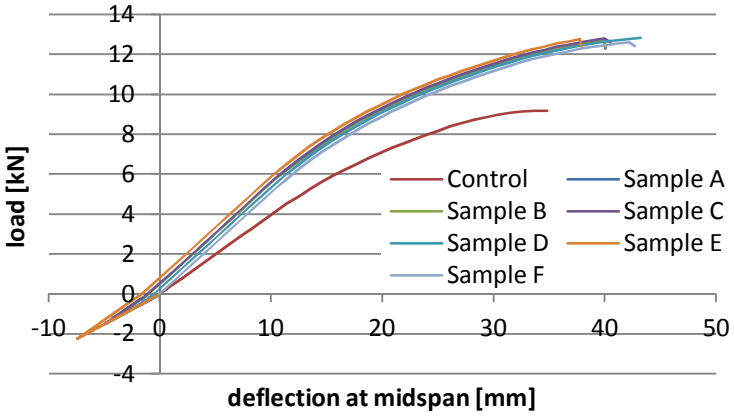

Figure 104: *Load as a function of the deflection at midspan (the cambering of the battens is also shown in the graph)*

There is no significant difference in the loadbearing capacity between the reinforced samples. However, the reinforcement leads to a clear gain compared to the controls (Table 22 and Figure 104).

Table 22: *Numerically-calculated results using the same timber properties for all specimens*

	Camber [mm]	**Prestress in CFRP** [MPa]	**Load-bearing capacity** [kNm]	**Deflection at max load** [mm]	**Stress in CFRP at max. load** [MPa]	**Deflection at 1 kNm** [mm]
Control	-	-	1.52	34.8	-	15.8
Sample A	-1.06	164	2.10	39.9	1486	11.0
Sample B	-1.06	164	2.10	39.9	1485	11.0
Sample C	-1.09	163	2.11	39.9	1476	10.9
Sample D	-0.54	82	2.12	43.2	1480	11.4
Sample E	-1.63	245	2.11	37.7	1512	10.3
Sample F	-		2.08	42.1	1368	12.0

The numerical calculations show that at failure load, the highest shear stress in the adhesive layer is not towards the end of the lamella but in the region where the force is applied during the four-point bending. The prestress level shows no influence on the peak stress; however, the modulus of elasticity of the adhesive had some influence. A high MOE led to higher shear stress in this region. However, the stress was still lower than the shear capacity of the adhesive and timber (Figure 105).

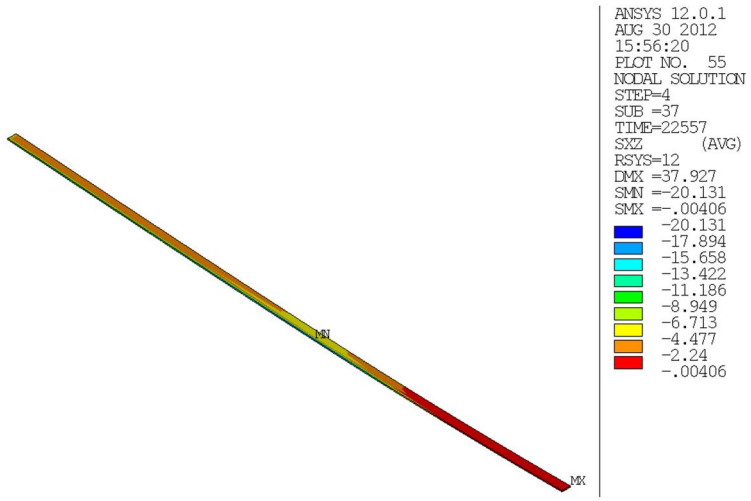

Figure 105: *Computed shear stress in the adhesive layer at failure. The symmetry at mid-span is in the lower right corner of the image.*

At the very end of the adhesive layer, a small area with active non-linearity was detected in the timber. The elements failed mainly due a combination of shear and tension perpendicular to the grain. Softening rules were only active in the outermost layer of the timber elements (0.7mm). This zone was, depending on the sample, between five (1.7 mm) and eight elements (2.7 mm) long. The modulus of elasticity of the adhesive seems to have had only a small influence on the length of this zone. However, the prestress level had some influence. The modelling approach used did not allow the determination if the numerical total failure started in this zone or was due to bending failure of the timber.

The stress distribution in the tension perpendicular clearly shows the progress of the non-linear zones in the various samples. There was no clear influence of the MOE of the adhesive on the stress distribution; it seems that a higher modulus of elasticity of the adhesive leads to a slightly higher peak stress in the adhesive. However, the peak is more or less on the same locus for all three adhesive types. The prestress level had a clear influence on the position of the stress peak. Higher prestress led to a larger distance between peak stress and the end of the lamella. This trend is in agreement with the larger area containing elements with active non-linearity in this zone. The maximal stress seems to be about the same for all tested prestress levels.

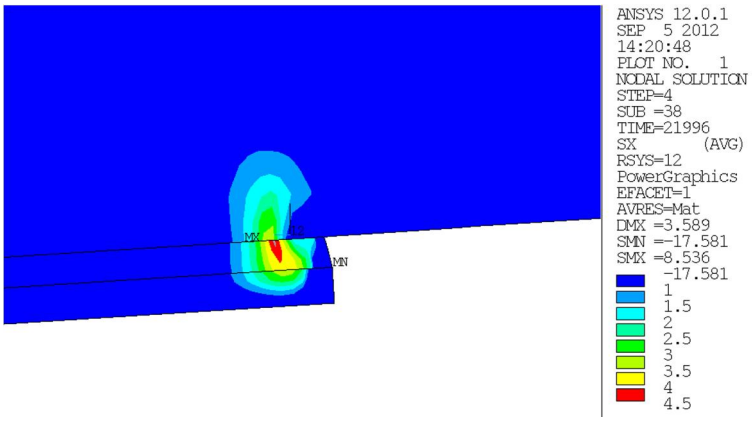

Figure 106: *Stress distribution perpendicular near the end of the CFRP-lamella*

The prestress level again had an influence on the shear stress distribution in the timber. A higher prestress level led to a larger area at the end of the lamella with low shear stress due to active softening rules (Figure 107). The prestress level also had an influence on the shear stress underneath the lamella. This influence was observed in areas without any influence from the reinforcement end. Higher prestress levels clearly led to higher shear stress in the timber.

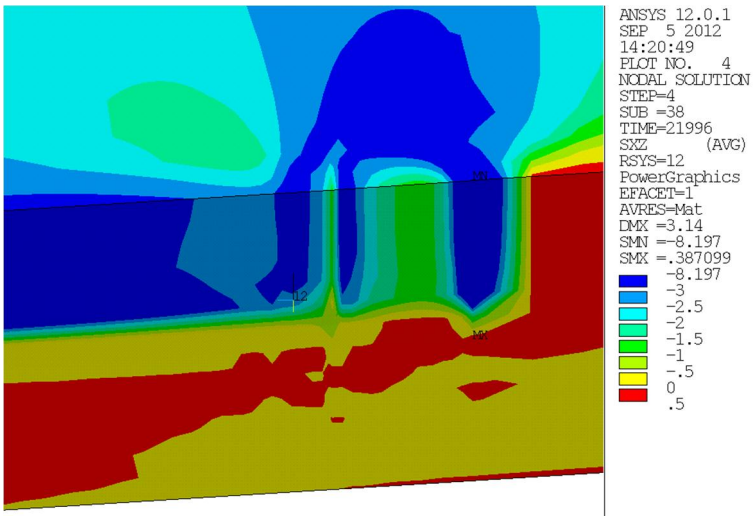

Figure 107: *Shear-stress distribution in the timber near the end of the CFRP-lamella*

5.2.2 Modelling of Series 2

The large specimens were also modelled using Ansys and the multi-surface plasticity model for timber included in the MultiPlas material library.

The ultimate strength parallel to the fibres was adjusted in the respect that structural and not clear timber was used. The other strength properties were set to the values presented above (Table 15). The tension strength was set to 38.6 MPa, which represents the average value at the first partial failure measured during the experiments (Table 13). The value for the compression strength was set to 36 MPa, which represents the value where a clear deviation from the linear relationship between the force and the compression strain in the timber was seen during the experiments (Figure 82). As the strain gauges were positioned in regions with clear timber, this deviation could not be seen for all specimens. Only the ones where

such a deviation was clearly visible were taken into account for the determination of the compression strength.

For the modelling of the structural-sized sample brick, elements with eight nodes were used. The adhesive layer was modelled with three elements in its thickness; along the height of the CRFP-lamella four elements were used. The element size was varied along the height of the timber beam. In order to reduce the model size, some irregular shapes were accepted in zones were no active plasticity or large strains were expected. However, in zones where active plasticity and high strain were expected, reasonably small, regular-shaped elements were used (Figure 108).

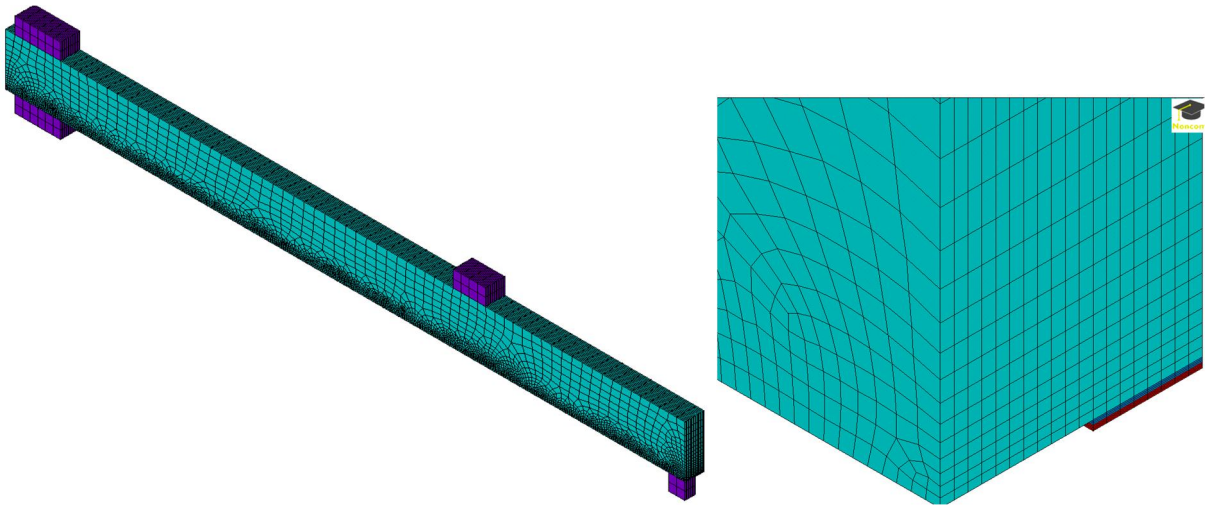

Figure 108: *Element-size distribution for the structural-sized specimens.* ***Left:*** *complete model with the loading and support plates.* ***Right:*** *detailed view of the symmetry plane at midspan (the loading plates and the dummy material are not shown)*

5.2.2.1 Comparison with the Experiments

Determining the governing material properties during the experiments allowed the minimising of the influence of natural variations in the mechanical properties on the calculated results. Therefore the force-crosshead displacement graph shows a very good correlation between the experiments and the numerical calculation (Figure 109).

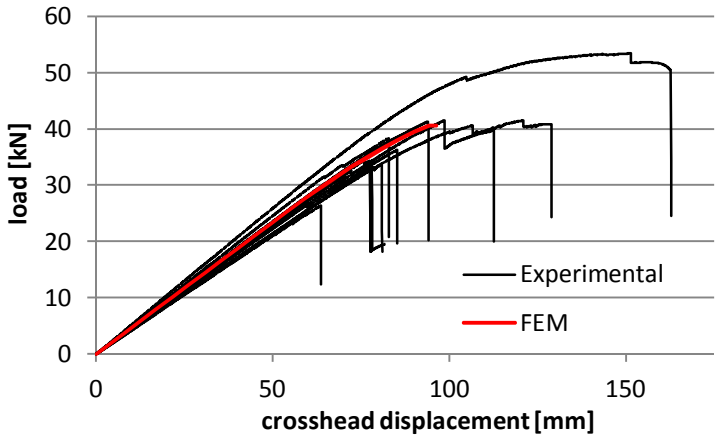

Figure 109: *Load as a function of the crosshead displacement (**black**: experimental measurements; **red**: FEM)*

The numerically calculated camber is 3.3mm due to prestressing and shows good agreement with the camber measured during the experiments at 4.1mm. One has to consider that the camber measured during the experiments has a COV of 39% (Table 12). The numerically calculated prestress in the CFRP-lamella is only 5.5% lower than the one measured experimentally. The computed prestress distribution in the CFRP-lamella corresponds well with the measured one (Figure 110). The numerically calculated maximal load-bearing capacity is overestimated by 6.1 % compared with the average, determined experimentally (Table 23).

Table 23: *Comparison of the numerical calculations with the experiments*

	Camber [mm]	**Prestress in CFRP** [MPa]	**Load-bearing capacity** [kNm]	**Gain due to CFRP**
experimental	4.1	253	25.4	
FEM	3.3	239	27	25.6%*

*The load-bearing capacity of an unreinforced beam was numerically determined using the same material properties as for the reinforced ones.

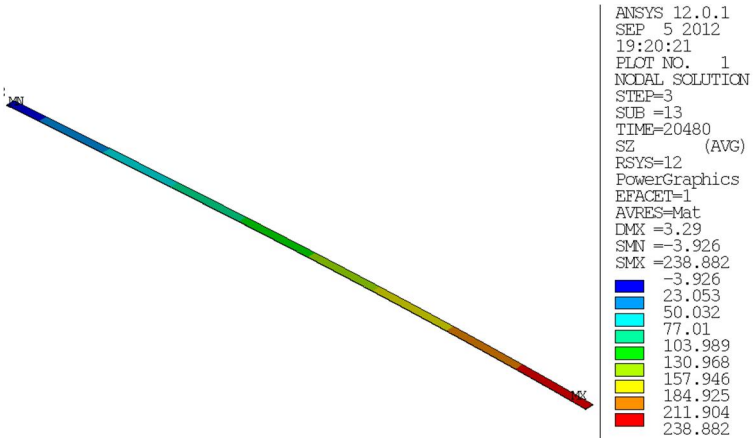

Figure 110: *Computed prestress distribution in the CFRP-lamella*

The tension strain measured on the timber corresponds well with the calculation (Figure 111). The activation of the softening at the maximal stress led to a small deviation of the ex-

pected behaviour. This small error is introduced by the material model, but has no significant influence.

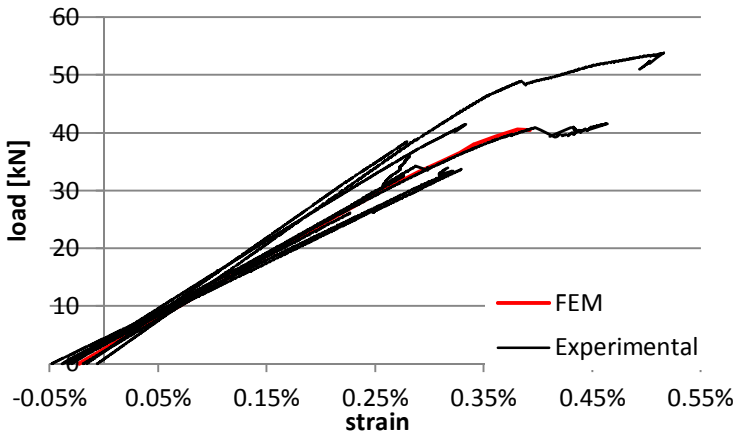

Figure 111: *Load as a function of tension strain on timber at gauge position 5, where strain at zero force is due to the prestressing (**black**: experimental measurements **red**: FEM)*

The compression strain measured on the timber corresponds well in the elastic part (Figure 112). As the strain gauges were placed on clear areas of the timber, the crushing of the timber during the bending tests was not measured even if it did occur. There were two exceptions where it was clearly visible; however, this visible crushing occurred before it could be detected in the strain-gauge measurements. In the numerical model, knots and the variability of the timber over the length of the beam, were not considered. In order to be able to represent the global behaviour of the beam, an average over the length was estimated. The result led to an overestimation of the non-linear deformation in the clear part and to an underestimation in weaker regions. Again, the activation of the plasticity led to a small shift in the graph. As there was no physical reason for this shift, it indicates some numerical problems in the material model used.

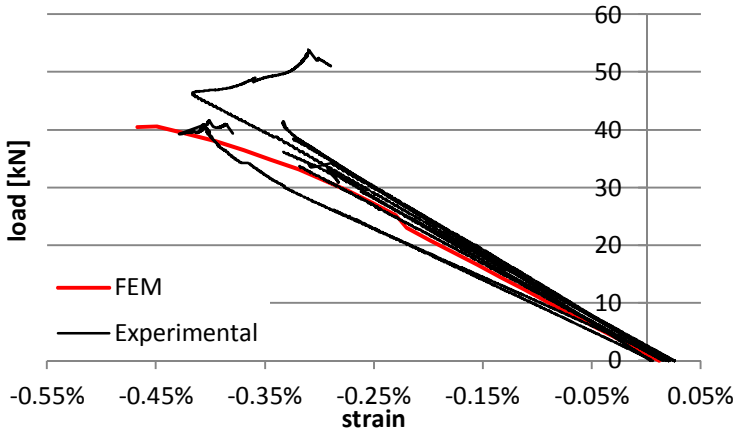

Figure 112: *Load as a function of compression strain on timber at gauge position 5, where strain at zero force is due to the prestressing (**black**: experimental measurements **red**: FEM)*

5.2.2.2 Results

The computed shear-stress distribution in the adhesive layer shows a fairly regular stress distribution over the entire length. Only towards of the end of the lamella can higher stresses be detected. However, this higher stress is less than 2 MPa and far lower than the stress that could be expected if the prestress force were constant over the whole length of the lamella (Figure 113).

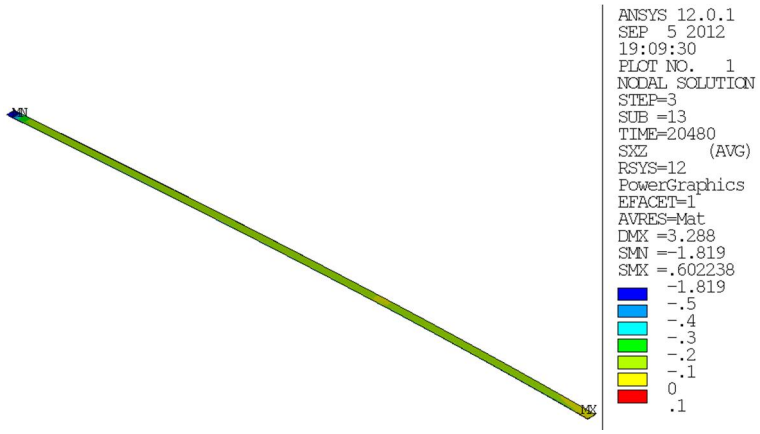

Figure 113: *Computed shear-stress distribution in the adhesive after prestressing*

At the very end of the CRFP-lamella, a small zone in the timber with active non-linearity was detected (Figure 114). The elements failed due to the interaction of shear and tension perpendicular to the fibres. This zone was only 1mm long at failure load and may have indicated the start of debonding. In the chosen modelling approach, whether the starting debonding or the bending failure led to the numerical complete failure cannot be distinguished. However, the zone with active non-linearity was clearly smaller than for the small specimens and also smaller than for the numerical calculations using CFRP-lamellas with a higher modulus of elasticity. Therefore, it can be assumed that this zone was not governing the failure for calculations using lamellas with an MOE of 165 GPa. Furthermore, the nominal shear flow and stress was lower than for the small specimens. The peak stresses perpendicular to the adhesive layer were only at the outermost node at the free corner of the CRFP-lamella. In the next node, the stress was already significantly lower. The reason may be numerical and not physical, however, especially as this element was quite distorted due to the lateral moving of the lamella during the cambering of the beam. During load step one where the camber was introduced, the elements modelling the adhesive were inactive.

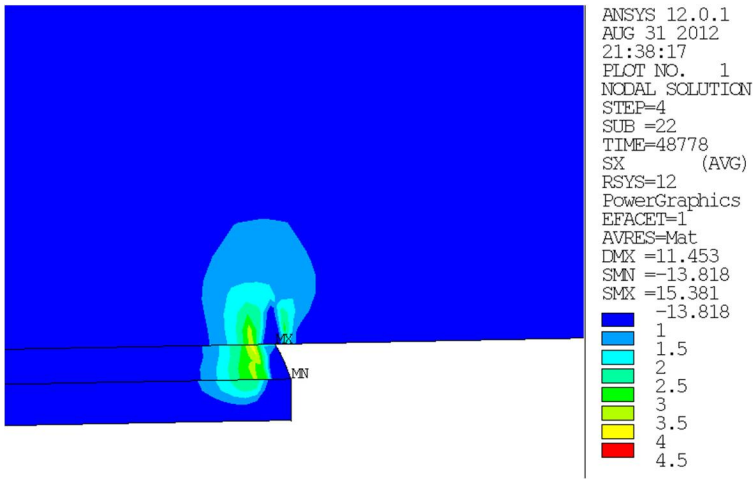

Figure 114: *Tension perpendicular at the end of the reinforcement, where the stress distribution clearly shows the active non-linearity in a small zone of the timber*

The shear stress distribution in the timber clearly shows a narrow peak at the end of the reinforcement (Figure 115). This peak is lower than the expected shear strength of timber. However, as the peak is in combination with tension perpendicular to the grain, some stress redistribution due to non-linear behaviour can be expected, and this is also visible in the numerical results. Compared to elastic calculations of adhesively-bonded shear connections, the stresses are quite low. According to Vallée, Tannert, Lehmann et al. [118], computed peak stresses using linear elastic-material models can reach values above 20 MPa for shear and tension perpendicular to the grain before leading to failure. The results allow the conclusion that the multi-surface plasticity model used reduces the peak stresses by active softening functions and that active non-linearity does not necessarily lead to delamination.

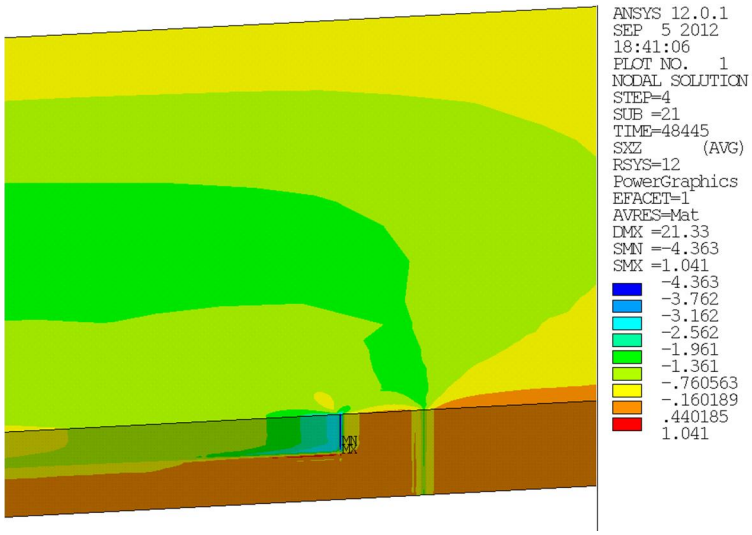

Figure 115: *Shear-stress distribution in timber at the end of the reinforcement*

The distribution of the longitudinal stress in the CFRP-lamella clearly shows the bending of the CFRP-lamella towards its end (Figure 116). The bending is due to the eccentric force in the CRFP-lamella. This introduces tension perpendicular to the grain in combination with shear stresses, which can lead to the peeling of the reinforcement. Schnüriger, Brunner and Lehmann [98] also report such debonding of the multilayered CFRP reinforcement during

bending tests using highly prestressed CFRP-lamellas. However, during the experiments described in Chapter 4, no such debonding before timber failure was detected, and the prestress level introduced with the camber method is quite low compared to other methods. Therefore, one can assume that no additional end anchorage is needed as long as lamellas with an MOE of 165 GPa and the camber method are used for prestressing.

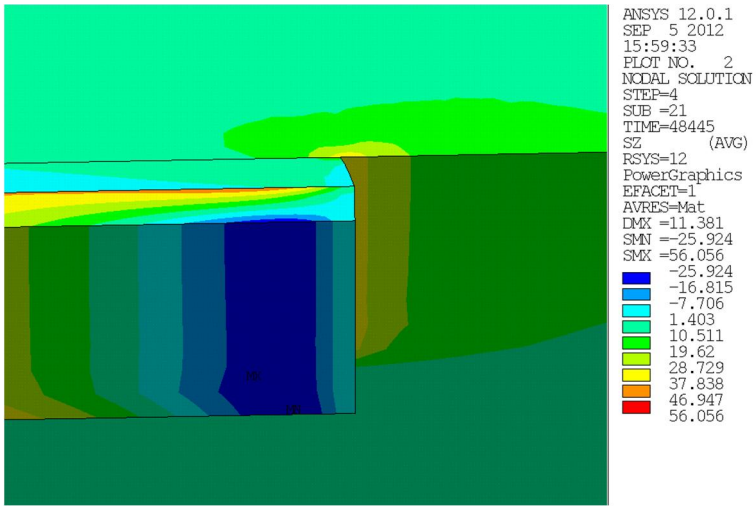

Figure 116: *Stress parallel to the fibres at the end of the reinforcement, where only the last four centimetres of the lamella are shown*

At the loadbearing limit, the shear-stress distribution in the adhesive shows a clear peak towards the end of the lamella. Otherwise, the stress distribution is quite regular and corresponds well with the expectations. The peak stress under the loading point is not as clearly visible as in the small samples. This is possibly due to the relatively small area that has already passed its elastic limit (Figure 117).

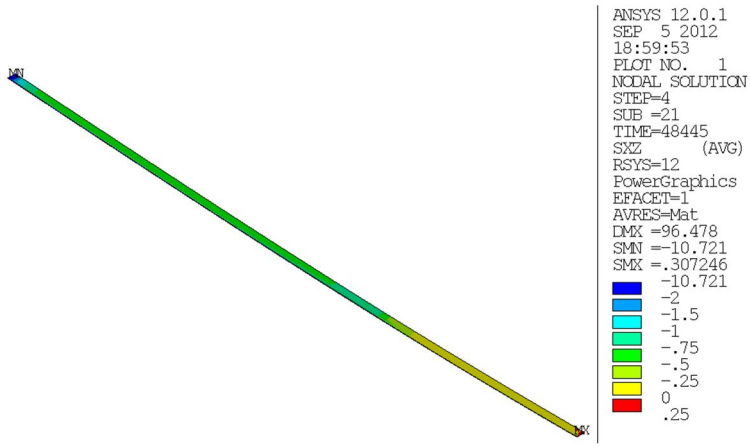

Figure 117: *Shear-stress distribution in the adhesive at ultimate load*

5.3 Optimisation using FEM

As already shown in the modelling and in the experiments, the CRFP-lamella is not used to its full capacity. As the proposed prestressing method depends on the difference of the MOE in the fibre direction of the two materials, a high modulus carbon fibre may allow the use of the lamella to its full capacity and to higher failure loads. Unfortunately, the lamellas with high

MOEs are quite expensive, and therefore not often used in the building industry. The HM carbon fibres and lamellas produced using such fibres have a significant lower ultimate tension strain and also lower tension strength. CFRP-lamellas with MOE up to 400 GPa are produced for the building industry [5, 7]. The design strain (0.16 %) of such lamellas exactly equals the theoretical strain in GL24h at design-bending stress for beams with a height less than 230mm. As the lamellas are prestressed in this work, the use of this CFRP-lamella type may not be efficient (Table 24).

Table 24: *Overview of the results using CRFP-lamella with different modulus of elasticity compared with the unreinforced beam*

	Unreinforced beams	**Reinforced beams**			
MOE of the lamella	-	165 GPa	210 GPa	300 GPa	400 GPa
camber	-	3.3 mm	4 mm	5.2 mm	6.4 mm
prestress in CFRP	-	239 MPa	285 MPa	375 MPa	459 MPa
load-bearing capacity	21.5 kNm	27 kNm	27.9 kNm	27.9 kNm*	21.0 kNm*
deflection at max load	85 mm	91.8 mm	91.7 mm	87 mm	52.3 mm
deflection at 15kNm	53.8 mm	44.1 mm	42.2 mm	38.4 mm	34.6 mm
stress in CFRP at max. load	-	927 MPa	1157 MPa	1500 MPa	1450MPa
utilisation CFRP**	-	30%	36%	100%	100%

*Failure due to CFRP rupture.

**Calculated using the average tension strength stated by the producer [5].

Beams reinforced using CRFP-lamellas with an MOE of 300 GPa fail due to CFRP failure if the bending stress in timber during bonding of the lamella is 20 MPa. However, the loadbearing capacity of such a composite beam is the same as for a beam reinforced using lamellas with a MOE of 210 GPa. A reduction of the bending stress during bonding to 13 MPa allows the full utilisation of the prestressed composite system, and increases the load-bearing capacity by about 8 %. In this system, the strength of the CFRP and the timber is reached at nearly the same load level. However, the reduction of the prestress leads to 35 % less camber (Table 25). For lamellas with an MOE of 400 GPa, a camber of 6.4mm can be achieved. Unfortunately, the ultimate strength of the CFRP is reached on a level lower than the unreinforced beam, and therefore, the reinforcement for such a beam is for service-limit state only. If lamellas with an MOE of 400 GPa are used without prestress, the composite still fails due to CFRP failure but on a load level higher than for beams using lamellas with an MOE of 210 GPa. Depending on whether the deformation or the strength is governing, one can chose the prestress level using high modulus CFRP-lamellas. Lamellas with an MOE of 400 GPa should be used only if the service-limit state is governing the design and/or in combination with low-grade timber.

Table 25: *Computed results for beams using high modulus CRFP-lamella and different prestress levels*

MOE of the lamella	300 GPa	300 GPa	400 GPa	400 GPa
stress in timber during bonding	20 MPa	13 MPa	20 MPa	-
camber	5.2 mm	3.4 mm	6.4 mm	-
prestress in CFRP	375 MPa	244 MPa	459 MPa	-
load-bearing capacity	27.9 kNm*	30.1 kNm	21.0 kNm*	28.7 kNm*
deflection at max load	87 mm	96.4 mm	52.3 mm	88 mm
deflection at 15 kNm	38.4 mm	41.3 mm	34.6 mm	41.7 mm
stress in CFRP at max. load	1500 MPa	1500 MPa	1450 MPa	1450 MPa
utilisation CFRP**	100%	100%	100%	100%

*Failure due to CFRP rupture.

**Calculated using the average tension strength stated by the producer [5].

The modulus of elasticity of the CFRP-Lamella has a clear influence on the shear stress in the timber at ultimate load. This influence is clearly visible towards the end of the lamella. A higher MOE leads to a significantly higher shear stress (Figure 118). The prestress level may have some influence on the shear-stress distribution but it is far less obvious. One reason is as for the high modulus CRFP-lamella the strength of the CFRP is design governing and therefore at ultimate load the tension force in the CRFP-lamella is the same.

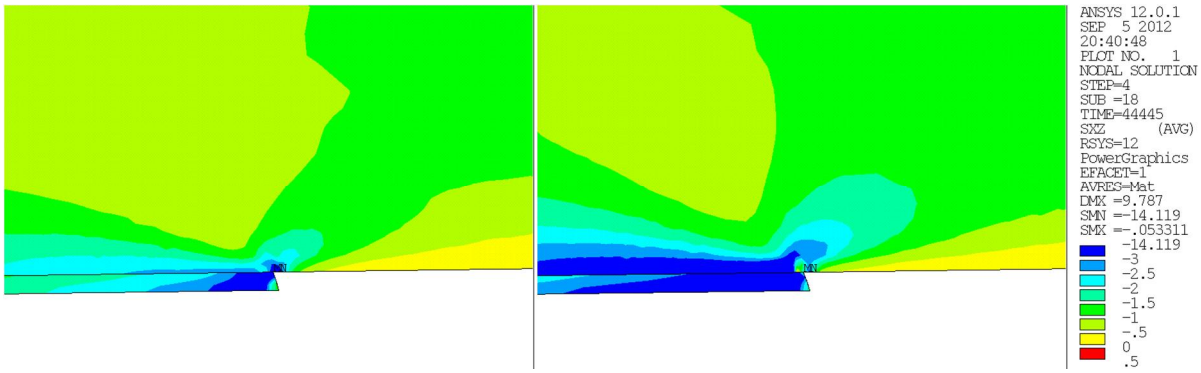

Figure 118: *Shear-stress distribution at ultimate load towards the end of the lamella (only the last 15mm is visible).* ***Left:*** *The MOE of the CFRP is 165 GPa;* ***Right:*** *The MOE of the CFRP is 300 GPa.*

The MOE of the CFRP-lamella has a clear influence on the tension perpendicular to the fibre in the timber. Higher MOE leads to higher stress and the peak is further away from the end of the lamella which corresponds with the larger area containing timber elements with non-linear behaviour. Again the prestress level had little influence.

5.4 Discussion and conclusion

In Series 2, the governing strength properties were determined during the tests on the specimens; leading to a good conformity between the experiments and the numerical modelling. However, the strength properties of the timber used in Series 1 were not determined using the same specimens as for the bending tests. Consequently, some adjustment based on the values presented in literature [48, 80, 85, 118] had to be made for Series 1, in order to reach an acceptable agreement between the experiments and the numerical calculations. This factor shows the importance of determining the parameters during the experiments using the same specimens, unless one prefers to achieve the correlation by curve fitting.

The shear-stress distribution in the adhesive layer indicates that there is no pronounced anchorage zone towards the end of the lamella. There is a zone with higher stresses and also some stress peaks at the end of the lamella. However, not the whole force of the lamella is anchored in this region. For concrete, the model with an anchorage zone is developed where the CFRP reinforcement often fails due to peeling of the lamella. This failure mostly occurs in the concrete underneath the adhesive [116]. In concrete, a large part of the tension zone is fissured and therefore the design model defines the anchorage zone in the non-fissured part of the beam towards the end of the lamella [11]. For the concrete model in this zone, the whole force in the CFRP is anchored. As timber has different load-bearing behaviour than concrete, the force in the lamella is anchored over the whole length. Therefore the author recommends that the calculation model for the anchorage force proposed for concrete in the Swiss pre-standard SIA 166:2004 externally-bonded reinforcement [11] is not applied for timber structures. Furthermore, the differentiation between the anchorage and active zones needs to be questioned for timber structures. The use of the camber method for prestressing in timber structures leads to an anchorage of the prestress force over the whole length of the lamella. However, if a prestressing frame or similar method is used, the whole prestress force is anchored in the very end of the lamella [114] and the anchorage zone has to be considered for design.

The design strain stated in the applications guide for CFRP-lamellas [5, 7] is based on the load-bearing behaviour of concrete, where strain peaks in the fissured zone have to be considered. However, as timber has no fissured zone, a reductions factor of 2 between the minimum ultimate strain and the design strain can be questioned. The factors γ_M and η_M are given with 1.3 and 0.8 in the Swiss standard [11] which leads to a reductions factor of 1.625. Therefore, one could suggest dividing the five percentile by 1.625, which leads to significantly higher values than stated in the applications guide [5, 7], and to a significantly higher design capacity for timber beams reinforced using high or ultrahigh modulus CFRP-lamellas. However, if lamellas with an MOE of 165 GPa or 210 GPa are used, the design strain does not govern the design.

For the large specimens using high modulus CFRP as reinforcement, the stress peaks towards the end of the lamella have about the same values and the same locus as the ones in the small specimens, and therefore one can assume that no delamination should occur before timber failure. This assumption is confirmed by the fact that the numerical model had no convergence issues with loads significantly higher than at the point where CFRP rupture was expected.

The timber model used allows the numerical estimation of the failure load if the input parameters are properly determined. However, it does not allow modelling the post peak behaviour. Furthermore, this model does not consider the variability of the timber unless one is modelling the knots and the fibre angle. This leads to a limitation if local effects have to be analysed. However, a model considering the variability of the timber would be quite expensive considering the calculation-power and time necessary. According to Frese [32], hundreds of calculation runs with different beams would be needed in order to determine the characteristic strength, using numerical calculations to consider the natural variability.

6 Overall Discussion and Conclusion

The analytical calculations model corresponds well with the results for the prestressing obtained by the numerical modelling. The camber and the prestress present in the CFRP are exactly the same for both methods. There is only a small difference in stress in the timber at midspan after prestressing. The origin of this deviation is due to the fact that the analytical calculation model does not consider the local influence of the loading plates during the cambering. The example used to illustrate the analytical model (Chapter 3) was also calculated using Ansys. The modelling approach was the same as described in Chapter 5; however, instead of a four-point bending, the distributed load was force controlled applied . The difference at ultimate design load was lower than 2%. For the reinforcement using CFRP-lamella with a MOE of 165 GPa, all timber elements stayed within the elastic limits. Therefore, no debonding was expected. In a case where a lamella with an MOE of 300 GPa is used, a few elements at the end of the lamella are beyond the elastic limits. As this area is only two elements long (0.7mm), which is far less than was detected during the modelling of the experiments, one can assume that no delaminating will occur as long as the timber in this zone is of a good quality and no strength-reducing features are present.

The numerical calculations showed that using high modulus CFRP-lamellas may be a reasonable solution when reinforcing using the camber method to prestress the lamella. Therefore the influence of high modulus CFRP-lamella on the design of the example structure used in Chapter 3 was determined using the analytical calculations model. Using CFRP with an MOE of 210 GPa leads to a 10 % higher margin in the timber for the ultimate-limit state, and the utilisation of the timber drops to 88 %. The gain in the service-limit state leads to a fulfilment of the limit given for near-permanent loads considering the appearance; the limit given for fittings with ductile behaviour is only surpassed by 1.6 %. This is an improvement of the service-limit state by about 5 % and 12 % respectively, compared to a reinforcement using CFRP with an MOE of 165 GPa. The utilisation of the CRFP-lamella regarding the design strain is, at 49 %, about 9 % higher for the lamella with an MOE equivalent to steel.

Using CFRP-lamella with an MOE of 300 GPa allows for a utilisation of 100%, regarding the design strain of the lamella. The utilisation of the timber drops to 81 %. In order to avoid a violation of the design strain of the CFRP, a reduction of the bending stress in timber to 14 MPa during bonding is necessary. Even with this reduction, the service-limit state can easily be fulfilled. Beside the greater margin towards the design limits, the lower bending stress during bonding and the lower utilisation shows that high modulus CRFP-lamellas may be a good solution if the timber quality is not completely sound.

Using CRFP-lamellas with 400 GPa leads to an almost complete utilisation of the lamella without any prestress, and the utilisation of the timber is also nearly 100% considering the ultimate-limit state. However, the service-limit state for near-permanent loads regarding the appearance cannot be met. The deflection is 3.2 mm above the limit, representing a violation of the limit by 24 %. The results show that the use of ultrahigh modulus CFRP-lamellas does not lead to an improvement of the design compared to the other lamellas.

The lamella with an MOE of 300 GPa clearly shows the best performance of all types investigated. However, one has to consider that high modulus CFRP-lamellas are far more expen-

sive than lamellas with an MOE of 165 GPa. As the camber method is proposed for the reinforcing of both heritage and contemporary timber structures where the material costs are usually kept lower than the labour costs, the use of all types of CFRP may be justified. Moreover, the camber method is far less labour intensive and destructive than most other reinforcing methods. However the costs would prohibit the use of CFRP in a new construction in order to reduce the timber consumption.

The investigations show that the analytical calculation model presented allows for a safe design and shows good agreement with the experiments and numerical modelling. The calculations and experiments demonstrate that the reinforcing of timber beams using the camber method is efficient. The example presented shows that existing structures can be upgraded to withstand the higher deal and live loads due to renovation and change from residential building to office use. The investigations show that the MOE of the adhesive has no significant influence on the load-bearing behaviour. However, the experiments show that the adhesive type may have some influence on the failure and post-failure behaviour. The numerical calculations demonstrate that there are stress peaks towards the end of the lamella. A higher modulus of elasticity of the CFRP-lamella leads to higher stresses in this region, although they were reasonable at design loads and no delaminating is expected. The calculations show that the use of high modulus CFRP-lamellas leads to a complete utilisation of the CFRP at design level and a significant reduction of the deflection. An adjustment of the bending stress during the bonding of the lamella leads to higher failure loads and a lower camber after prestressing.

The reaction to climatic variations and the long-term behaviour of timber beams reinforced with CFRP using the camber method needs to be studied further. In addition, and especially for high or ultra-high modulus CFRP-lamellas, the performance of the bond towards the end of the lamella needs to be studied carefully. Furthermore, the proposed analytical calculations model for long-term design has to be experimentally verified.

The experiments demonstrated that the use of a heating system allows the curing of the adhesive in one hour, although this involves clamping the lamellas to the timber, which is inconvenient on a building site. Therefore, the optimal parameters for hot curing need to be determined in the future.

Abbreviations

CFRP	carbon fibre-reinforced polymer
COV	Coefficient of variation
EI	bending stiffness = modulus of elasticity multiplied by the moment of inertia
FEM	finite-element method
FRP	fibre-reinforced polymer
GL24h	glue-laminated timber (glulam) with a 5-percentile stress in bending of 24 MPa, where the whole section contains the same strength grade of lamellas (see also SIA 265 [51])
HDT	heat distortion temperature
HBM	Hottinger Baldwin Messtechnik
MOR	modulus of rupture (maximal-bending stress)
MOE	modulus of elasticity

SIA Schweizerischer Ingenieur- und Architektenverein

Index of Figures

Index of Tables

References

[1] Agthe R. 1974: *Die Ausführung der Klebearbeiten;* Schweizerische Bauzeitung, **92**(19) pp.471-474

[2] Anonymous 1974: *Telefongebäude Füsslistrasse in Zürich - Umbau und Renovation;* Schweizerische Bauzeitung, **92**(19) pp.457

[3] Anonymous 2001: *Shear Strengthening*. Sika Schweiz AG: Zürich.

[4] Anonymous 2008: *Sika CarboDur Heizgerät, Heizgerät für beschleunigte Aushärtung*. Sika Schweiz AG: Zürich.

[5] Anonymous 2008: *Sika CarboDur Lamellen, Hochfestes CFK-Lamellen-Verstärkungssystem*. Sika Schweiz AG.

[6] Anonymous 2009: *Biresin CR 141 - Compositeharz-System für Heisshärtung*. Sika Schweiz AG: Zürich.

[7] Anonymous 2010: *Sika CarboDur Lamellen, Hochfestes CFK-Lamellen-Verstärkungssystem*. Sika Schweiz AG.

[8] Anonymus 2009: *Sikadur-30, Armierungskleber*. Sika Schweiz AG: Zürich.

[9] Anonymus 2009: *Sikadur-330, Armierungskleber und Imprägnierharz*. Sika Schweiz AG: Zürich.

[10] Anonymus 2009: *Sikadur-331W, 2-Komponenten Epoxy Dispersionsspachtel*. Sika Schweiz AG: Zürich.

[11] Arbeitsgruppe SIA 162-8 Klebebewehrungen 2004: *Klebebewehrungen*, in *Vornorm SIA 166:2004*. SIA Schweizerischer Ingenieur- und Architektenverein: Zürich.

[12] Baumann R.W. 1922: *Die bisherigen Ergebnisse der Holzprüfungen in der Materialprüfungsanstalt an der Technischen Hochschule Stuttgart*, Forschungsarbeiten auf dem Gebiete des Ingenieurwesens, Vol. 231, Verein Deutscher Ingenieure, Berlin

[13] Berset T. 2010: *e-mail 16/02/2010*. Sika Schweiz AG: Zürich.

[14] Blass H.J., Krams J. and Romani M. 2002: *Verstärkung von BS-Holz-Trägern mit horizontal und vertikal angeordneten CFK-Lamellen;* Bautechnik, **79**(10) pp.684-690

[15] Blass H.J. and Romani M. 2000: *Trag- und Verformungsverhalten von Verbundträgern aus Brettschichtholz und faserverstärkten Kunststoffen;* Forschungsbericht, Universität Fridericiana Karlsruhe, Karlsruhe

[16] Blass H.J. and Romani M. 2001: *Tragfähigkeitsuntersuchungen an Verbundträgern aus BS-Holz und Faserverbundkunstoff-Lamellen;* Holz als Roh- und Werkstoff, **59** pp.364-373

[17] Blass H.J. and Romani M. 2002: *Biegezugverstärkung von Brettschichtholz mit CFK- und AFK-Lamellen;* Bautechnik, **79**(4) pp.216-224

[18] Bohannan B. 1962: *Prestressing Wood Members;* Forest Products Journal, **12**(12) pp.596-602

[19] Borri A., Corradi M. and Grazini A. 2003: *FRP Reinforcement of Wood Elements under Bending Loads*; in proceedings of the *Structural Faults and Repair* London.

[20] Borri A., Corradi M. and Grazini A. 2005: *A method for flexural reinforcement of old wood beams with CFRP materials;* Composites: Part B, **36**(2) pp.143-153

[21] Bourban P.-E., Carlsson L., Mercier J.P., et al. 2004: *Traité des Matériaux - 15. Matériaux Composites à Matrice Organiques*, Presses Polytechniques et Universitaires Romandes, Lausanne

[22] Brunner M. 2000: *On the Plastic design of timber beams with a complex cross-section*; in proceedings of the *WCTE2000*; Whistler, Canada.

[23] Brunner M. and Lehmann M. 2008: *Strengthening glulam beams with prestressed multilayer FRP carbon laminates*; in proceedings of the *Final Conference of COST E34 Bonding of Timber*; Sopron.

[24] Buell T.W. and Saadatmanesh H. 2005: *Strengthening Timber Bridge Beams Using Carbon Fibre;* Journal of Structural Engineering, **131**(1) pp.173-187

[25] Butterfield B.G. and Meylan B.A. 1980: *Tree-dimensional structure of Wood - an ultastructural approach*; second edition, Chapman and Hall, London

[26] CEN/TC 124 "Holzbauwerke" 2003: *Holzbauwerke - Bauholz für tragende Zwecke und Brettschichtholz - Bestimmung einiger physikalischer und mechanischer Eigenschaften*, in *SN EN 408:2003*. SIA Schweizerischer Ingenieur- und Architektenverein: Zürich.

[27] CEN/TC 250 "Structural Eurocodes" 2005: *Eurocode 5 Bemessung und Konstruktion von Holzbauten - Teil 1-1: Allgemeine Regeln für den Holzbau*, in *SN EN 1995-1-1:2004*. SIA Schweizerischer Ingenieur- und Architektenverein: Zürich.

[28] Cruz H. and Custódio J. 2010: *Adhesives for On-Site Rehabilitation of Timber Structures;* Journal of Adhesion Sciense and Technology, **24**(8-10) pp.1473–1499

[29] de Castro San Román J. 2005: *Experiments on Epoxy, Polyurethane and ADP Adhesives;* technical report, CCLab2000.1b/1; École Polytechnique Fédéralede Lausanne,

[30] Dziuba T. 1985: *The Ultimate Strength of Wooden Beams with Tension Reinforcement;* Holzforschung und Verwertung, **37**(6) pp.115-119

[31] Fengel D. and Wegener G. 2003: *Wood; Chemistry, Ultrastructure, Reactions*, Kessel Verlag, Remagen (Germany)

[32] Frese M. 2010: *Computer-aided simulation of glulam strength parallel to grain*; in proceedings of the *IV European Congress on Computational Mechanics (ECCM IV)*; Paris.

[33] Fuhrmann C. and Steurer A. 1995: *Massnahmen zur Leistungssteigerung bei Kleinquerschnitten in Holz;* Forschungsbericht, Bericht Nr. 208; ETH Zürich, Zürich

[34] Furuta T., Kanakubo T., Nemoto T., et al. 2001: *Sprayed-up FRP Strengthening for Concrete Structures*; in proceedings of the *FRP Composites in Civil Engineering*; Hong Kong, Elsevier.

[35] Furuta T., Kanakubo T., Nemoto T., et al. 2002: *Sprayed Up FRP Strengthening for Reinforced Concrete Beams*; in proceedings of the *International Conference on Composites in Infrastructure*; San Francisco.

[36] Goris A. ed. *Bautabellen für Ingenieure*. Vol. 20. 2012, Werner Verlag: Köln.

[37] Grosse M. 2005: *Zur numerischen Simulation des physikalisch nichtlinearen Kurzzeittragverhaltens von Nadelholz am Beispiel von Holz-Beton-Verbundkonstruktionen*; Dissertation, Bauhaus-Universität Weimar, Weimar

[38] Habenicht G. 2009: *Kleben: Grundlagen, Technologien, Anwendungen*; 6. Auflage, Springer Verlag Berlin, Berlin

[39] Hammer U., Müller D. and Bücheler L. 2005: *Instandsetzung der Nektartalbrücke der BAB 6 bei Heilbronn unter Verwendung von Carbonfaser-Spannglieder;* Tiefbau, **117**(3) pp.130-141

[40] Hartnack R. 2004: *Langzeitverhalten von druckbeanspruchten Bauteilen aus Holz*; Dissertation, Bauhaus-Universität Weimar, Weimar

[41] Herzog M. 2001: *Sanierung von Holzbalkendecken mit CFK Lamellen*; Diplomarbeit, Universität Stuttgart, Stuttgart

[42] Heuer R. 2009: *Mechanik mehrschichtiger Verbundkonstruktionen*, Skriptum zur Vorlesung 206.167 Technische Universität Wien, Wien

[43] Hill R. 1998: *The mathematical theory of plasticity*; Oxfords classic series, Oxford University Press, New York

[44] Holzenkämpfer P. 1994: *Ingenieurmodelle des Verbunds geklebter Bewehrung für Beton Bauteile*; Dissertation, Technischen Universität Braunschweig, Braunschweig

[45] Hörsting O.-P. 2008: *Zum Tragverhalten druck- und biegbeanspruchter Holzbauteile*; Dissertation, Technischen Universität Braunschweig, Braunschweig

[46] Kim Y.J. and Harries K.A. 2010: *Modeling of timber beams strengthened with various CFRP composites;* Engineering Structures, **32**(10) pp.3225-3234

[47] Klaus P.W. and Tausky R. 1974: *Bericht des Architekten und des Bauingenieurs;* Schweizerische Bauzeitung, **92**(19) pp.459-462

[48] Kollmann F. 1951: *Technologie des Holzes und der Holzwerkstoffe*; 2. Auflage; Band 1, Springer Verlag Berlin, Berlin

[49] Kommision SIA 161 "Stahlbauten" 2003: *Stahlbau*, in *SIA 163:2003*. SIA Schweizerischer Ingenieur- und Architektenverein: Zürich.

[50] Kommision SIA 162 2003: *Betonbau*, in *SIA 262:2003*. SIA Schweizerischer Ingenieur- und Architektenverein: Zürich.

[51] Kommision SIA 164 "Holzbau" 2003: *Holzbau*, in *SIA 265:2003*. SIA Schweizerischer Ingenieur- und Architektenverein: Zürich.

[52] Kommission SIA 160 "Einwirkungen auf Tragwerke" 2003: *Grundlagen der Projektierung von Tragwerken*, in *SIA 260:2003*. SIA Schweizerischer Ingenieur- und Architektenverein: Zürich.

[53] Kraemer O. 1929: *Untersuchung über den Einfluss von Aufbau und Faserverlauf auf Zugfestigkeit, Biegung und Dehnung an Birkenfurnieren und Birkensperrholz;* 122. Bericht; Deutsche Versuchsanstalt für Luftfahrt, Berlin-Adlershof

[54] Kreistelefondirektion Zürich 1974: *Ersatz der Telefonzentrale Füssli (Zürich-City);* Schweizerische Bauzeitung, **92**(19) pp.457-458

[55] Krueger G.P. and Eddy F.M. 1974: *Ultimate-Strength Design of Reinforced Timber: Moment Rotation Characteritics;* Wood Sciences, **6**(4) pp.330-344

[56] Krueger G.P. and Sandberg L.B. 1974: *Ultimate-Strength Design of Reinforced Timber: Evaluation of design Parameters;* Wood Sciences, **6**(4) pp.316-329

[57] Kucera L.J. and Gfeller B. 1994: *Einheimische und fremdländische Nutzhölzer: Merkmale und Eigenschaften der in der Schweiz gebräuchlichsten Holzarten* Professur Holzwissenschaften Zürich

[58] Lander M. and Flüehler P. 1974: *Versuche an Stahlbetonbauteilen mit geklepter Armierung;* Schweizerische Bauzeitung, **92**(19) pp.463-470

[59] Lantos G. 1970: *The Flexural Behavior of Steel Reinforced Laminated Timber Beams;* Wood Sciences, **2**(3) pp.136-143

[60] Lauterbach H. 1974: *Epoxid - Bindemittel für Klebearbeiten Stahl - Beton;* Schweizerische Bauzeitung, **92**(19) pp.470-471

[61] Lehmann M. 2006: *Renforcement sur site de poutres en bois avec lamelles de carbone précontraintes*; MSc. Thesis, Université Henri Poincaré, Nanncy

[62] Lehmann M. 2008: *LGA Holzbalken, Bestimmung von einigen mechnaischen Eigenschaften eines Historischen Holzbalkens;* Prüfbericht (confidential), 7774-SB-01; Berner Fachhochschule, Biel/Bienne

[63] Lehmann M. 2009: *Sonotan; Entwicklung von tanningebundenen Akustikplatten;* Forschungsbericht, 2692-SB-01; Berner Fachhochschule, Biel

[64] Lehmann M. 2009: *Verstärkung von Holz mittels vorgespannten CFK-Lamellen*; in proceedings of the *41. Fortbildungskurs der SAH: Werkstoffkombinationen – ein Mehrwert für Holz*; Weinfelden (Switzerland), Lignum.

[65] Lehmann M., Brunner M., Schober K.-U., et al. 2008: *Testing and Numerical Simulation of Prestressed CFRP Reinforced Timber Structures*; in proceedings of the *Final Conference of COST E34 Bonding of Timber*. Sopron.

[66] Lehmann M., Clénin R., Richter K., et al. 2007: *Kohlefaserlamellen zur Verstärkung von Holzbalken;* Baublatt, (41) pp.28-30

[67] Lehmann M., Clénin R., Richter K., et al. 2007: *Kohlefaserlamellen zur Verstärkung von Holzbalken;* der bauingenieur, (10) pp.28-32

[68] Lehmann M., Grosse M. and Tannert T. 2010: *Multi Surface Plasticity Model for Timber Bending Members*; in proceedings of the *ECCM 2010*; Paris, France.

[69] Lehmann M., Properzi M. and Pichelin F. 2008: *Strengthening of timber structures using pre-stressed carbon fibre lamellas*; in proceedings of the *1st MEDACHS 08 Conference*. Lisbon.

[70] Lehmann M., Properzi M., Pichelin F., et al. 2006: *Pre-stressed FRP for the in-situ strengthening of timber structures*; in proceedings of the *World Conference on Timber Engineering (WCTE 2006)*; Portland.

[71] Lehmann M., Vallée T., Tannert T., et al. 2009: *Adhesively bonded Joints Composed of Wooden Load -Bearing Elements*; in proceedings of the *ICF12*; Ottawa, Canada.

[72] Luggin W.F. 2000: *Die Applikation vorgespannter CFK-Lamellen auf Brettschichtholz*; Dissertation, Universität für Bodenkultur, Wien

[73] Manson J.-A.E. 2005: *Les Composites Travaux Pratiques*, Skriptum zur Vorlesung, École polytechnique fédérale de Lausanne, Lausanne

[74] Mazza P.P.A., Martini F., Sala B., et al. 2006: *A new Palaeolithic discovery: tar-hafted stone tools in a European Mid-Pleistocene bone-bearing bed;* Journal of Archaeological Science, **33**(9) pp.1310-1318

[75] Meier H. 2000: *Verstärkung einer Holzbrücke;* Schweizer Holzzeitung, **112**(31/32) pp.8

[76] Meier U. 1987: *Grundlagen zur Bemessung von Kunststoffbauteilen*, Skriptum zur ETH Vorlesung 20-638 Teil 1, ETH Zürich, Zürich

[77] Meier U. 1995: *Eigenschaften von unidirektionalen CFK-Lamellen* in: *SIA D 0128 - Nachträgliche Verstärkung von Bauwerken mit CFK-Lamellen* pp. 19 - 23, SIA Schweizerischer Ingenieur- und Architektenverein: Zürich.

[78] Meier U. 2004: *Ausblick, weitere Entwicklungen - Wo sind Systemverbesserungen noch denkbar?*; in: *Dokumentation D 0209 Klebebewehrung - Einführung in die Norm SIA 166*, pp. 53-58, SIA Schweizerischer Ingenieur- und Architektenverein: Zürich.

[79] Michaeli W. and Wegener M. 1989: *Einführung in die Technologie der Faserverbundwerkstoffe*, Carl Hanser Verlag, Wien

[80] Mitsuhashi K., Poussa M. and Puttonen J. 2008: *Method for predicting tension capacity of sawn timber considering slope of grain around knots;* Journal of Wood Science, **54**(3) pp.189-195

[81] Navi P. and Heger F. 2005: *Comportement thermo-hydromécanique du bois: applications technologiques et dans les structures*, Presses Polytechniques et Universitaires Romandes, Lausanne

[82] Negrão J., Brunner M. and Lehmann M. 2008: *Pre-stressing of timber*; in: *Lignovisionen Book Series of the institute of wood science and technology University of Vienna Issue 18/ Special edition*, pp.: Vienna.

[83] Neubauer U., Rostasy F.S. and Budelmann H. 2001: *Verbundtragfähigkeit geklebter CFK-Lamellen für die Bauteilverstärkung* Bautechnik, **78**(10) pp.681-692

[84] Neuhaus F.-H. 1981: *Elastizitätszahlen von Fichtenholz in Abhängigkeit von der Holzfeuchtigkeit*; Dissertation, Ruhr-Universität Bochum, Bochum

[85] Niemz P. 1993: *Physik des Holzes und der Holzwerkstoffe*, DRW-Verlag, Leinfelden-Echterdingen

[86] Onken P., vom Berg W. and Neubauer U. 2002: *Verstärkung der West Gate Bridge, Melbourne;* Beton- und Stahlbau, **97**(2) pp.94-104

[87] Pichelin F. 2000: *Manufacture of oriented strand board with high moisture tolerant adhesives*; Dissertation, Universität Hamburg, Hamburg

[88] Plevris N. and Triantafillou T.C. 1992: *FRP-Reinforceed Wood as Structural Material;* Journal of Materials in Civil Engineering, **4**(3) pp.300-317

[89] Preising R. 2006: *Otto Hetzer - Pionier des Holzleimbaus;* bauen mit holz, **108**(6) pp.34 - 36

[90] Properzi M. and Lehmann M. 2006: *OnSite. An innovative approach for the on-site reinforcement and rehabilitation of timber structures;* Scientific Report COST E34 project, Bern University of Applied Sciences, Architecture, Timber and Civil Engineering, Biel/Bienne

[91] Rautenstrauch K. 1989: *Untersuchungen zur Beurteilung des Kriechverhaltens von Holzbiegeträgern* Dissertation, Universität Hannover, Hannover

[92] Richter K., Cruz H. and Negrão J. 2008: *Bonding on Site; Introduction*; in: *Core document of the COST Action E34 Bonding of Timber*, pp. 7-8, Universität für Bodenkultur: Wien.

[93] Richter K., Lehmann M. and Properzi M. 2008: *Long-Term behaviour of pre-stressed timber-CFRP composites*; in proceedings of the *Final Conference of COST E34 Bonding of Timber*. Sopron.

[94] Romani M. and Blass H.J. 2001: *Design Model for FRP Reinforced Glulam Beams*; in proceedings of the *CIB-W18/34-12-3*; Venice.

[95] Rosenkranz A., Pichelin F., Lehmann M., et al. 2011: *Nigerian agricultural waste products for the production of particleboard*; in proceedings of the *Italic 6 - Science & Technology of Biomass: Advances and Challenges* Viterbo (Italy).

[96] S&P Clever Reinforcement Company: *Applikationshandbuch für S&P FRP Systeme*, [cited: 18. August 2009]; Available from: http://www.sp-reinforcement.ch.

[97] Schnell R. 1992: *Das Kriechverhalten eines quasi-isotropen CfK-Laminats unter Zugbeanspruchung bei unterschiedlicher symmetrischer Anordnung der Einzellagen*; Dissertation, Universität Stuttgart,

[98] Schnüriger M., Brunner M. and Lehmann M. 2007: *Gradientenvorspannung; Verstärkung von Holzbalken mit vorgespannten CFK-Lamellen welche in Gradienten Verankert sind;* Forschunungsbericht, Berner Fachhochschule, Biel

[99] Schober K.-U. 2008: *Untersuchungen zum Tragverhalten hybrider Verbundkonstruktionen aus Polymerbeton, faserverstärkten Kunststoffen und Holz*; Dissertation, Bauhaus-Universität Weimar, Weimar

[100] Schober K.-U. and Rautenstrauch K. 2006: *Post-strengthening of timber structures with CFRP's;* Materials and Structures, **40**(1) pp.27-35

[101] Schwegler G. 1995: *CFK-Verstärkungen im Mauerwerks- und Holzbau*; in: *SIA D 0128 - Nachträgliche Verstärkung von Bauwerken mit CFK-Lamellen*, pp. 61 - 65, SIA Schweizerischer Ingenieur- und Architektenverein: Zürich.

[102] Sliker A. 1962: *Reinforced Wood Lamianted Beams;* Forest Products Journal, **12**(1) pp.61-96

[103] Smedley D., Cruz H. and Paula R. 2008: *Quality Control On Site*; in: *Core document of the COST Action E34 Bonding of Timber*, pp. 80-90, Universität für Bodenkultur: Wien.

[104] Steiger R. 2004: *Bonding of carbon reinforced plastics (CRFP) with wood*; in proceedings of the *COST E34 Innovations in Wood Adhesives*; Biel, Switzerland, Bern University of Applied Sciences, Architecture, Timber and Civil Engineering.

[105] Stern G.E. and Kumar V.K. 1973: *Flitch Beams;* Forest Products Journal, **23**(5) pp.40-47

[106] Steurer A. 1999: *Holzkonstruktionen mit Stahl- und Kunststoffverstärkung*; in proceedings of the *SAH Tagung 1999: Tragende Verbundkonstruktionen mit Holz*; Weinfelden, SAH.

[107] Stöcklin I. 2003: *Vorgespannte CFK-Lamellen mit Gradientenverankerung*; in: *CFK im Bauwesen - heute Realität; Festschrift zum 60. Geburtstag von Professor Urs Meier*, pp. 11-15, EMPA-Akademie: Dübendorf.

[108] Strahm T. 2009: *Verbindungen mit grosser Leistung*; in proceedings of the *41. Fortbildungskurs SAH; Werkstoffkombinationen - ein Mehrwert für Holz*; Weinfelden.

[109] Stüssi F. 1946: *Holzfestigkeit bei Beanspruchung schräg zur Faser;* Schweizerische Bauzeitung, **128**(20) pp.251-252

[110] Terrasi G.P. 2003: *CFK-vorgespannte Tragwerkelemente aus Hochleistungsbeton*; in: *CFK im Bauwesen - heute Realität; Festschrift zum 60. Geburtstag von Professor Urs Meier*, pp. 25-33, EMPA-Akademie: Dübendorf.

[111] Thomsing M. 1998: *Spannbeton; Grundlagen - Berechnungsverfahren - Beispiele*, B.G. Teubner, Stuttgart

[112] Triantafillou T.C. 1997: *Shear Reinforcement of Wood Using FRP Materials;* Journal of Materials in Civil Engineering, **9**(2) pp.65-69

[113] Triantafillou T.C. and Deskovic N. 1991: *Innovative Prestressing with FRP Sheets: Mechanics of Short-Term Behavior;* Journal of Engineering Mechanics, **117**(7) pp.1652-1672

[114] Triantafillou T.C. and Deskovic N. 1992: *Prestressed FRP Sheets as External Reinforcement of Wood Members;* Journal of Structural Engineering, **118**(5) pp.1270-1284

[115] Tsai S.W. and Wu E.M. 1971: *A General Theory of Strength for Anisotropic Materials* Journal of composite materials, **5**(1) pp.58-80

[116] Ulaga T. 2003: *Lamellenverstärkte Stahlbetonträger: experimentelle Erfahrung, Analysen, Bemessung*; in: *CFK im Bauwesen - heute Realität; Festschrift zum 60. Geburtstag von Professor Urs Meier*, pp. 35-41, EMPA-Akademie: Dübendorf.

[117] Ulaga T. and Meier U. 2002: *Kohlenstofffaserverstärkte thermoplastische Lamellen für die Verstärkung von Betontragwerken;* Forschungsbericht, EMPA Bericht 260; Eidgenössische Materialprüfungs und Forschungsanstalt, Dübendorf

[118] Vallée T., Tannert T., Lehmann M., et al. 2009: *Probalistic Strength Prediction of Adhesively Bonded Joints Composed of Wooden Adherends*; in proceedings of the *ICF12*; Ottawa, Canada.

[119] vom Berg W. and Beecken C.A. 2007: *Geklebte Bewehrung aus Faserverbundwerkstoffen;* adhäsion, **51**(4) pp.45-49

[120] von Mises R. 1928: *Mechanik der plastischen Formänderung von Kristallen (pages 161–185);* Zeitschrift für angewandte Mathematik und Mechanik **8**(3) pp.161-185

[121] Widmann R., Meier U., Brönnimann R., et al. 2010: *Design, Construction and Monitoring of a Bowstring Arch Bridge Made Exclusively of Timber, CFRP and GFRP.*; in proceedings of the *WCTE 2010*; Riva del Garda.

[122] Wiedemann J. 1989: *Leichtbau; Band 2 Konstruktion*, Springer Verlag Berlin, Berlin

Affidavit

Ich erkläre hiermit ehrenwörtlich, dass ich die vorliegende Arbeit ohne unzulässige Hilfe Dritter und ohne Benutzung anderer als der angegebenen Hilfsmittel angefertigt habe. Die aus anderen Quellen direkt oder indirekt übernommenen Daten und Konzepte sind unter Angabe der Quelle gekennzeichnet.

Bei der Auswahl und Auswertung folgenden Materials haben mir die nachstehend aufgeführten Personen in der jeweils beschriebenen Weise entgeltlich/unentgeltlich geholfen:

- Bei der Auswahl und Auswertung wurde keine Hilfe in Anspruch genommen

Weitere Personen waren an der inhaltlich-materiellen Erstellung der vorliegenden Arbeit nicht beteiligt. Insbesondere habe ich hierfür nicht die entgeltliche Hilfe von Vermittlungs- bzw. Beratungsdiensten (Promotionsberater oder anderer Personen) in Anspruch genommen. Niemand hat von mir unmittelbar oder mittelbar geldwerte Leistungen für Arbeiten erhalten, die im Zusammenhang mit dem Inhalt der vorgelegten Dissertation stehen.

Die Arbeit wurde bisher weder im In- noch im Ausland in gleicher oder ähnlicher Form einer anderen Prüfungsbehörde vorgelegt.

Ich versichere ehrenwörtlich, dass ich nach bestem Wissen die reine Wahrheit gesagt und nichts verschwiegen habe.

Bern, 1. Dezember 2012

Curriculum Vitae

Professional experience

since 11.2009	University of Applied Sciences Bern – Architecture, Wood and Civil Engineering R&D department, Biel Scientific collaborator
10.2004–11.2009	University of Applied Sciences Bern – Architecture, Wood and Civil Engineering R&D department, Biel Assistant
03.2003–02.2004	University of Melbourne Trainee
08.2000–10.2000	Baur & Cie AG, Abt. Holzbau, Wettswil a. A. Carpenter
05.1996–12.1998	Baur & Cie AG, Abt. Holzbau, Wettswil a. A. Carpenter
10.1995–12.1995	Kletterzentrum Gaswerk, Schlieren Climbing wall builder
05.1995–07.1995	Baur & Cie AG Abt. Holzbau, Wettswil a. A. Carpenter
08.1994–02.1995	Wöcke Zimmerei, Herferswil Carpenter
07.1991–07.1994	Spaltenstein Holzbau AG, Zürich Apprentice Carpenter

Education

since 2007	Bauhaus University, Weimar Doctoral candidate Theme: Reinforcement of timber-bending beams using pre-stressed CFRP-lamellas Supervisor: Prof. Dr. Ing. Karl Rautenstrauch
10.2005–09.2006	Université Henri Poincaré UHP, Nancy (Frankreich) Master de recherche, ‘Sciences du Bois et des Fibres’ Title of thesis: Renforcement sur site de poutres en bois avec lamelles de carbone précontraintes
10.2000–09.2004	University of Applied Sciences Bern – Architecture, Wood and Civil Engineering Structural timber engineer Title of thesis: The Development of Vintorg 2, mechanical testing of the first trial production
01.1999–08.2000	Language holiday in America, New Zealand and Australia

07.1991–07.1994	Gewerbliche Berufsschule Wetzikon Full carpentry qualifications with technical baccalaureate
06. 1991	Completed education at secondary school, Opfikon

Memberships

since 2011	SNV Swiss standardisations committee: INB NK 2193 ‘Adhesives’
2005–2008	COST Action E34: Bonding of Timber, WG1 Bonding on-site

Publications List

Peer-reviewed journals

2010 M. Brunner, M. Lehmann, S. Kraft, J. Conzett, K. Richter and U. Fankhauser: *A flexible adhesive layer to strengthen glulam beams*; in: Journal of Adhesion Science and Technology 24/9 pp. 1665–1701

National journals

2007 M. Lehmann, R. Clénin, K. Richter and M. Properzi: *Kohlefaserlamellen zur Verstärkung von Holzbalken*; in: Baublatt 41/2007, pp. 28–30

2007 M. Lehmann, R. Clénin, K. Richter and M. Properzi: *Kohlefaserlamellen zur Verstärkung von Holzbalken*; in: der bauingenieur 10/2007, pp. 28–32

2002 M. Lehmann and B. Kenel: *Mehrgeschossiger Wohnungsbau*; in: Lignarius 14/2002, pp. 20–21

Chapters in edited books

2010 M. Brunner, M. Lehmann, S. Kraft, K. Richter, U. Fankhauser and J. Conzett: *A flexible adhesive layer to strengthen glulam beams*; in: Wood Adhesives, A. Pizzi and K.L. Mittal (eds.); Brill, Leiden, Netherlands

2008 J. Negrão, M. Brunner and M. Lehmann: *Pre-stressing of timber*; in: Core document of the COST Action E34 'Bonding of Timber', M. Dunky, B. Källander, M. Properzi, K. Richter and M. Van Leemput (eds.); Universität für Bodenkultur, Wien, Austria

Conference proceedings

2012 M. Lehmann, T. Vallée, K. Rautenstrauch: *Testing and Modelling of Prestressed Timber Beams Using a Multi Surface Plasticity Model*; in: Proceedings of the 12th WCTE 2012, 16–19 July 2012, Auckland, New Zealand

2012 C. Sigrist, M. Lehmann: *Development of a Cross Laminated, Post Tensioned Bridge Deck*; in: Proceedings of the 12th WCTE 2012, 16–19 July 2012, Auckland, New Zealand

2012 C. Sigrist, M. Lehmann: *An Integral Production Chain to Reliably Produce Glued Laminated Timber*; in: Proceedings of the 12th WCTE 2012, 16–19 July 2012, Auckland, New Zealand

2012 M. Brunner, M. Lehmann: *Bending Tests on the Continuous Glulam Beam*; in: Proceedings of the 12th WCTE 2012, 16–19 July 2012, Auckland, New Zealand

2012 C. Ganne-Chédeville, T. Volkmer, B. Letsch, M. Lehmann: *Measures for the Maintenance of Untreated Wood Facades;* in: Proceedings of the 12th WCTE 2012, 16–19 July 2012, Auckland, New Zealand

2011 A. Rosenkranz, F. Pichelin, M. Lehmann, C. Job, H. Tata Kimeng, S. Mustapha O.E. Nduka and C. Aghaegbusi Mgbemene: *Nigerian Agricultural Waste Products for the Production of Particleboard*; in: Proceedings of Italic 6 – Science & Technology of Biomass: Advances and Challenges, 5–8 September 2011, Viterbo, Italy

2010 M. Lehmann, M. Grosse, T. Tannert: *Multi-Surface Plasticity Model for Timber Bending Member;* In: Proceedings of the 4th ECCM 2010, 16–21 May 2010, Paris, France

2010 M. Lehmann, M. Brunner, S. Kraft: *Higher Load-Bearing Capabilities with Elastic Glue Lines for Glulam*; in: Proceedings of the 11th WCTE 2010, 20–24 June 2010, Riva del Garda, Italy

2010 M. Lehmann, M. Brunner, S. Kraft, U. Fankhauser, K. Richter: *Super Glulam: A Flexible Adhesive Layer Boosts the Bending Resistance of Glulam*; in: Proceedings of the 11th WCTE 2010, 20–24 June 2010, Riva del Garda, Italy

2009 M. Lehmann, T. Vallée, T. Tanner, M. Brunner: *Adhesively Bonded Joints Composed of Wooden Load-Bearing Elements*; in: Proceedings of the 12th ICF, 12–17 July, Ottawa, Canada

2009 T. Vallée, T. Tanner, M. Lehmann, M. Brunner: *Probabilistic Strength Prediction of Adhesively Bonded Joints Composed of Wooden Adherends*; in: Proceedings of the 12th ICF, 12–17 July, Ottawa, Canada

2009 M. Brunner, M. Lehmann: FRP-Prestressed Timber: *Losses in Prestressing Force due to Elastic, Creep and Shrinkage Deformations of the Timber*; in: Proceedings of the 9th FRPRCS, 13–15 July, Sydney, Australia

2009 M. Lehmann: *Verstärkung von Holz mittels vorgespannten CFK-Lamellen*; in: Proceedings of 41. Fortbildungskurs der SAH: Werkstoffkombinationen – ein Mehrwert für Holz, 27–28 October, Weinfelden, Switzerland

2009 R. Rauscher, F. Spang, M. Lehmann, T. Vallée: *Strength Prediction of a Joint Composed of a Pultruded FRP Tube Bonded to an FRP Lamella*; in: Proceedings of the 17th ICCM, 27–29 July, Edinburgh, Scotland

2008 M. Lehmann M. Properzi, P. Pichelin: *Strengthening of timber structures using pre-stressed carbon fibre lamellas*; in: Proceedings of the 1st MEDACHS 08 Conference, 20–23 January 2008, Lisbon, Portugal

2008 M. Lehmann: *Ductile Adhesive Interface for Glulam*; in: Proceedings of Holzbau Forschung und Praxis, 5–6 March 2008, Stuttgart, Germany

2008 M. Lehmann, M. Brunner, K.U. Schober, K. Rautenstrauch: *Testing and Numerical Simulation of Prestressed CFRP Reinforced Timber Structures*; in: Proceedings of the Final Conference of COST E34 Bonding of Timber, 6–7 May, Sopron, Hungary

2008 M. Brunner, M. Lehmann: *Strengthening glulam beams with prestressed multilayer FRP carbon laminates*; in: Proceedings of the Final Conference of COST E34 Bonding of Timber, 6–7 May, Sopron, Hungary

2008 K. Richter, M. Lehmann, M. Properzi: *Long-term behaviour of pre-stressed timber-CFRP composites*; in: Proceedings of the Final Conference of COST E34 Bonding of Timber, 6–7 May, Sopron, Hungary

2006 M. Lehmann, M. Properzi, F. Pichelin, P. Triboulot: *Pre-stressed FRP for the in-situ strengthening of timber structures*; in: Proceedings of the 9th WCTE 2006, 6–10 August, Portland, USA

Scientific reports

2012 M. Lehmann, A. Rosenkranz, J. Froidevaux: *Buche Ultraleicht – Entwicklung einer leistungsfähigen Bauplatte aus Buchenholz*; scientific report BAFU project

2010 M. Lehmann: *Duktile Klebefugen für Brettschichtholz*; scientific report CTI project

2009 M. Lehmann: *Sonotan Entwicklung von tanningebundenen Akustikplatten*; scientific report CTI project

2008 M. Lehmann: *Stress Distribution in Pre-stressed Timber Constructions*; scientific report COST-STSM-E34-03165

2007 M. Brunner, M. Schüriger, M. Lehmann: *Gradientenvorspannung: Verstärkung von Holzbalken mit vorgespannten CFK-Lamellen, die in Gradienten verankert sind*; scientific report BUWAL project

2006 M. Properzi, M. Lehmann: *OnSiteOn-site – An innovative approach for the on-site reinforcement and rehabilitation of timber structures*; scientific report COST E34 project

2005 M. Lehmann, S. Wieland: *Mikrowellenbehandlung als Alternative zur phytosanitären Hitzebehandlung von Holz: Machbarkeitsstudie*; scientific report BUWAL project

Edited books

2004 M. Properzi, F. Pichelin, M. Lehmann (eds.): COST E34 Innovations in Wood Adhesives, School of Architecture, Civil and Wood Engineering HSB, Biel

Academic reports

2006 M. Lehmann: *Renforcement sur site de poutres en bois avec lamelles de carbone précontraintes*; Mémoire de Master -Sciences du Bois et des Fibres-, Université Henri Poincaré UHP, Nancy

2004 M. Lehmann: *The development of Vintorg 2 -Mechanical testing of the first trial production-*; Diploma thesis, Hochschule für Architektur Bau und Holz, Biel

Appendix

A.1 Modelling of Series 1

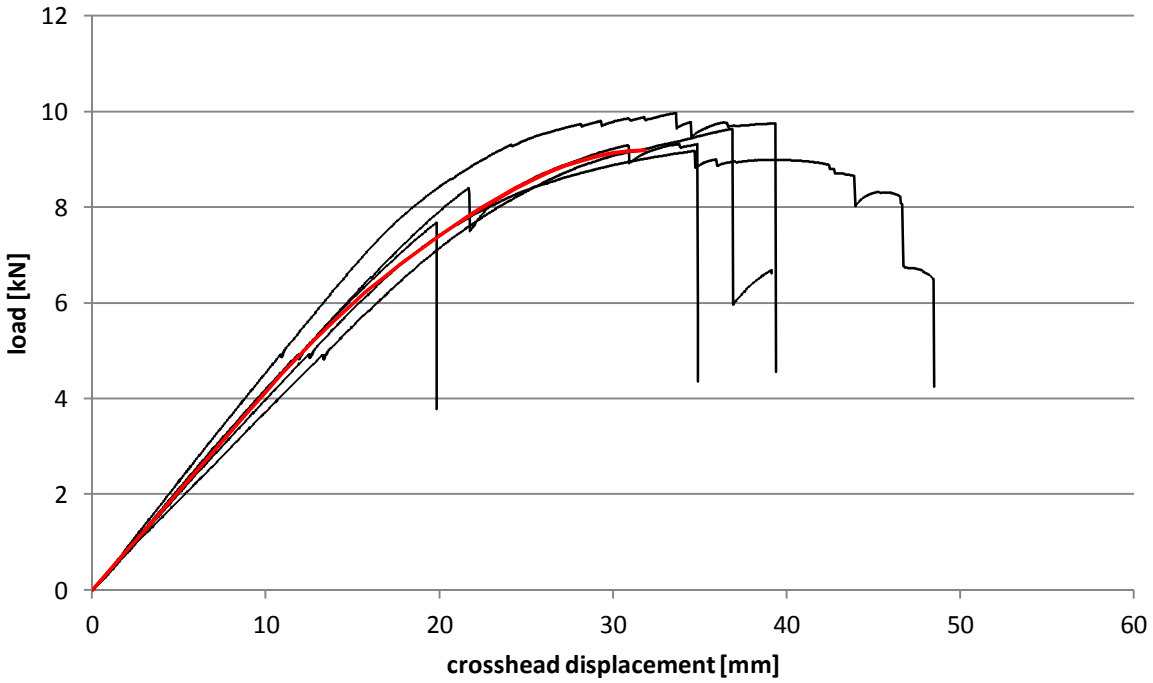

Figure A 1: *Load as a function of the crosshead displacement of the control specimens (**black**: experimental measurements; **red**: FEM)*

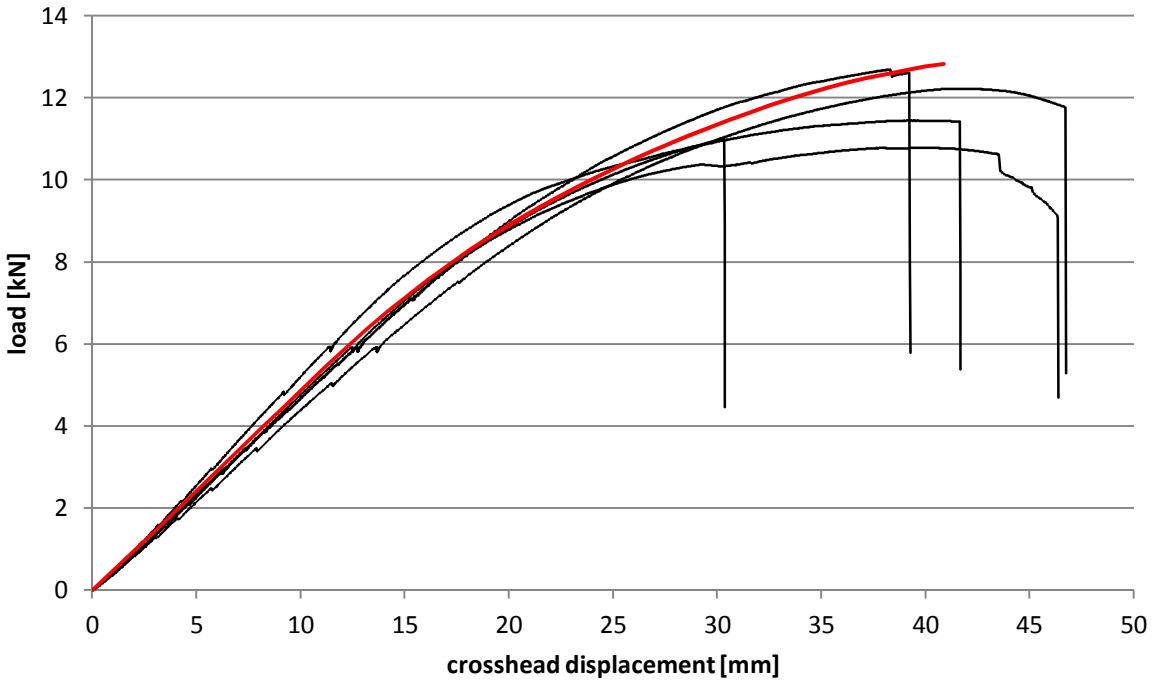

Figure A 2: *Load as a function of the crosshead displacement of Sample A (**black**: experimental measurements; **red**: FEM)*

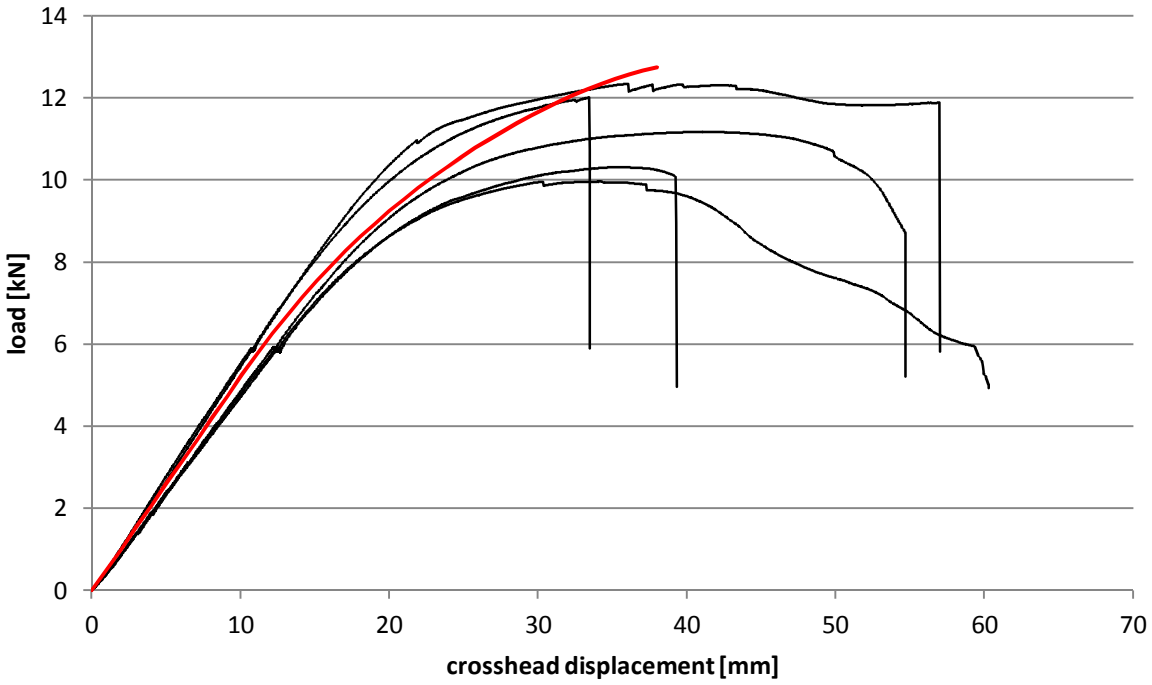

Figure A 3: *Load as a function of the crosshead displacement of Sample B (**black**: experimental measurements; **red**: FEM)*

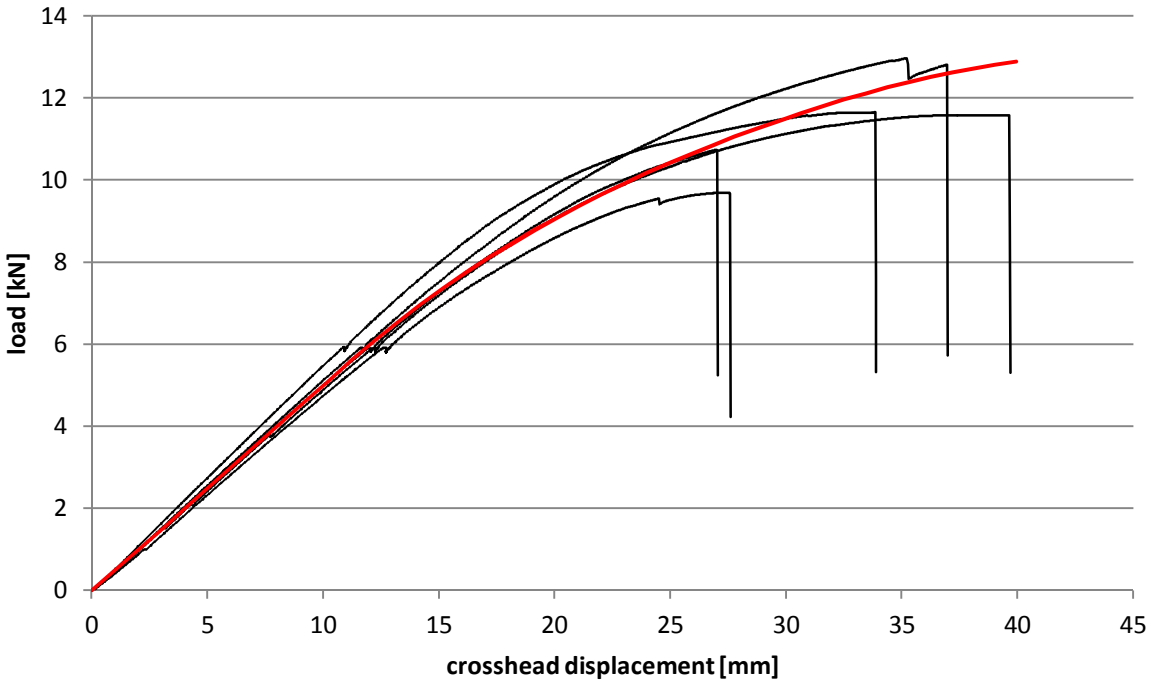

Figure A 4: *Load as a function of the crosshead displacement of Sample C (**black**: experimental measurements; **red**: FEM)*

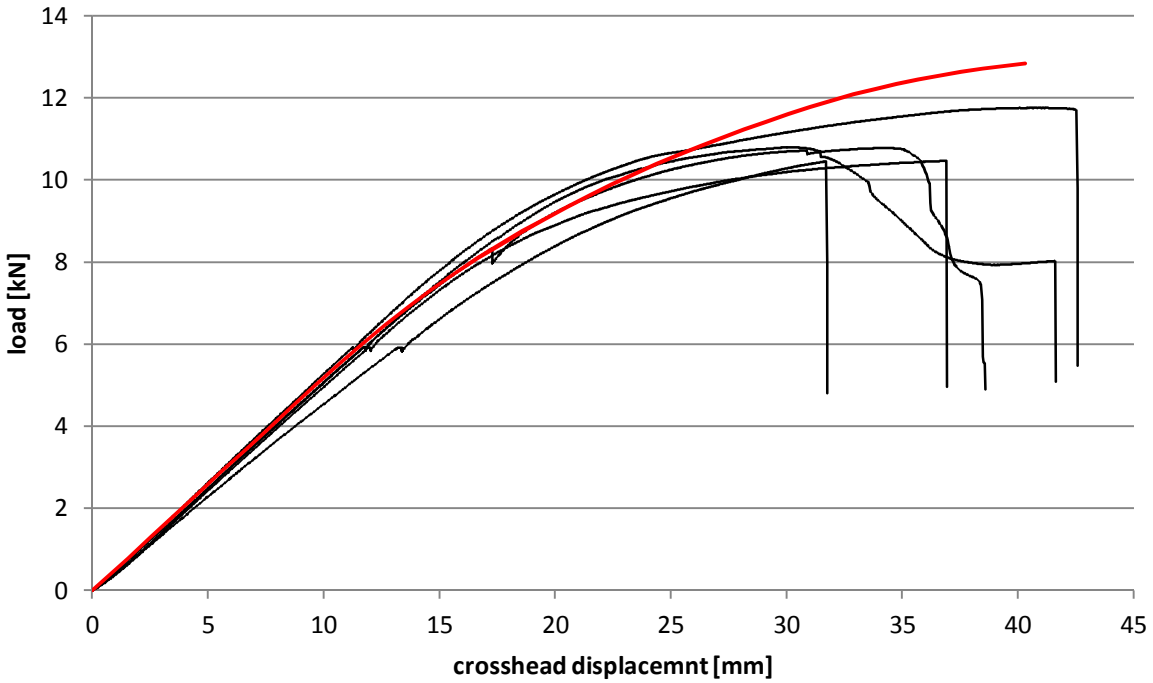

Figure A 5: *Load as a function of the crosshead displacement of Sample D (**black**: experimental measurements; **red**: FEM)*

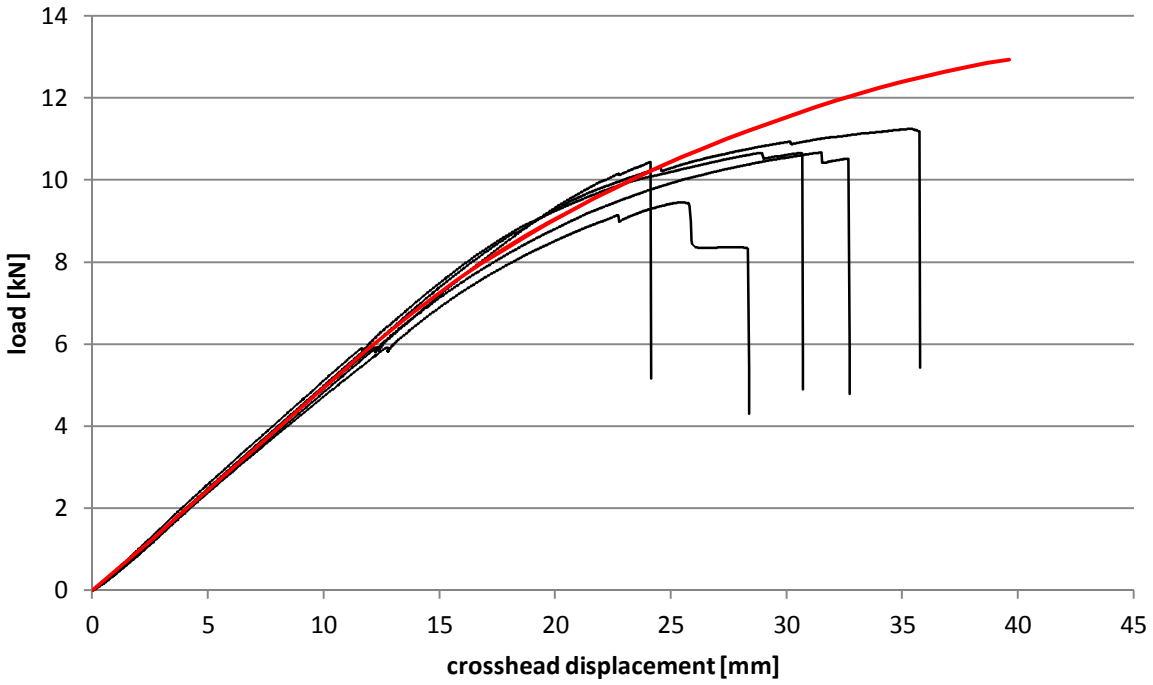

Figure A 6: *Load as a function of the crosshead displacement of Sample E (**black**: experimental measurements; **red**: FEM)*

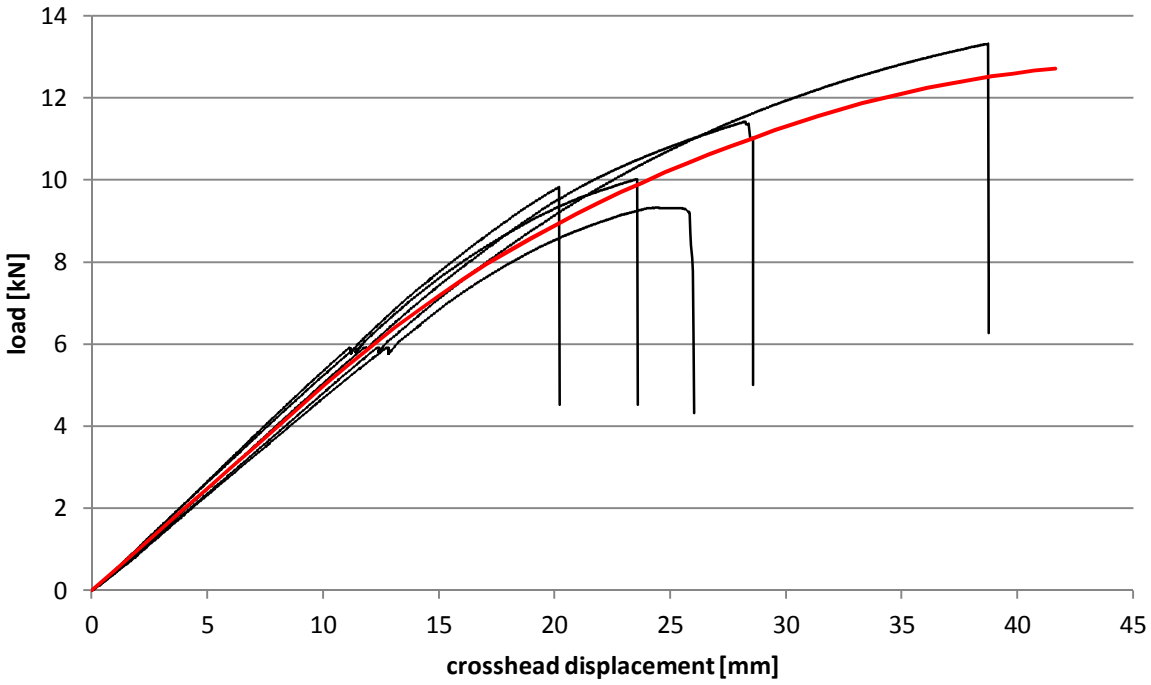

Figure A 7: *Load as a function of the crosshead displacement of Sample F (**black**: experimental measurements; **red**: FEM)*